GALACTIC RADIO SOURCES

III. SPECTRA AND PHYSICAL CHARACTERISTICS

By P. A. SHAVER* and W. M. GOSS†

[*Manuscript received February* 3, 1970]

Abstract

Spectral indices for over 250 galactic radio sources have been determined from high resolution observations at 408 and 5000 MHz. About 14% of the sources have nonthermal spectra. A comparison with results from an H109α line survey shows that the line-to-continuum temperature ratios for thermal sources are greater than about 2.5%, and no recombination line above the detectable threshold has been found in a nonthermal source. A search for optical emission from the vicinity of the thermal and nonthermal radio sources resulted in positive identifications for one-third of them. In 16 cases the radio contours are shown superimposed on optical photographs.

Electron temperatures have been determined directly from the 408 MHz brightness distribution for 50 thermal sources and are found to be consistent with values obtained from H109α recombination line work, indicating that any departures from local thermodynamic equilibrium, and their effects on the recombination lines, are small. Physical properties of the thermal sources have been computed assuming a spherical HII region model. It is shown that HII regions have a strong tendency to cluster, and that the cluster sizes are comparable with those of open star clusters. No HII regions were found with turnover frequencies greater than 1400 MHz, indicating that high density sources ($N_e > 5 \times 10^3$ cm^{-3} over a region > 0.1 pc in extent) are very rare. The largest, least dense HII regions have shell structure which is consistent with current ideas about the dynamical effects of radiation pressure on the dust within HII regions.

Fifteen new supernova remnants have been identified and distances and physical properties computed for them. For the well-resolved supernova remnants the shell thickness is a constant fraction of the diameter. It is shown that supernova remnants are frequently located in OB associations.

I. INTRODUCTION

The investigation of galactic radio sources is often plagued by confusion problems due to variations in the background radiation near the source and blending of adjacent sources. In order to obtain accurate spectral indices the same regions should be investigated at two widely different frequencies with similar beamwidths and signal-to-noise ratios. The latter requirement is important in recognizing low-lying emission which may extend over large angular distances; this emission can make a substantial contribution to the flux density.

Recently about 70 regions in the galactic plane were observed at 5000 MHz with a 4′ arc beam using the Parkes 210 ft radio telescope (Part I of the present Supplement, pp. 1–75) and at 408 MHz with a 3′ arc beam using the Molonglo radio telescope

* School of Physics, University of Sydney, Sydney, N.S.W. 2006.
† Division of Radiophysics, CSIRO, P.O. Box 76, Epping, N.S.W. 2121.

(Part II of the present Supplement, pp. 77–131). Contour maps, positions, and integrated flux densities are given in these papers for all of the sources. The 5000 MHz survey was carried out in conjunction with an H109α recombination line investigation of the southern Milky Way (Wilson *et al.* 1970). The continuum observations are of similar high resolution and sensitivity, and the frequency ratio is 12; from them we have been able to derive accurate spectral indices and physical parameters for over 200 sources. This analysis is reported in the present paper (preliminary results for two sources near $l^{II} = 312^{\circ}$ have already been given by Shaver and Goss 1969). Electron temperatures have also been determined from the continuum observations for 50 sources that are sufficiently opaque and well resolved at 408 MHz; these results are not dependent on theories for the relative population of the excited levels of atoms and ions and provide a reliable check on methods of temperature determination using spectral lines.

In Section II of the present paper the radio spectra of all the sources are examined. The results of a search for optical features in the neighbourhood of these sources are reported in Section III. Sections IV and V deal with the thermal and nonthermal sources respectively. Individual sources are discussed in detail in the Appendix.

II. SOURCE SPECTRA

All the sources in Parts I and II, and in Mills and Shaver (1968) and Shaver (1969*a*), are listed in Table 1. The criteria used in determining what features on the maps should be considered sources were not well defined; it is difficult to hold to a rigorous criterion because in some extreme cases sources with steep spectral indices (positive or negative) appearing on either the 408 or 5000 MHz map do not show up at all on the other. Generally a feature was called a source if it was fairly localized and stood out against the background. In some cases several of the "sources" dealt with in this section are part of single HII regions or supernova remnants which are discussed in Sections IV and V (this is especially true for supernova remnants).

In order to obtain accurate spectral indices it is essential that the sources be measured in a consistent way from the 408 and 5000 MHz maps—in particular that they be separated from the varying background in the same way in both cases. A considerable effort was made to ensure that this was done. All the measurements for one source were made at the same time from both the high and low frequency maps by fitting Gaussians to the brightness distributions.

The galactic "G" numbers of the sources are listed in column 1 of Table 1; whenever the 408 and 5000 MHz source numbers differ slightly, the 408 MHz one is used here. The next 10 columns list the Gaussian source parameters measured at the low and high frequencies: the baselevel determined for the source and the measured peak temperatures (T_{1p}, T_{2p}), half-power widths (M_1, M_2), and computed flux densities* for a Gaussian model, the subscripts 1 and 2 referring to the 408 and 5000 MHz observations respectively. The 408 MHz flux densities for the thermal sources are generally $\sim$ 5% too small because the baselevel was taken to be flat and the absorption of the background neglected; however, fitting small sources with a Gaussian distribution overestimates the flux density because the beam pattern is sharper than that of a

* 1 flux unit (f.u.) = 10^{-26} W m^{-2} Hz^{-1}.

Gaussian. The two effects often cancel each other, and both have been neglected. It should also be noted that, even for well-resolved sources, the half-power widths in right ascension and declination have been used in computing the flux density rather than those of the major and minor axes; this results in a further underestimation of the flux densities.

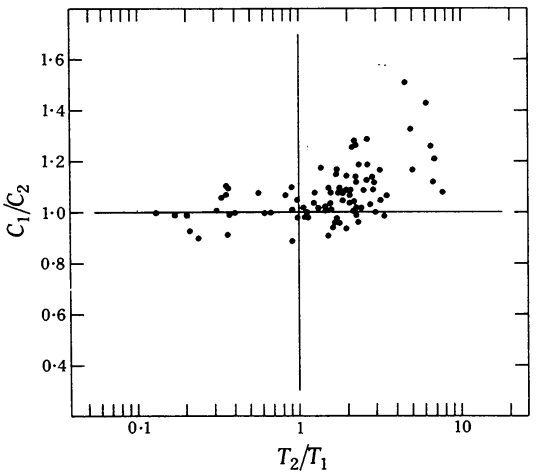

Fig. 1.—Dependence of the ratio of low frequency to high frequency half-power widths on the ratio T_2/T_1 (for sources with $T_{1p} > 1000°$K), which is related to the spectral index α by equation (7).

A convenient way of comparing the observations at the two frequencies is to convolve the map with highest resolution to match the resolution of the other. The half-power beamwidth at 408 MHz is 2′.65 in right ascension and 2′.86 sec (δ+35°.51) in declination, and for the circular beam at 5000 MHz it is 4′.0 arc. Usually the resolution at 408 MHz was highest, and the following equations were used.

$$C_{1\alpha}^2 = B_2^2 - B_{1\alpha}^2 + M_{1\alpha}^2 , \qquad C_{1\delta}^2 = B_2^2 - B_{1\delta}^2 + M_{1\delta}^2 , \qquad (1, 2)$$

$$C_1 = (C_{1\alpha}\, C_{1\delta})^{1/2} , \qquad C_2 = (M_{2\alpha}\, M_{2\delta})^{1/2} , \qquad (3, 4)$$

$$T_1 = (M_{1\alpha}\, M_{1\delta}/C_1^2) T_{1p} , \qquad T_2 = 195\, T_{2p} . \qquad (5, 6)$$

In a few cases the declination beamwidth at 5000 MHz was smaller than that at 408 MHz and the above procedure had to be reversed for the declination coordinate. In equations (1)–(6) C represents the measured source width (M) after convolution and B is the half-power beamwidth. C_1 and T_1 are the geometric mean half-power width and peak temperature respectively of the source at 408 MHz convolved to match the resolution at 5000 MHz. C_2 and T_2 are the geometric mean half-power width and peak temperature respectively of the source as observed at 5000 MHz for which the temperature scale has been augmented by the ratio of the optical depths, using Oster's (1961) formula $\tau_1/\tau_2 \approx 195$ for $T_e = 7000°$K. This is the ratio of the brightness temperature of an optically thin thermal source at 408 MHz to that at 5000 MHz, and is independent of the properties of the source except for a weak dependence on the electron temperature. For a nonthermal source we expect to find $C_1/C_2 = 1$ and $T_2/T_1 < 1$ (see equation (7)). For a thermal source, $C_1/C_2 \geqslant 1$ and $T_2/T_1 \geqslant 1$ and both ratios should increase with increasing opacity.

1970AuJPA..14..133S

TABLE 1

Measured Continuum Data for All Sources

(1)	(2)	(3)	(4)	(5)	(6)	(7)	(8)	(9)	(10)	(11)	(12)	(13)	(14)	(15)	(16)
	408 MHz Measured Parameters					5000 MHz Measured Parameters									
G Number	Base-level (^oK)	Peak Temp. T_{1p} (^oK)	Half-power Widths $M_{1\alpha}$ (min of arc)	$M_{1\delta}$ (min of arc)	Flux Density S_1 (f.u.)	Base-level (^oK)	Peak Temp. T_{2p} (^oK)	Half-power Widths $M_{2\alpha}$ (min of arc)	$M_{2\delta}$ (min of arc)	Flux Density S_2 (f.u.)	Widths Ratio C_1/C_2	Conv. Temps. T_2/T_1	Error in T_2/T_1	Nature of Source	Temp. Ratio T_L/T_C (%)
206.0 -1.7	50	130	14.8	13.0	12.3	-	-	-	-	-	-	-	-	-	-
206.0 -2.1	70	160	12.2	11.6	11.1	-	-	-	-	-	-	-	-	-	-
206.2 -2.3	70	160	7.7	11.6	7.0	-	-	-	-	-	-	-	-	-	-
206.5-16.4	50	3850	5.3	4.7	47.0	0.5	31.5	5.0	4.7	54.4	1.14	1.99	0.20	T	4.9
206.6 -1.7	30	200	15.5	28.4	43.2	-	-	-	-	-	-	-	-	-	-
207.1 -1.3	0	700	2.7	3.8	3.5	-	-	-	-	-	-	-	-	NT	-
208.5-19.2	-	-	-	-	-	0.2	0.4	5.1	5.2	0.8	-	-	-	-	-
208.9-19.3	50	1560	3.4	3.8	9.9	0.2	10.3	4.7	4.7	16.7	0.94	1.97	0.21	T	6.0
209.0-19.4	50	6750	7.2	6.6	157.2	0.2	183.8	5.1	5.1	351.5	1.43	6.07	0.01	T	4.3
265.1 +1.5	0	2900	3.8	4.0	21.6	0.2	15.0	4.6	4.7	23.8	1.04	1.55	0.16	T	4.4
267.8 -0.9	0	780	8.0	7.3	22.3	0.6	4.6	9.0	8.5	25.9	0.93	1.31	0.16	T	6.8
268.0 -1.1	0	5100	4.2	5.2	54.6	1.0	124.0	4.2	4.5	172.3	1.26	6.55	0.66	T	3.4
268.1 -1.0	0	1050	6.5	5.8	19.4	0.8	5.8	7.1	6.2	18.8	1.02	1.31	0.15	T	-
282.0 -1.2	100	2850	3.5	4.1	20.0	0.4	17.8	4.4	4.5	25.9	1.05	1.88	0.19	T	4.1
283.1 -1.0	80	340	4.9	4.4	3.6	0.4	1.5	5.9	4.5	2.9	1.07	1.16	0.24	-	-
283.2 -1.1	80	450	2.6	3.2	1.8	0.3	0.2	4.0	4.0	0.2*	1.00	0.17	0.17	NT	-
283.3 -0.6	70	280	6.7	8.5	7.8	0.5	1.2	8.8	10.6	8.2	0.83	0.96	0.23	-	-
283.3 -1.0	80	350	6.4	6.0	6.6	0.5	1.8	5.6	6.5	4.8	1.12	1.20	0.23	-	LT 2.5
283.5 -1.0	110	520	3.8	9.0	8.7	0.8	2.0	4.8	9.0	6.4	1.02	0.99	0.16	-	-
284.0 -1.0	350	470	4.0	7.7	7.1	1.7	1.7	7.5	10.0	9.4	0.71	0.93	0.16	-	6.5
284.3 -0.3	100	5300	7.0	9.4	171.0	1.0	53.0	6.2	7.4	178.8	1.27	2.20	0.22	T	3.3
284.6 -0.2	0	420	6.2	7.5	9.6	0.8	1.9	6.8	8.2	7.8	0.99	1.03	0.18	-	LT 2.3
284.6 -0.5	60	310	6.7	5.2	5.3	0.3	1.1	6.5	6.5	3.4	0.99	0.84	0.21	-	-
285.3 -0.0	0	2180	3.4	4.5	16.3	0.2	11.6	4.4	4.4	16.5	1.08	1.58	0.16	T	4.0
287.4 -0.6	300	5050	6.2	9.2	141.2	-	-	-	-	-	-	-	-	T	4.5

287.6 -0.6	300	4400	8.2	6.8	120.3	-	-	-	-	-	-	-	-	T	3.2
287.7 -1.3	200	700	2.7	3.2	3.0	-	-	-	-	-	-	-	-	NT	-
287.8 -0.8	700	930	11.0	7.2	36.1	-	-	-	-	-	-	-	-	-	3.7
287.9 -1.0	700	950	6.2	5.7	16.5	-	-	-	-	-	-	-	-	-	6.1
288.0 -0.8	700	930	6.2	6.7	18.9	-	-	-	-	-	-	-	-	-	4.6
289.1 -0.4	50	820	3.9	4.7	7.4	0.4	4.0	5.2	5.1	7.8	0.99	1.35	0.16	T	2.8
289.8 -1.2	120	580	8.7	7.3	18.1	1.0	3.6	8.4	7.6	16.9	1.05	1.35	0.18	T	3.7
289.9 -0.8	140	310	2.8	5.5	2.3	1.3	2.1	4.2	4.4	2.9	1.05	2.11	0.40	T	-
290.1 -0.8	0	1430	12.4	11.4	99.1	-	-	-	-	-	-	-	-	NT	-
290.4 -0.9	80	420	2.6	3.2	1.7	-	-	-	-	-	-	-	-	NT	-
290.6 -1.2	30	200	5.0	4.2	2.1	-	-	-	-	-	-	-	-	-	-
291.0 -0.1	30	870	7.3	7.8	24.3	0.5	3.3	5.8	6.0	8.4	1.36	0.84	0.11	NT	LT 1.3
291.1 -0.8	30	340	4.0	3.6	2.4	0.7	1.7	5.8	4.8	3.5	0.88	1.46	0.28	T	-
291.2 -0.3	40	400	5.7	5.8	6.5	0.8	1.5	6.7	6.6	4.9	0.95	0.89	0.17	-	-
291.3 -0.7	50	3150	3.1	4.1	19.6	0.7	77.3	4.1	4.1	97.4	1.08	7.68	0.77	T	3.8
291.5 -0.1	30	370	6.4	7.8	9.1†	0.5	1.7	6.3	6.5	5.1	1.18	1.04	0.20	-	-
291.6 -0.5	50	4650	7.0	8.6	137.2	1.0	56.0	5.5	7.6	172.1	1.29	2.66	0.27	T	2.9
291.9 -0.7	80	590	3.0	3.6	3.1	1.0	2.3	4.0	4.4	3.0	1.02	1.29	0.19	T	5.8
292.0 +1.8	0	1750	4.0	4.7	16.1	0.2	5.2	4.7	4.9	8.8	1.07	0.82	0.09	NT	LT 2.5
295.1 -1.7	60	440	4.0	6.0	5.2	0.8	1.6	7.0	8.2	6.8	0.74	0.95	0.17	-	11.1
295.2 -0.6	100	630	5.0	4.3	6.6	0.7	3.7	6.3	5.8	9.9	0.88	1.52	0.20	T	3.0
298.2 -0.8	-	-	-	-	-	0.4	2.4	4.0	4.0	2.8	-	-	-	-	-
298.2 -0.3	100	1950	3.3	4.4	13.9	1.0	21.0	4.4	4.5	30.6	1.05	3.20	0.33	T	3.4
298.5 -0.3	200	700	4.5	4.8	7.4	1.5	1.4	7.0	7.5	5.4	0.74	0.52	0.10	NT	-
298.6 -0.0	190	360	4.3	7.4	5.6	1.4	0.9	7.5	6.4	3.2	0.90	0.62	0.17	NT	-
298.9 -0.4	100	2400	4.9	4.9	28.2	0.6	16.5	5.5	4.9	32.7	1.08	1.74	0.18	T	5.2
301.0 +1.2	0	560	2.8	3.9	3.0	0.0	2.4	4.0	4.0	2.8	1.04	1.43	0.21	T	6.5
301.1 +1.0	0	560	2.8	3.3	2.5	0.0	3.0	4.0	4.0	3.6	1.00	1.90	0.27	T	3.7
304.6 +0.1	0	1470	6.0	6.9	29.8	0.0	2.1	6.2	7.0	6.7	1.06	0.33	0.05	NT	-
305.1 +0.1	120	740	5.5	7.5	15.0	0.9	4.3	6.4	7.0	14.2	1.04	1.35	0.17	T	4.6
305.2 +0.0	130	1370	5.5	7.5	27.7	1.0	12.6	5.4	5.6	28.0	1.26	2.14	0.23	T	5.8
305.2 +0.2	130	1970	5.5	7.0	37.2	1.0	14.2	6.3	7.9	52.0	0.96	1.69	0.17	T	5.5
305.3 +0.1	130	840	3.4	4.5	6.3	1.0	5.1	4.7	5.2	9.2	0.96	1.78	0.21	T	-
305.4 +0.2	130	2040	4.8	4.9	23.5	1.2	22.8	5.0	4.7	39.4	1.14	2.85	0.29	T	6.2
305.5 +0.4	100	600	3.1	3.6	3.3	0.9	2.5	4.2	4.3	3.3	1.01	1.34	0.19	T	-

* † See footnotes at end of table.

1970AuJPA..14..133S

(1)	(2)	(3)	(4)	(5)	(6)	(7)	(8)	(9)	(10)	(11)	(12)	(13)	(14)	(15)	(16)
	408 MHz Measured Parameters					5000 MHz Measured Parameters									
G Number	Base-level (^{o}K)	Peak Temp. T_{1p} (^{o}K)	Half-power Widths $M_{1\alpha}$ (min of arc)	$M_{1\delta}$	Flux Density S_1 (f.u.)	Base-level (^{o}K)	Peak Temp. T_{2p} (^{o}K)	Half-power Widths $M_{2\alpha}$ (min of arc)	$M_{2\delta}$	Flux Density S_2 (f.u.)	Widths Ratio C_1/C_2	Conv. Temps. T_2/T_1	Error in T_2/T_1	Nature of Source	Temp. Ratio T_L/T_C (%)
305.6 +0.0	130	1020	5.3	6.3	16.7	1.0	6.2	6.1	6.4	17.8	1.02	1.45	0.16	T	8.6
307.1 +1.2	0	6700	2.7	3.2	28.4	0.0	3.2	4.2	4.0	4.0	0.99	0.17	0.02	NT	LT 2.1
308.6 +0.6	0	550	4.2	6.1	6.9	0.3	3.1	5.3	7.5	9.1	0.93	1.45	0.20	T	2.9
309.6 +1.7	0	4750	4.1	4.8	45.8	0.3	4.3	5.6	6.0	10.6	0.90	0.24	0.03	NT	-
309.8 +1.8	0	7400	6.6	5.7	136.5	0.4	6.2	7.2	6.3	20.7	0.99	0.20	0.02	NT	LT 1.8
311.1 -0.3	80	250	5.6	6.2	4.3	0.5	1.3	8.2	8.1	6.3	0.80	1.23	0.30	-	-
311.3 +0.1	90	230	4.2	5.8	2.7	0.7	0.9	6.5	8.5	3.7	0.76	1.01	0.30	-	-
311.5 +0.4	100	460	3.8	5.8	5.0	0.9	2.3	5.0	6.0	5.1	0.99	1.34	0.21	T	3.9
311.5 -0.5	100	350	4.5	5.5	4.2	0.7	1.5	5.7	5.7	3.6	0.99	1.09	0.22	-	-
311.5 -0.3	120	750	3.8	4.1	5.7	0.6	1.0	4.9	4.8	1.7	0.98	0.38	0.09	NT	-
311.6 +0.3	40	70	2.6	3.2	0.3	0.8	2.4	4.0	4.0	2.8	1.00	12.56	7.36	T	4.6
311.9 +0.1	150	820	3.8	4.3	6.6	1.0	4.4	5.0	4.4	7.1	1.05	1.52	0.18	T	8.6
311.9 +0.2	100	770	4.4	4.6	7.6	0.7	4.0	5.0	5.3	7.8	1.02	1.38	0.17	T	8.3
314.2 +0.3	0	330	3.1	5.3	2.7	0.2	1.4	4.8	6.0	3.0	0.90	1.26	0.27	-	-
314.2 +0.4	0	550	3.5	3.9	3.7	0.2	3.0	4.8	4.9	5.2	0.95	1.64	0.23	T	9.6
316.2 +0.0	20	630	5.3	13.0	21.3	-	-	-	-	-	-	-	-	NT	-
316.3 -0.0	20	790	4.4	9.4	16.0	-	-	-	-	-	-	-	-	NT	-
316.4 -0.4	40	360	4.5	4.6	3.7	-	-	-	-	-	-	-	-	-	-
316.8 -0.1	100	2300	4.4	4.5	22.3	0.8	20.2	4.6	4.2	28.7	1.19	2.36	0.24	T	5.6
317.0 +0.3	100	620	7.4	8.7	19.6	0.8	3.0	7.3	9.1	14.7	1.04	1.06	0.14	-	7.4
317.3 +0.2	110	320	6.3	8.4	8.3	0.9	1.3	7.4	9.5	6.7	0.93	0.92	0.20	-	23.9
319.2 -0.4	0	480	6.3	6.3	9.3	0.2	2.8	6.5	6.1	8.2	1.09	1.36	0.20	T	4.0
319.4 -0.0	0	690	6.0	4.3	8.7	0.2	3.8	6.4	4.6	8.2	1.07	1.39	0.18	T	7.6
319.9 +0.8	0	350	2.9	3.2	1.6	-	-	-	-	-	-	-	-	NT	-
320.1 -0.5	100	330	3.7	4.3	2.6	0.3	1.0	5.5	5.8	2.3	0.86	0.88	0.22	-	-

320.2	+0.8	0	1450	3.4	3.8	9.2	0.3	5.9	4.2	4.2	7.7	1.08	1.26	0.14	T	4.5
320.2	-1.4	0	600	5.5	5.8	9.4	-	-	-	-	-	-	-	-	NT	-
320.3	-0.3	100	950	4.0	4.3	8.0	0.3	4.1	4.8	5.0	7.2	1.01	1.21	0.14	T	4.3
320.3	-0.2	100	850	4.2	3.5	6.1	0.3	4.4	4.2	4.3	5.8	1.07	1.51	0.18	T	6.6
320.3	-1.4	0	630	7.6	7.1	16.7	-	-	-	-	-	-	-	-	NT	-
320.4	-1.0	0	2200	6.2	6.4	42.8	0.5	3.5	7.0	6.8	12.2	0.99	0.37	0.04	NT	LT 1.3
320.4	+0.2	90	260	4.3	3.9	2.1	0.2	1.2	5.1	5.0	2.3	0.96	1.30	0.32	-	-
320.4	-1.4	0	660	6.7	8.0	17.3	-	-	-	-	-	-	-	-	NT	-
320.5	-1.0	0	700	4.9	4.8	8.1	-	-	-	-	-	-	-	-	NT	-
321.0	-0.5	0	980	4.2	4.0	8.1	0.3	4.5	5.1	4.6	7.8	1.02	1.29	0.15	T	6.4
321.1	-0.5	0	740	4.6	5.7	9.5	0.3	3.4	5.5	5.7	7.8	1.04	1.17	0.15	T	7.2
322.2	+0.6	60	1040	2.8	3.2	4.6	0.3	9.8	4.1	4.1	12.2	0.99	3.39	0.37	T	5.7
324.2	+0.2	0	450	4.8	5.0	5.3	-	-	-	-	-	-	-	-	-	-
324.2	+0.1	40	180	2.7	3.1	0.7	0.0	2.8	4.0	4.0	3.3	1.00	5.89	1.50	T	4.8
326.4	+0.9	50	720	2.8	3.1	3.1	0.3	5.9	4.1	4.1	7.2	1.00	3.03	0.36	T	4.9
326.6	+0.6	60	1940	6.0	6.1	34.8	0.4	18.0	4.9	5.5	35.7	1.28	2.20	0.23	T	5.9
327.3	-0.6	150	1630	3.7	3.7	10.9	1.0	36.0	4.1	4.1	44.9	1.12	6.74	0.69	T	5.5
327.6	-0.4	70	530	4.9	5.1	6.5	0.6	2.5	5.3	5.9	5.7	1.02	1.21	0.18	T	7.1
327.8	-0.4	70	510	2.6	3.7	2.4	0.6	2.8	4.3	5.2	4.6	0.92	1.98	0.29	T	-
327.8	+0.1	70	280	6.5	5.7	5.1	0.7	1.1	6.7	7.3	4.0	0.95	0.93	0.23	-	-
328.0	-0.1	80	880	3.6	3.5	5.4	0.7	3.0	4.5	4.4	4.4	1.01	1.07	0.14	-	7.4
328.0	+0.3	80	350	4.0	5.8	4.0	0.5	0.4	5.0	6.3	1.0	1.00	0.32	0.16	NT	-
328.1	+0.1	80	250	3.2	3.0	1.2	0.5	0.7	4.4	4.2	1.0	0.98	1.01	0.34	-	-
328.3	+0.4	40	940	3.6	4.0	6.6	0.5	6.6	4.5	4.6	10.0	1.03	2.12	0.24	T	5.4
328.4	+0.2	40	2460	3.9	4.1	19.3	0.6	7.6	4.4	4.4	10.8	1.10	0.90	0.09	NT	LT 0.3
330.7	-0.4	70	430	3.3	3.4	2.4	0.6	1.8	4.7	4.5	2.8	0.95	1.39	0.24	T	-
330.9	-0.4	100	1000	3.7	3.8	6.9	0.8	6.8	4.4	4.3	9.5	1.07	2.07	0.23	T	7.8
331.0	-0.2	120	680	5.6	4.8	9.0	0.8	3.0	6.1	6.2	8.3	0.95	1.11	0.15	-	13.3
331.1	-0.5	150	570	2.8	4.3	3.4	1.0	2.5	4.0	4.4	3.2	1.03	1.46	0.21	T	8.0
331.3	-0.2	150	730	2.9	3.4	3.5	1.0	3.2	4.2	4.2	4.2	1.00	1.55	0.20	T	4.2
331.3	-0.3	140	980	3.9	4.6	8.6	1.0	4.9	4.7	4.6	7.8	1.09	1.41	0.16	T	6.8
331.4	+0.5	0	220	3.3	5.8	2.1	0.4	1.1	6.2	6.6	3.3	0.79	1.44	0.40	T	-
331.4	-0.0	150	750	3.4	5.3	6.6	0.9	3.9	4.4	5.2	6.6	1.06	1.50	0.19	T	6.3
331.5	-0.1	150	2450	4.1	4.6	22.7	1.0	20.0	4.7	4.5	31.1	1.12	2.27	0.23	T	7.4
332.0	+0.2	90	460	4.2	4.4	4.2	-	-	-	-	-	-	-	-	NT	-

1970AuJPA..14..133S

(1)	(2)	(3)	(4)	(5)	(6)	(7)	(8)	(9)	(10)	(11)	(12)	(13)	(14)	(15)	(16)
	408 MHz Measured Parameters					5000 MHz Measured Parameters									
G Number	Base-level (^{o}K)	Peak Temp. T_{1p} (^{o}K)	Half-power Widths $M_{1\alpha}$ (min of arc)	$M_{1\delta}$ (min of arc)	Flux Density S_1 (f.u.)	Base-level (^{o}K)	Peak Temp. T_{2p} (^{o}K)	Half-power Widths $M_{2\alpha}$ (min of arc)	$M_{2\delta}$ (min of arc)	Flux Density S_2 (f.u.)	Widths Ratio C_1/C_2	Conv. Temps. T_2/T_1	Error in T_2/T_1	Nature of Source	Temp. Ratio T_L/T_C (%)
332.0 +0.1	90	510	4.8	5.4	6.5	-	-	-	-	-	-	-	-	NT	-
332.2 -0.4	100	1300	3.0	3.0	5.7	0.6	10.4	4.2	4.1	13.2	1.00	2.93	0.31	T	5.1
332.4 -0.4	100	2100	7.5	7.8	60.2	0.7	3.3	6.8	7.9	13.0	1.11	0.35	0.04	NT	LT 1.3
332.4 +0.2	150	990	6.0	3.3	9.6	0.7	1.5	7.2	5.1	4.0	0.82	0.42	0.07	NT	-
332.5 +0.0	150	1100	3.9	4.9	10.3	0.8	1.4	5.8	5.6	3.3	0.91	0.36	0.06	NT	-
332.5 -0.1	160	390	3.4	3.7	2.4	0.8	1.7	4.4	4.0	2.2	1.08	1.39	0.26	T	7.8
332.7 -0.6	200	1420	4.4	4.5	13.8	1.2	9.2	5.4	5.5	20.1	0.96	1.77	0.19	T	10.1
332.8 -0.8	200	300	4.2	3.8	2.3	0.6	0.8	5.2	4.6	1.5	1.00	0.82	0.24	-	-
332.8 -0.6	200	1000	6.3	6.0	18.5	1.2	6.4	5.1	7.8	18.7	1.10	1.51	0.17	T	7.6
332.8 -0.3	190	150	3.2	3.4	0.8	1.0	0.3	4.6	4.3	0.5	0.98	0.76	0.50	-	-
333.0 +0.8	0	1900	2.8	3.9	10.3	0.4	5.0	4.2	4.3	6.6	1.01	0.90	0.10	NT	-
333.0 -0.6	200	500	3.9	6.8	6.5	1.2	2.1	5.8	6.7	6.0	0.93	1.11	0.18	-	-
333.0 -0.4	200	1800	4.0	6.0	21.2	1.2	15.6	6.3	5.5	39.7	0.96	2.30	0.24	T	10.5
333.1 -0.4	200	1800	4.2	7.2	26.7	1.2	17.8	5.1	6.3	42.1	1.09	2.52	0.26	T	8.4
333.1 +0.0	100	250	4.6	5.5	3.1	0.8	1.4	5.3	6.5	3.5	0.99	1.45	0.34	T	-
333.2 -0.1	100	650	4.3	5.3	7.3	0.8	3.7	5.8	7.8	12.3	0.83	1.51	0.20	T	9.6
333.3 +0.1	80	390	2.9	3.1	1.7	0.7	1.6	4.8	5.0	2.8	0.84	1.50	0.29	T	-
333.3 -0.4	200	1300	3.2	6.5	13.3	1.2	22.8	4.0	5.1	34.2	1.17	5.04	0.53	T	6.3
333.6 -0.1	150	1250	5.2	5.2	16.6	1.0	5.6	5.7	6.4	15.0	0.98	1.13	0.13	T	5.9
333.6 -0.2	150	2750	4.0	4.3	23.2	1.0	67.0	4.1	4.1	84.4	1.21	6.96	0.70	T	3.1
333.7 -0.5	50	230	5.1	5.3	3.0	0.7	1.3	5.3	6.3	3.2	1.03	1.43	0.36	T	12.0
335.7 -0.2	90	570	6.8	5.1	9.7	0.8	3.2	6.0	5.4	7.6	1.14	1.35	0.19	T	6.2
336.0 +0.1	140	310	6.0	3.8	3.5	1.0	1.4	6.2	4.5	2.9	1.05	1.20	0.26	-	-
336.4 -0.2	170	530	5.6	7.0	10.2	1.3	2.7	6.4	6.0	7.6	1.11	1.21	0.18	T	8.2
336.4 -0.3	170	730	5.2	5.2	9.7	1.3	3.5	6.5	6.0	10.0	0.95	1.21	0.15	T	8.9

336.5 +0.0	170	380	4.4	5.0	4.1	1.3	1.4	5.2	6.2	3.3	0.97	0.99	0.20	-	11.1
336.5 -1.5	100	430	3.2	3.2	2.2	0.8	7.2	4.0	4.0	8.6	1.05	5.80	0.81	T	4.9
336.5 +0.1	300	270	2.9	3.1	1.2	2.0	0.4	4.0	4.0	0.5	1.01	0.55	0.29	NT	-
336.5 -0.2	170	690	5.5	5.5	10.2	1.3	3.1	7.1	9.0	14.6	0.78	1.11	0.15	-	5.7
336.7 +0.5	60	380	5.9	4.1	4.5	0.5	0.6	6.6	4.9	1.4	1.00	0.41	0.15	NT	-
336.8 +0.6	60	290	6.6	3.5	3.3	0.2	0.4	7.2	4.3	0.8	1.03	0.33	0.19	NT	-
336.8 +0.0	180	1390	9.7	6.3	41.6	1.4	9.4	11.4	7.3	57.5	0.91	1.50	0.16	T	5.7
337.0 -0.1	180	2020	6.1	6.1	36.8	1.4	4.8	5.3	7.7	14.4	1.08	0.56	0.06	C	7.4
337.1 -0.2	180	1520	3.9	3.9	11.3	1.4	11.4	4.1	4.4	15.1	1.14	2.23	0.23	T	5.5
337.2 +0.1	250	350	2.7	3.1	1.4	1.7	0.6	4.0	4.0	0.7	1.00	0.66	0.24	NT	-
337.3 -0.1	170	600	6.1	7.2	12.9	1.3	3.1	5.3	6.1	7.4	1.27	1.20	0.16	T	4.3
337.5 -0.3	-	-	-	-	-	0.5	1.3	7.7	7.7	5.7	-	-	-	-	-
337.6 -0.0	300	420	5.8	6.0	7.2	1.5	2.2	5.9	6.4	6.1	1.06	1.26	0.21	T	8.1
337.7 -0.3	130	220	3.3	4.2	1.5	0.5	0.8	5.3	5.0	1.6	0.91	1.13	0.37	-	-
337.8 -0.1	300	2340	5.5	5.0	31.5	1.5	3.3	5.9	5.0	7.2	1.10	0.36	0.04	NT	LT 1.3
337.9 -0.5	50	1450	3.6	3.6	9.2	0.5	13.3	4.2	4.2	17.3	1.09	2.90	0.30	T	5.3
338.0 -0.1	300	660	10.0	7.5	24.3†	1.5	3.0	7.2	7.0	11.1	1.28	0.99	0.13	-	5.9
338.1 +0.0	300	590	5.0	7.0	10.1†	1.5	3.8	4.6	5.7	7.3	1.30	1.57	0.21	T	7.6
338.1 -0.2	300	600	8.2	8.2	15.0†	1.5	2.4	5.3	6.7	6.3	1.30	0.91	0.13	-	5.5
338.2 +0.4	40	310	2.6	5.7	2.3	0.3	0.4	4.0	6.2	0.8	1.00	0.45	0.22	NT	-
338.3 -0.1	300	770	6.0	5.5	12.5†	1.5	0.8	6.7	6.0	2.4	1.01	0.25	0.07	NT	-
338.4 +0.2	200	2030	5.0	7.0	34.8	1.0	8.6	5.7	7.3	26.3	1.02	1.03	0.11	-	-
338.4 -0.2	140	560	3.5	3.7	3.6	1.1	2.9	4.3	4.3	3.9	1.06	1.64	0.23	T	4.6
338.4 +0.0	200	2150	5.5	9.0	52.2	1.0	10.2	6.4	9.7	46.6	0.97	1.10	0.11	-	8.1
338.5 -0.3	100	400	3.1	3.1	1.9	0.6	1.0	4.3	4.0	1.3	1.00	0.89	0.22	-	-
338.5 +0.1	200	1950	5.5	7.0	36.8†	1.0	4.7	6.2	7.5	16.1	1.00	0.57	0.06	NT	-
338.7 +0.6	50	310	4.4	3.2	2.1	0.4	1.4	4.3	5.0	2.2	0.99	1.39	0.30	T	-
338.9 +0.6	50	770	4.7	4.7	8.3	0.5	5.0	5.1	5.3	9.9	1.05	1.73	0.21	T	8.4
338.9 -0.1	50	600	3.7	4.2	4.6	0.4	2.4	4.4	4.4	3.4	1.10	1.19	0.17	T	8.3
338.9 +0.4	50	330	3.8	5.0	3.1	0.6	1.1	4.4	5.1	1.8	1.11	0.94	0.23	-	-
340.3 -0.2	90	780	3.7	4.1	5.8	0.6	3.3	4.4	4.6	4.9	1.07	1.27	0.16	T	8.1
340.8 -1.0	0	700	2.8	3.0	2.8	0.6	7.8	4.0	4.0	9.4	1.00	4.30	0.51	T	6.3
340.9 -1.0	0	800	4.3	4.1	6.9	-	-	-	-	-	-	-	-	-	-
343.5 -0.0	80	1070	4.3	4.0	9.0	0.6	6.0	5.3	5.4	12.6	0.94	1.61	0.18	T	5.2
345.0 +1.5	160	360	5.3	9.3	8.7	0.8	2.1	8.0	12.0	14.8	0.77	1.36	0.24	T	5.3

† See footnote at end of table.

1970AuJPA..14..133S

(1)	(2)	(3)	(4)	(5)	(6)	(7)	(8)	(9)	(10)	(11)	(12)	(13)	(14)	(15)	(16)
	408 MHz Measured Parameters					5000 MHz Measured Parameters									
G Number	Base-level (^oK)	Peak Temp. T_{1p} (^oK)	Half-power Widths $M_{1\alpha}$ (min of arc)	$M_{1\delta}$	Flux Density S_1 (f.u.)	Base-level (^oK)	Peak Temp. T_{2p} (^oK)	Half-power Widths $M_{2\alpha}$ (min of arc)	$M_{2\delta}$	Flux Density S_2 (f.u.)	Widths Ratio C_1/C_2	Conv. Temps. T_2/T_1	Error in T_2/T_1	Nature of Source	Temp. Ratio T_L/T_C (%)
345.2 +1.0	90	1160	2.9	3.9	6.4	0.4	7.8	4.2	4.3	10.4	1.02	2.29	0.25	T	8.0
345.3 +1.5	150	1000	3.8	4.9	9.1	0.8	6.0	5.5	5.2	12.6	0.96	1.70	0.19	T	4.4
345.4 +1.4	150	1650	3.8	3.5	10.8	0.8	10.1	4.2	4.2	13.1	1.09	1.92	0.20	T	7.5
345.6 +1.5	70	490	3.0	3.1	2.2	0.4	1.3	4.2	4.0	1.6	1.01	0.97	0.19	-	-
348.7 -1.0	100	2600	3.8	4.4	21.3	1.0	23.5	4.3	4.5	33.4	1.13	2.64	0.27	T	7.4
351.1 +0.7	350	1390	8.8	8.3	49.8	0.7	11.0	8.0	7.4	47.9	1.17	1.72	0.18	T	-
351.2 +0.7	350	1990	4.4	4.4	18.9	0.7	11.3	5.3	5.1	22.5	1.01	1.58	0.16	T	-
351.2 +0.5	350	1140	5.6	5.5	17.2	0.7	8.6	5.9	5.6	20.9	1.08	1.87	0.20	T	-
351.4 +0.7	350	3250	7.3	10.3	119.8	0.8	30.8	7.5	9.3	158.0	1.09	2.07	0.21	T	6.6
351.6 +0.5	-	-	-	-	-	0.5	1.2	4.0	4.9	1.7	-	-	-	-	-
353.1 +0.4	-	-	-	-	-	1.0	6.5	10.0	7.9	37.8	-	-	-	-	5.0 N
353.1 +0.7	350	3090	7.6	5.5	63.3	1.2	31.8	6.8	7.0	111.3	1.02	2.42	0.24	T	5.2
353.2 +0.9	350	3750	7.0	4.0	51.5	1.2	46.8	5.5	4.6	87.1	1.17	3.22	0.32	T	4.7
5.9 -0.4	180	900	3.5	4.0	6.2	-	-	-	-	-	-	-	-	T	6.5 N
6.0 +0.0	300	620	11.0	3.4	11.4	-	-	-	-	-	-	-	-	NT	-
6.0 -1.2	100	2600	5.1	5.5	35.7	0.5	22.5	5.8	5.7	54.7	1.04	2.18	0.22	T	5.0 N
6.1 -0.1	450	400	5.4	12.2	12.9	-	-	-	-	-	-	-	-	T	12.1
6.2 +0.2	300	330	5.4	9.5	8.3	-	-	-	-	-	-	-	-	NT	-
6.3 -0.2	500	420	8.1	8.8	14.7	-	-	-	-	-	-	-	-	NT	-
6.4 -0.5	400	700	5.4	8.8	16.3	-	-	-	-	-	-	-	-	NT	-
6.5 +0.1	700	1000	6.7	4.2	13.8	-	-	-	-	-	-	-	-	NT	3.8
6.6 -0.3	600	1900	4.0	7.4	27.6	-	-	-	-	-	-	-	-	NT	-
6.6 -0.1	800	350	4.0	5.5	3.8	-	-	-	-	-	-	-	-	T	4.7
6.6 -0.6	300	330	4.1	7.5	5.0	-	-	-	-	-	-	-	-	NT	-
6.7 -0.3	1100	1200	5.4	6.0	19.1	-	-	-	-	-	-	-	-	NT	2.8

7.0	-0.3	250	650	5.5	7.4	13.0	-	-	-	-	-	-	-	-	-	5.2 N
9.9	-0.7	100	420	5.3	5.8	6.3	0.3	1.5	5.5	6.0	3.6	1.08	0.88	0.17	-	-
10.0	-0.3	220	310	5.5	6.5	5.4	0.4	0.2	6.3	7.1	0.8	0.99	0.18	0.16	NT	-
10.2	-0.3	200	3100	4.1	4.3	26.8	0.5	32.5	4.6	4.4	48.4	1.12	2.96	0.30	T	6.3
10.3	-0.2	300	1600	3.5	4.2	11.5	0.7	9.5	4.3	4.3	12.9	1.10	1.79	0.19	T	5.3 N
10.5	+0.0	-	-	-	-	-	0.5	1.4	4.1	4.3	1.8	-	-	-	-	-
10.6	-0.4	180	450	3.9	4.9	4.2	0.5	5.3	4.3	4.6	7.7	1.17	3.27	0.46	T	7.8 N
11.2	-0.3	100	4050	4.3	4.2	35.9	0.4	5.1	4.7	4.8	8.5	1.07	0.35	0.04	NT	LT 0.8 N
12.7	-0.2	140	860	5.6	6.5	15.3	0.7	4.9	5.0	6.8	12.2	1.16	1.36	0.16	T	-
12.8	-0.2	400	700	2.7	3.0	2.8	2.0	23.0	4.0	4.0	27.1	1.00	12.54	1.45	T	3.9 N
15.0	-0.7	250	6950	8.0	11.5	313.4	0.7	146.3	5.7	7.8	478.3	1.51	4.50	0.45	T	4.2
16.9	+0.7	70	1450	7.7	9.5	52.0	0.8	7.4	8.5	9.5	43.9	1.00	1.11	0.12	-	5.6 N
17.0	+0.9	70	1330	12.0	11.0	86.1	0.9	6.3	11.5	12.5	66.6	0.98	0.98	0.11	-	-
18.2	+1.9	100	320	9.5	9.5	14.2	0.8	1.4	8.9	8.5	7.8	1.13	0.93	0.20	-	-
18.3	+1.9	100	330	7.0	11.5	13.0	0.8	1.4	7.7	9.6	7.6	1.09	0.92	0.20	-	-
18.5	+1.9	80	450	17.0	10.0	37.5	0.7	2.0	22.3	15.0	49.2	0.73	0.91	0.15	-	13.1 N
18.7	+2.0	80	1070	4.0	4.0	8.4	1.0	5.5	5.0	4.6	9.3	1.01	1.46	0.16	T	-
18.9	+1.8	80	320	8.0	9.2	11.5	0.7	2.0	9.3	14.7	20.1	0.78	1.35	0.25	T	-
19.2	+2.2	-	-	-	-	-	0.2	0.9	4.2	4.7	1.3	-	-	-	-	-
21.8	-0.6	50	2250	11.3	5.7	71.0	0.3	3.2	10.5	6.5	16.1	1.01	0.31	0.04	NT	LT 1.1 N
21.9	-0.4	50	570	10.2	4.6	13.1	0.3	1.1	9.0	6.0	4.4	0.97	0.44	0.10	NT	-
22.7	-0.1	200	400	11.5	9.0	20.3	1.2	0.6	11.9	9.4	4.9	0.99	0.31	0.11	NT	-
22.8	-0.5	150	510	4.0	4.1	4.1	0.9	2.1	4.4	4.2	2.9	1.12	1.15	0.18	-	-
22.8	-0.2	460	240	4.7	5.0	2.8	2.0	1.0	5.3	5.3	2.1	1.04	1.06	0.30	-	3.6 N
22.9	-0.1	220	480	2.7	3.2	2.0	1.2	0.4	4.0	4.0	0.5*	1.00	0.30	0.15	NT	-
23.1	-0.2	250	1350	5.0	11.5	38.1	1.5	1.2	7.3	10.0	6.4	0.93	0.21	0.04	NT	LT 1.6 N
23.1	+0.6	50	300	4.8	4.8	3.4	-	-	-	-	-	-	-	-	-	-
23.3	-0.3	250	720	7.0	7.0	17.3	1.5	1.7	7.3	4.7	4.3	1.34	0.53	0.09	NT	-
23.4	-0.2	550	900	4.5	4.0	7.9	1.5	5.4	4.6	4.5	8.2	1.08	1.62	0.19	T	6.1 N
23.6	-0.0	220	530	6.8	7.1	12.5	1.3	2.1	7.2	6.9	7.7	1.05	0.89	0.14	-	-
23.6	+0.3	150	400	8.1	6.5	10.3	1.2	1.0	13.5	7.5	7.4	0.78	0.55	0.14	NT	-
23.7	+0.2	150	300	2.7	3.3	1.3	1.2	1.6	4.0	4.0	1.9	1.00	1.88	0.39	T	-
23.9	-0.1	200	250	3.5	6.4	2.7	1.0	0.8	4.5	4.5	1.2	1.18	0.87	0.27	-	-
24.0	+0.2	100	200	2.8	3.4	0.9	0.9	2.1	4.0	4.0	2.5	1.03	3.60	0.88	T	-
24.2	+0.6	0	400	2.6	3.4	1.7	-	-	-	-	-	-	-	-	NT	-

* See footnote at end of table.

1970AuJPA..14..133S

(1)	(2)	(3)	(4)	(5)	(6)	(7)	(8)	(9)	(10)	(11)	(12)	(13)	(14)	(15)	(16)
	408 MHz Measured Parameters					5000 MHz Measured Parameters									
G Number	Base-level (^{o}K)	Peak Temp. T_{1p} (^{o}K)	Half-power Widths $M_{1\alpha}$ (min of arc)	$M_{1\delta}$	Flux Density S_1 (f.u.)	Base-level (^{o}K)	Peak Temp. T_{2p} (^{o}K)	Half-power Widths $M_{2\alpha}$ (min of arc)	$M_{2\delta}$	Flux Density S_2 (f.u.)	Widths Ratio C_1/C_2	Conv. Temps. T_2/T_1	Error in T_2/T_1	Nature of Source	Temp. Ratio T_L/T_C (%)
24.4 +0.1	230	340	4.3	4.8	3.4	-	-	-	-	-	-	-	-	-	-
24.5 +0.2	150	750	5.7	5.8	12.2	-	-	-	-	-	-	-	-	NT	-
24.5 +0.5	50	700	2.9	3.4	3.4	-	-	-	-	-	-	-	-	-	-
24.5 -0.2	230	590	3.9	4.6	5.2	-	-	-	-	-	-	-	-	-	7.3 N
24.7 +0.6	70	370	11.5	9.0	18.8	-	-	-	-	-	-	-	-	NT	-
24.7 -0.2	180	520	3.7	5.0	4.7	-	-	-	-	-	-	-	-	-	-
24.8 +0.1	180	670	4.9	6.8	10.9	-	-	-	-	-	-	-	-	-	6.3 N
25.3 -0.1	150	1050	2.8	3.3	4.8	0.8	0.4	4.0	4.0	0.5*	1.00	0.13	0.07	NT	-
25.3 +0.3	250	200	5.2	8.0	4.1	0.8	0.7	5.8	7.4	2.2	1.07	0.82	0.30	-	-
25.4 -0.2	150	1550	3.8	5.0	14.4	0.8	11.7	4.9	4.9	20.7	1.04	2.05	0.21	T	4.2 N
25.4 +0.0	210	340	3.5	4.7	2.7	0.8	1.0	4.8	5.8	2.0	0.93	0.83	0.21	-	-
28.8 +3.5	0	1700	6.6	6.5	35.7	0.5	9.3	6.8	6.6	30.7	1.04	1.23	0.13	T	4.4 N
29.7 -0.2	50	2650	3.0	3.7	14.4	-	-	-	-	-	-	-	-	NT	-
29.9 -0.0	80	1220	5.0	5.6	16.7	0.8	8.6	5.1	5.1	16.4	1.15	1.70	0.18	T	5.0 N
30.2 -0.1	200	430	3.8	5.1	4.1	1.4	1.7	4.2	4.6	2.4	1.17	1.05	0.19	-	15.0 N
30.4 -0.2	200	420	4.5	6.1	5.7	1.5	1.8	6.5	5.4	4.6	0.99	1.05	0.19	-	-
30.5 -0.3	100	280	7.1	7.3	7.1	1.1	1.5	9.7	6.1	6.5	1.01	1.18	0.26	-	-
30.6 +0.0	250	290	3.9	5.2	2.9	1.8	1.3	4.0	4.7	1.8	1.21	1.18	0.27	-	-
30.7 -0.3	200	440	4.2	5.5	5.0	1.6	2.2	4.7	5.2	4.0	1.11	1.27	0.21	T	-
30.8 -0.0	180	3120	6.1	6.5	60.6	1.4	36.2	5.8	5.6	86.5	1.19	2.64	0.27	T	5.0
31.1 +0.1	-	-	-	-	-	1.5	1.8	6.0	5.5	4.4	-	-	-	-	6.9 N
31.1 +0.5	-	-	-	-	-	0.8	1.0	4.2	4.3	1.3	-	-	-	-	-
35.1 -1.5	0	240	4.8	7.8	4.4	0.5	1.3	7.5	6.0	4.3	0.99	1.27	0.32	-	-
35.2 -1.8	0	1360	2.9	4.1	7.9	0.3	12.5	4.1	4.1	15.5	1.03	2.77	0.29	T	5.0 N
35.4 -1.8	0	370	5.0	7.6	6.9	0.2	1.3	5.8	5.3	3.0	1.20	0.84	0.18	-	-

1970AuJPA..14..133S

37.4	-0.2	100	260	2.7	3.8	1.3	-	-	-	-	-	-	-	-	NT	-
37.5	-0.1	100	300	6.4	6.0	5.6	0.5	1.8	6.3	6.1	5.1	1.06	1.33	0.27	T	6.6 N
37.7	+0.1	70	270	7.8	5.6	5.8	0.4	1.3	6.7	6.1	3.9	1.07	1.04	0.24	-	-
37.8	-0.2	100	530	3.8	4.8	4.7	0.5	2.9	5.3	4.8	5.4	0.97	1.41	0.20	T	-
37.9	-0.4	100	330	6.0	6.4	6.2	0.5	4.1	4.9	4.6	6.8	1.39	2.77	0.46	T	5.6 N
39.2	-0.3	130	2070	4.8	6.4	31.2	-	-	-	-	-	-	-	-	NT	LT 1.1 N
39.3	-0.0	130	270	3.8	5.9	3.0	-	-	-	-	-	-	-	-	-	-
39.4	-0.6	50	300	2.7	4.1	1.6	-	-	-	-	-	-	-	-	NT	-
43.2	-0.0	100	2140	5.2	4.6	25.1	0.3	33.7	4.9	4.6	55.9	1.07	3.51	0.36	T	4.3
43.3	-0.2	100	5550	4.9	4.4	58.7	0.3	9.7	5.1	4.6	16.7	1.00	0.40	0.04	NT	LT 1.9 N
45.1	+0.1	0	420	3.2	4.6	3.0	-	-	-	-	-	-	-	-	-	-
45.5	+0.1	0	850	3.1	4.7	6.1	0.3	6.7	4.3	4.3	9.1	1.02	2.04	0.23	T	LT 1.1 N
48.6	+0.0	230	1120	3.8	5.3	11.1	0.5	4.3	5.2	5.8	9.5	0.89	0.90	0.10	-	5.2
48.6	+0.2	-	-	-	-	-	0.8	1.0	5.8	5.1	2.2	-	-	-	-	-
49.0	-0.3	630	1520	5.1	12.2	46.4	3.0	9.4	5.5	9.0	34.2	1.18	1.37	0.14	T	5.4
49.0	-0.6	100	1170	23.0	13.0	171.5	0.5	4.0	23.0	13.0	87.9	1.00	0.67	0.08	NT	-
49.1	-0.4	840	1140	5.4	7.3	22.0	4.0	5.2	5.7	6.9	15.0	1.05	0.98	0.11	-	5.6
49.2	-0.3	1270	1150	3.0	4.6	7.9	4.0	10.4	4.2	4.2	13.7	0.99	2.24	0.24	T	5.8
49.2	-0.7	100	960	11.0	14.0	72.5	0.5	3.8	12.0	15.0	50.3	0.94	0.80	0.10	NT	LT 0.1
49.2	-1.0	100	660	2.7	4.4	3.8	0.5	0.2	4.0	4.0	0.3*	1.00	0.09	0.08	NT	-
49.4	-0.3	150	1840	4.2	6.0	22.7	1.0	18.0	5.3	5.3	37.2	1.01	2.19	0.23	T	4.8
49.5	-0.4	150	2620	6.0	6.9	53.2	1.0	62.5	5.0	5.0	114.9	1.33	4.85	0.49	T	4.9

* Flux density at 5000 MHz is an upper limit.

† Parameters measured at 408 MHz have been corrected for contaminating effects of side lobes.

TABLE 2

Flux Densities from Other References

G Number	Frequency ν (MHz)	Flux Density S_ν (f.u.)	Spectral Index* α	Ref.†	G Number	Frequency ν (MHz)	Flux Density S_ν (f.u.)	Spectral Index* α	Ref.†
207.1−1.3	2650	⩽0.5	⩽−1.05	1	5.9−0.4	5000	23.3	+0.53	10
287.4−0.6	5000	125	NS	2	7.0−0.3	5000	13.3	NS	10
287.6−0.6	5000	103	NS	2	10.5+0.0	2650	1.5	NS	11
287.7−1.3	2650	⩽1.0	⩽−0.60	3	19.2+2.2	2650	1.5	NS	11
290.1−0.8	5000	24	−0.56	4	23.1+0.6	5000	4	NS	4
290.4−0.9	2650	⩽1.2	⩽−0.19	5	24.2+0.6	2650	⩽0.6	⩽−0.56	11
290.6−1.2	2650	~1.5	NS	5	24.4+0.1	2650	3.0	NS	11
298.2−0.8	2650	2.4	NS	5	24.5+0.2	2650	8.0	−0.22	11
316.2+0.0	2650	15	−0.47	6	24.5+0.5	2650	3.7	NS	11
316.3−0.0					24.5−0.2	2650	5.0	NS	11
316.4−0.4	2650	3.0	NS	6	24.7+0.6	2650	9.0	−0.38	11
319.9+0.8	2650	1.2	−0.15	6	24.7−0.2	2650	5.5	NS	11
320.2−1.4	2650	13	−0.65	6	24.8+0.1	2650	10.5	NS	11
320.3−1.4					29.7−0.2	2650	4.7	−0.60	12
320.4−1.4					31.1+0.1	2650	4.0	NS	12
320.5−1.0	2650	3.5	−0.45	6	31.1+0.5	2650	1.3	NS	12
324.2+0.2	2650	~5	NS	6	37.4−0.2	2650	0.9	⩽−0.20	12
332.0+0.2	2650	6.2	−0.44	7	39.2−0.3	10630	7.5	−0.44	13
332.0+0.1					39.3−0.0	10630	3.6	NS	13
337.5−0.3	408	~6	NS	8	39.4−0.6	3240	⩽0.35	⩽−0.74	13
351.5+0.5	2650	1.5	NS	9	45.1+0.1	2650	~5	NS	14
353.1+0.4	408	38	NS	8	48.6+0.2	611	~2	NS	15

* The spectral indices were computed by comparing the flux density values in this table with those available in Table 1 or sometimes in Parts I and II. NS indicates that the values are not significantly different from zero.

† References are: 1, Hill (1967); 2, Gardner and Morimoto (1968); 3, Beard and Kerr (1966); 4, Milne (1969); 5, Thomas and Day (1969*a*); 6, Day, Thomas, and Goss (1969); 7, Beard (1966); 8, Present work, unpublished observations; 9, Beard, Thomas, and Day (1969); 10, Reifenstein *et al.* (1970); 11, Goss and Day (1970); 12, Beard and Kerr (1969); 13, Hughes and Butler (1969); 14, Day, Warne, and Cooke (1970); 15, Terzian and Balick (1969).

The two ratios C_1/C_2 and T_2/T_1 are listed in columns 12 and 13 of Table 1, and in column 14 the estimated standard error is given for T_2/T_1. Figure 1 shows C_1/C_2 plotted against T_2/T_1 for sources with $T_{1p} > 1000°$K (this limitation is set in order to eliminate sources for which baselevel errors would have a large effect on the measured widths and peak temperatures). As expected, $C_1/C_2 \sim 1$ for $T_2/T_1 < 1$, and C_1/C_2 increases with $T_2/T_1 > 1$ (especially for the well-resolved sources).

Conclusions regarding the nature of the sources, as determined from the values of T_2/T_1, are summarized in column 15 of Table 1. An entry "T" means that the source is thermal, "NT" that the source is nonthermal, and "C" that both thermal and nonthermal components are known to be present in the source. A dash in column 15 signifies that T_2/T_1 is within one standard error of unity, and the nature of this flat-spectrum source cannot be determined from the radio continuum observations. For some of the sources in Table 1 data are not available at one of the two observing

frequencies, 408 or 5000 MHz. In these cases other references have been used to determine the spectral indices. The references used and the resulting spectral indices are given in Table 2 and the conclusions are again summarized in column 15 of Table 1. In some cases more details can be found in the Appendix.

The last column (16) in Table 1 lists the line-to-continuum temperature ratios from the H109α recombination line and 5000 MHz continuum surveys. Whenever possible the southern H109α line survey (Wilson *et al.* 1970) has been used throughout this paper, but for sources not covered by that survey the results of the northern H109α line survey (Reifenstein *et al.* 1970) have been used where available. The southern and northern H109α line surveys were made with beamwidths of 4′ and 6′ arc respectively.

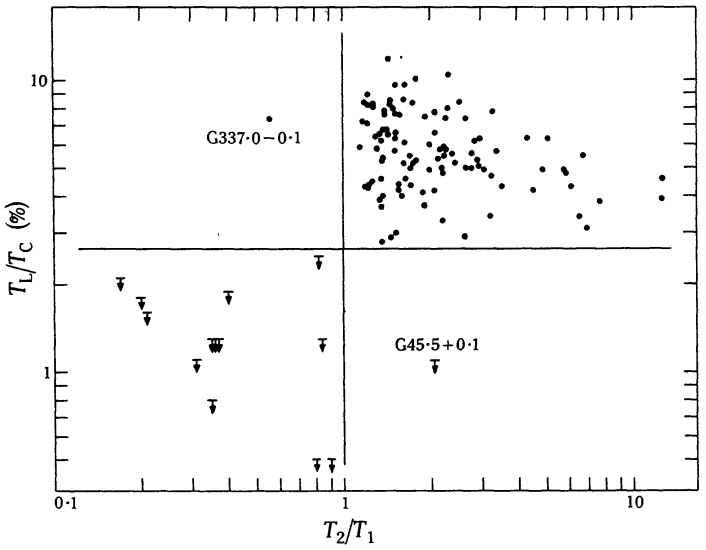

Fig. 2.—Relation between the H109α line-to-continuum temperature ratios and the ratio T_2/T_1, which is related to the spectral index α by equation (7).

In Table 1 the symbol "LT" preceding a value of T_L/T_C means "less than", and "N" following a value of T_L/T_C signifies that the H109α line observation was made in the northern survey. A dash indicates that no H109α line observations have been made for the source.

In Figure 2, T_L/T_C is plotted against T_2/T_1 for all cases in which entries other than dashes have been made in columns 13, 15, and 16 of Table 1. It is obvious that for thermal sources $T_L/T_C > 2.5\%$ and that no recombination lines above the detectable threshold are found in nonthermal sources. There are only two cases in Figure 2 which do not satisfy these conditions: G337.0–0.1 and G45.5+0.1. The former is known to contain both a thermal and a nonthermal component (see Appendix) and is therefore easily explained. The latter, however, remains a puzzle. From the radio continuum observations it appears to be a thermal source with turnover frequency ~ 1000 MHz; but if it is thermal, the H109α line upper limit imposes a lower limit on the electron temperature of ~ 14,000°K. The case of G45.5+0.1 is discussed in more detail in the Appendix.

Clearly the most accurate method of determining the thermal or nonthermal nature of galactic radio sources is to use values of T_2/T_1 over a wide frequency range obtained from observations with very high resolution and sensitivity. Lacking this, it is clear from Figure 2 that observations of recombination lines provide a reliable substitute. Milne *et al.* (1969) have arrived at similar conclusions using a number of selected galactic radio sources.

The ratio T_2/T_1 is related to the spectral index α ($S \propto \nu^{\alpha}$) of the source averaged over a 4′ arc beam by the equation

$$\alpha = \log(T_2/T_1)/\log(\nu_2/\nu_1) - 0.1 \ . \qquad (7)$$

Spectral indices have been computed in all possible cases and they are plotted in the histogram in Figure 3(*a*). There are two major peaks, at $\alpha \approx 0$ and -0.5.

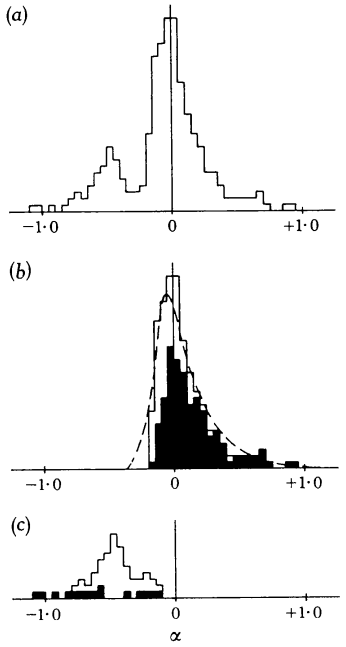

Fig. 3.—Frequency distribution of spectral indices α for
(*a*) all sources;
(*b*) thermal sources;
(*c*) nonthermal sources.
The open histogram in (*b*) represents all thermal sources, and the solid histogram represents all sources (except G337.0−0.1) in which the H109α line has been found. The dashed line is described in the text. The open histogram in (*c*) represents all nonthermal sources and the solid squares denote sources believed to be extragalactic.

The solid histogram in Figure 3(*b*) represents all the sources (except G337.0−0.1) in which the H109α line has been found. From Figure 2 we can conclude that these are all thermal. For the most part the peak at $\alpha \approx 0$ is not as pronounced in the filled histogram as in Figure 3(*a*) simply because many of these flat-spectrum sources were not strong enough to satisfy the H109α line survey selection criterion ($T_p \geqslant 2°K$) and line observations were not attempted. There are only two cases in which no lines were found in H109α observations of sources with flat spectra. Both of these sources are very weak, and one of them (G284.6−0.2) is known to be thermal from optical observations (see Appendix).

For the purposes of this paper, all sources that have flat spectra (indicated in column 15 of Table 1 by a dash) will be considered to be thermal. These sources are represented along with those known to be thermal (a"T" is shown in column 15) in the open histogram in Figure 3(*b*).

Evolutionary models of HII regions predict that the size increases with time and the density and emission measure decrease. Therefore we expect to find that at $\alpha = -0.1$ the number of thermal sources is a maximum, and that at higher α the number of thermal sources decreases steadily. If the real distribution of spectral indices for the thermal sources has the form

$$AH(\alpha+0.1)\ H(-\alpha+2.0)\ \exp[-B(\alpha+0.1)] \ ,$$

where A and B are constants and $H(x)$ is the Heaviside unit step function, we can predict the shape of the observed distribution by convolving that exponential curve

with a Gaussian curve of $\sigma \approx 0.10$ which represents the error in the spectral index for the flat-spectrum sources obtained from column 14 of Table 1. This expected distribution is shown as a dashed line in Figure 3(*b*), and is seen to match the observed distribution very well. In particular, it explains why the peak of the observed distribution is displaced from $\alpha = -0.1$. However, there is a discrepancy at the low end of the distribution, suggesting that a few thermal sources may have been taken to be nonthermal (see below). It should be noted that for positive spectral indices especially the shape of the distribution depends on the degree of resolution of the sources, because the spectral index varies across thermal sources.

The open histogram in Figure 3(*c*) represents all the sources registered as nonthermal in column 15 of Table 1. The solid squares denote sources believed to be extragalactic for reasons discussed below. The distribution of spectral indices for the galactic nonthermal sources can be represented satisfactorily by a Poisson distribution with an average value of $\alpha \approx -0.5$. The upper wing of the histogram is somewhat bigger than the lower wing, suggesting again that some thermal sources may have been wrongly classified as nonthermal; but a more serious error in classification stems from assuming that all flat-spectrum sources are thermal. The net result of this trade-off is likely to be that the proportion of sources classified as nonthermal is underestimated.

Earlier work (Altenhoff 1968; Kesteven 1968*a*) had suggested that there are about twice as many thermal as nonthermal sources in the Galaxy. However, the number of sources in Figure 3(*b*) is about three times the number in Figure 3(*c*), and when the extragalactic nonthermal sources are removed the ratio is more like four to one. It is shown in Sections IV and V that often several of the nonthermal sources in Table 1 actually comprise a single supernova remnant, whereas most of the thermal sources in Table 1 are individual HII regions; when this is taken into account the actual number of HII regions is about seven times the number of supernova remnants. There are several reasons for the difference between this and earlier results. First of all, the method used above in drawing the line between thermal and nonthermal sources is likely to favour thermal sources. Secondly, the selection of sources to be observed was biased in favour of thermal sources; for example, in the southern Milky Way, only regions around the sources observed in the H109α line survey (Wilson *et al.* 1970) were mapped. Finally, it is shown below that HII regions tend to cluster together. Therefore the high resolution observations used here have found many more HII regions than earlier observations with poorer resolution, even though the sensitivities may be equivalent.

III. OPTICAL IDENTIFICATIONS

A search has been made for optical features in all the areas observed in Parts I and II. The Palomar Sky Atlas, along with the Whiteoak and Matthews extensions, was used for regions north of -48° declination. For more southerly regions, Hα plates taken recently by G. Lyngå (personal communication) with the Uppsala Schmidt telescope at Mount Stromlo Observatory were generally used.

Positive identifications resulting from this search are described for individual cases in Table 3. Sixteen of the identifications are illustrated in Figure 4, which shows radioisophotes superimposed on the optical photographs. In Figures 4(*e*) and 4(*i*) (RCW 48, 49 and RCW 57) the positions of OH sources (Manchester, Robinson, and Goss 1970) are indicated.

TABLE 3

Optical Identifications

G Number	Figure Number	Optical Identification
206.0−1.7 206.0−2.1 206.2−2.3 206.6−1.7	4(*a*)	Rosette Nebula, NGC 2237−46
206.5−16.4	–	NGC 2024
208.5−19.2	4(*b*)	NGC 1973,5,7
208.9−19.3	4(*b*)	NGC 1982
209.0−19.4	4(*b*)	Orion Nebula, NGC 1976
265.1+1.5	4(*c*)	RCW 36
267.8−0.9 268.0−1.1 268.1−1.0	4(*d*)	RCW 38
282.0−1.2	–	RCW 46 is about 30′ away from G282.0−1.2; it is faint and quite extended, and is not likely associated with the radio source
283.5−1.0	4(*e*)	RCW 48, NGC 3199
284.0−1.0	4(*e*)	Weak nebulosity spread about the area
284.3−0.3	4(*e*)	RCW 49, NGC 3247
284.6−0.2	4(*e*)	Well-defined crescent, matching shape of radio contours
284.6−0.5	4(*e*)	Faint nebulosity
285.3−0.0	4(*f*)	Small bright knot outlying Carina Nebula
287.4−0.6 287.6−0.6 287.8−0.8 287.9−1.0 288.0−0.8	4(*g*)	Carina Nebula, RCW 53, NGC 3372
289.8−1.2	4(*h*)	Extended faint nebulosity, matching shape of radio contours
289.9−0.8	4(*h*)	A few small, fairly bright knots of emission
291.1−0.8	4(*i*)	Small nebulosity (~ 3′ diameter)
291.2−0.3	4(*i*)	Faint nebulosity, perhaps associated with cluster NGC 3590 (Sher 1965*a*)
291.3−0.7	4(*i*)	NGC 3576
291.5−0.1	4(*i*)	Faint nebulosity
291.6−0.5	4(*i*)	NGC 3603. The nominal position of RCW 57 coincides with G291.6−0.5, but RCW 57 actually includes both NGC 3576 and 3603
291.9−0.7	4(*i*)	Knot of emission ~ 2′ diameter
295.1−1.7	4(*j*)	λ Cen Nebula, RCW 62, IC 2944
301.0+1.2	–	RCW 65
301.1+1.0	–	RCW 66
305.1+0.1 305.2+0.0	–	RCW 74 appears to be faint foreground emission and may not be associated with the radio sources
308.6+0.6	–	RCW 79
320.2+0.8	–	RCW 87
320.4−1.0	–	RCW 89. Nebulosity with matted appearance ~ 6′ diameter. No such nebulosity was found at the positions of G320.2−1.4, G320.3−1.4, G320.4−1.4, or G320.5−1.0
321.0−0.5 321.1−0.5	–	RCW 91
322.2+0.6	–	RCW 92. Faint nebulosity. No concentration visible at radio peak

TABLE 3 (*Continued*)

G Number	Figure Number	Optical Identification
326.2+0.7	–	RCW 94
326.4+0.9	–	Appears to be associated with a faint nebula ~ ½′ diameter
326.6+0.6	–	Four main concentrations of nebulosity surrounded by extended faint emission. RCW 95 is ~ 15′ north-west of G326.6+0.6 and only weak radio emission has been found
327.3–0.6	–	RCW 97
332.4–0.4	–	RCW 103
332.7–0.6 332.8–0.8 332.8–0.6 333.0–0.6	–	RCW 106. Extended faint nebulosity with a bright knot near G332.7–0.6
336.5–1.5	4(*k*)	RCW 108. The radio source is located on a long sharply defined bright rim in RCW 108
336.4–0.2 336.4–0.3 336.5–0.2	–	RCW 107, NGC 6164. Located near the radio sources and may be associated. Considerable obscuration in the area
340.8–1.0 340.9–1.0	–	Small optical nebula ~ 5′ diameter, with bright knot near G340.9–1.0. RCW 110 and 111 are ~ 10′ to the north
345.0+1.5 345.2+1.0 345.3+1.5 345.4+1.4 345.6+1.5	4(*l*)	Large, bright emission complex
348.7–1.0	–	RCW 122. Faint optical emission but region heavily obscured
351.1+0.7 351.2+0.7 351.2+0.5 351.4+0.7	–	RCW 127, NGC 6334
353.1+0.4 353.1+0.7 353.2+0.9	–	RCW 131, NGC 6357
6.0–1.2	4(*m*)	Lagoon Nebula, RCW 146, M8
6.5+0.1 6.6–0.3 6.7–0.3	–	Faint nebulosity with matted appearance. Maximum dimension ~ 30′
7.0–0.3	–	Trifid Nebula, RCW 147, M20
15.0–0.7	–	Omega Nebula, RCW 160, M17
16.9+0.7 17.0+0.9	4(*n*)	RCW 165, M16
18.2+1.9 18.3+1.9 18.5+1.9 18.7+2.0 18.9+1.8	4(*o*)	RCW 167, NGC 6604. Small bright nebulosity at G18.7+2.0
23.1+0.6	–	RCW 171. Faint nebulosity ~ 5′ diameter
24.5–0.2	–	RCW 172. The radio source is located at the western edge of a faint extended region ~ 10′ diameter
25.3+0.3	–	RCW 173. The radio source is located at the western edge of a faint extended region 10′ diameter
28.8+3.5	4(*p*)	Extended weak emission in a region of heavy obscuration

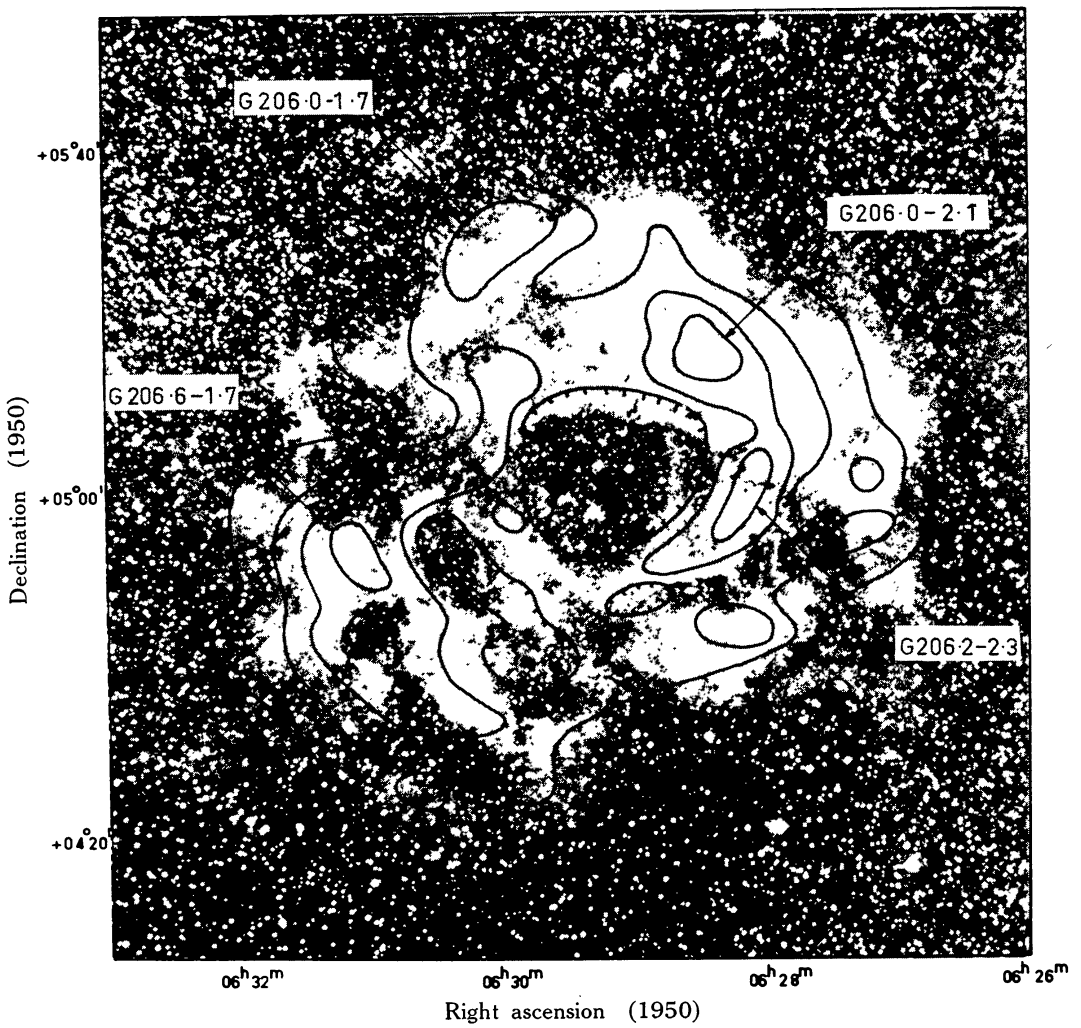

Figs 4(*a*)–4(*p*).–Radio-isophotes from Parts I and II superimposed on optical photographs of HII regions:
(*a*) Rosette Nebula. 408 MHz contours are shown superimposed on an Hα 48 in. Schmidt photograph (California Institute of Technology and Carnegie Institution of Washington).

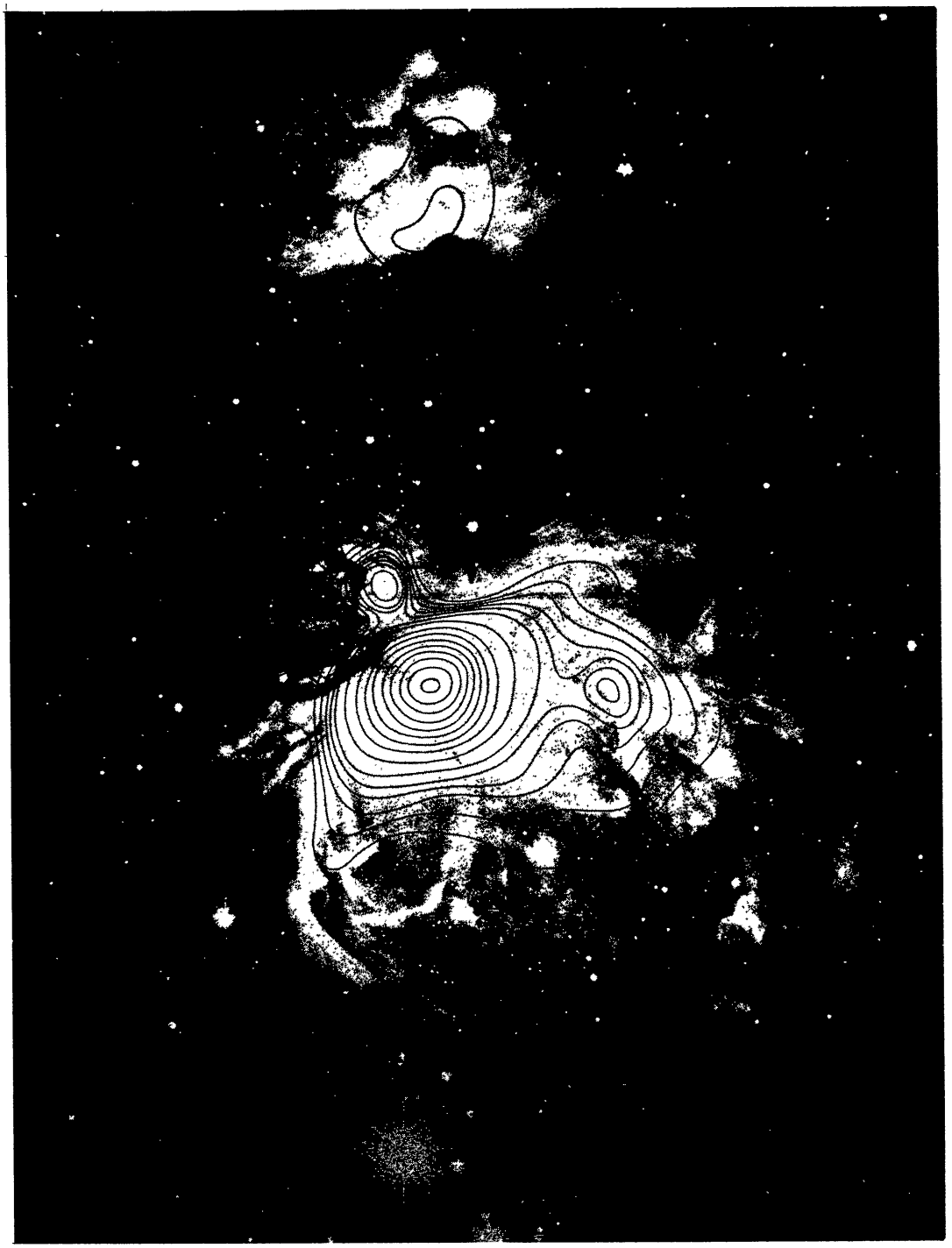

Fig. 4(*b*).–Orion Nebula. 408 MHz contours are shown for NGC 1976 and 1982, and 5000 MHz contours are shown for NGC 1973, 1975, and 1977 (Lick Observatory photograph).

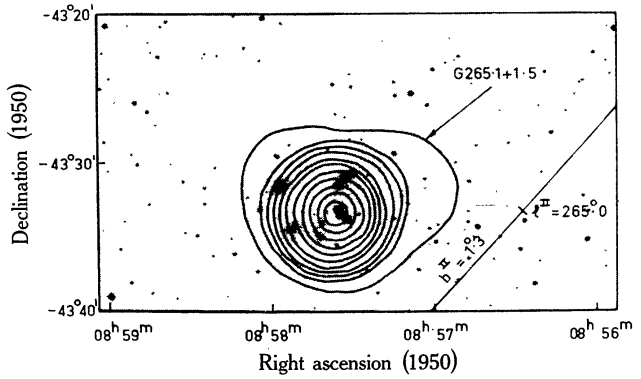

Fig. 4(*c*).–RCW 36. 5000 MHz contours are shown superimposed on a photograph taken from the Whiteoak extension of the Palomar Sky Survey.

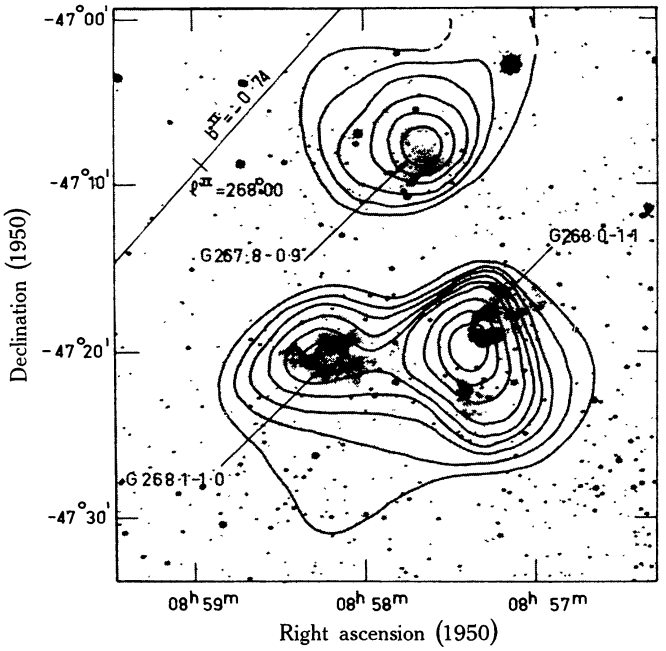

Fig. 4(*d*).–RCW 38. 408 MHz contours are shown superimposed on an Hα photograph taken by G. Lyngå with the 20/26 in. Uppsala Schmidt telescope at Mount Stromlo Observatory.

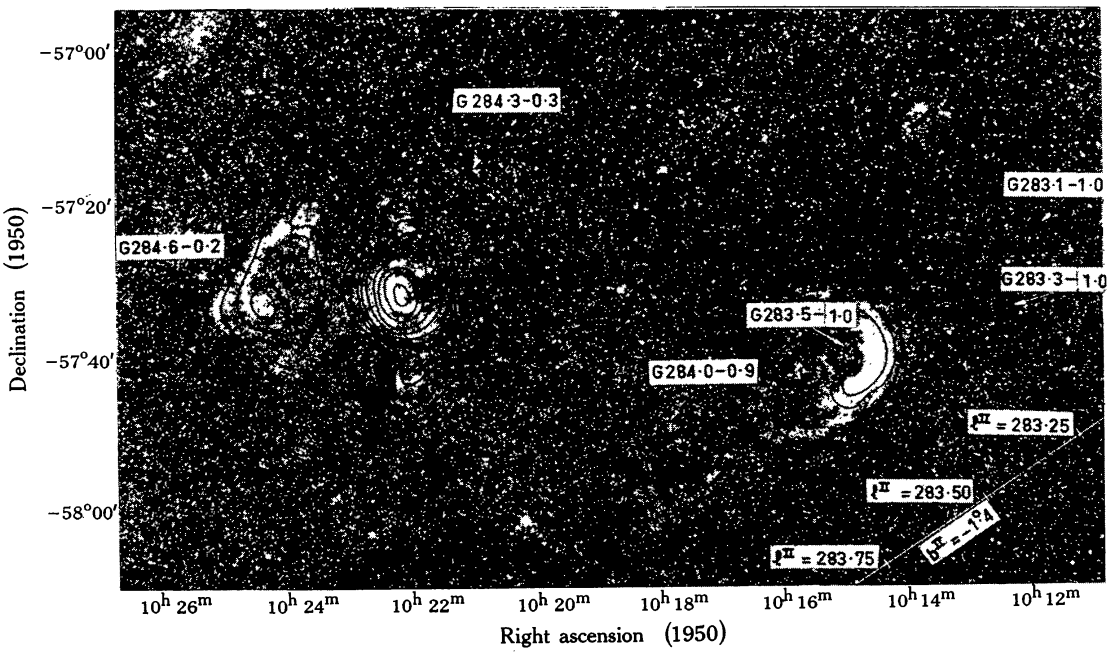

Fig. 4(*e*).—RCW 48, 49. 5000 MHz contours are shown superimposed on an Hα photograph taken by G. Lyngå with the 20/26 in. Uppsala Schmidt telescope at Mount Stromlo Observatory. The OH emission source G284.2−0.8 is indicated by a cross (Manchester, Robinson, and Goss 1970).

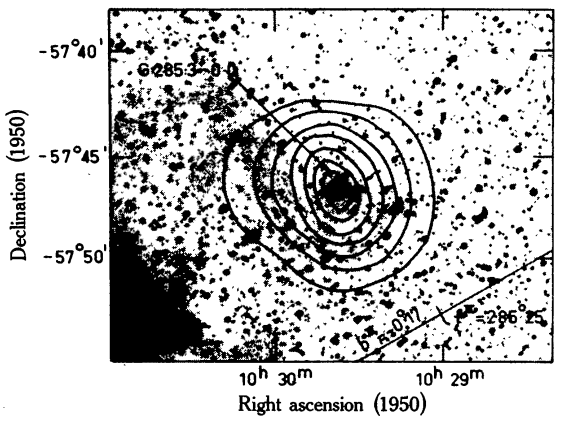

Fig. 4(*f*).—G285.3−0.0. 408 MHz contours are shown superimposed on an Hα photograph taken by G. Lyngå with the 20/26 in. Uppsala Schmidt telescope at Mount Stromlo Observatory.

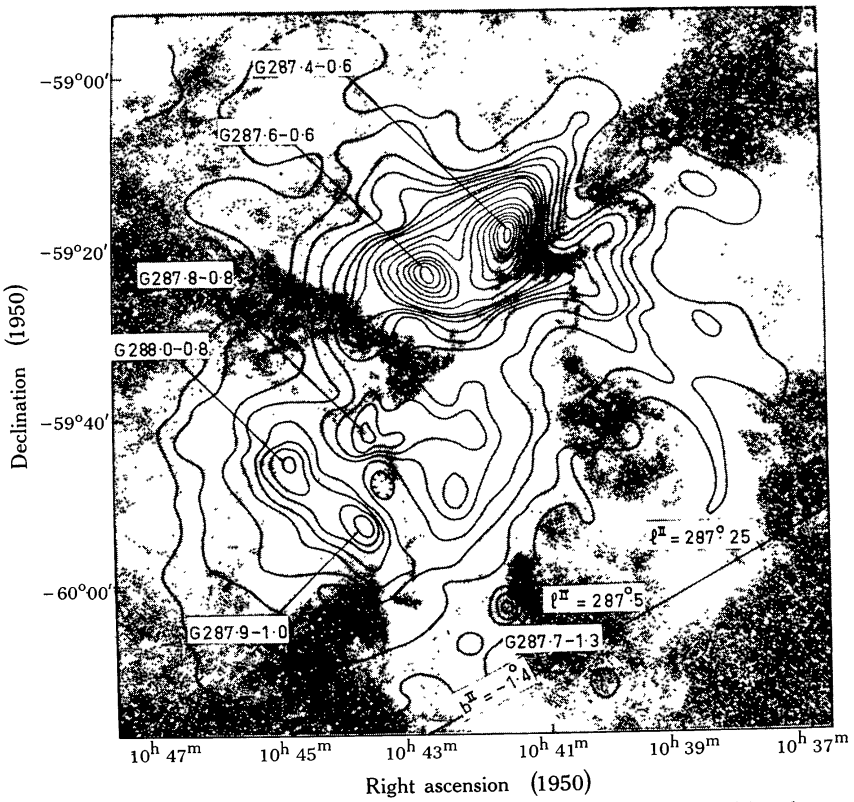

Fig. 4(*g*).–Carina Nebula. 408 MHz contours are shown superimposed on an Hα photograph taken by D. Faulkner with the 20/26 in. Uppsala Schmidt telescope at Mount Stromlo Observatory.

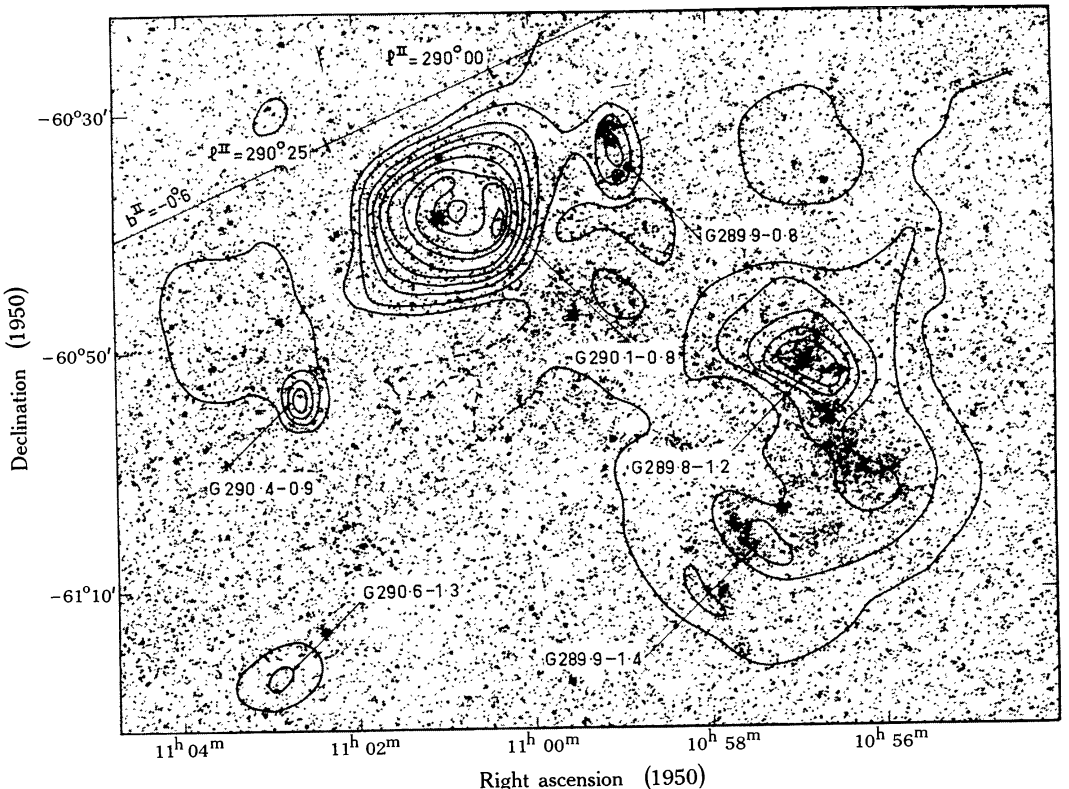

Fig. 4(*h*).–G289.8–1.2. 408 MHz contours are shown superimposed on an Hα photograph taken by G. Lyngå with the 20/26 in. Uppsala Schmidt telescope at Mount Stromlo Observatory.

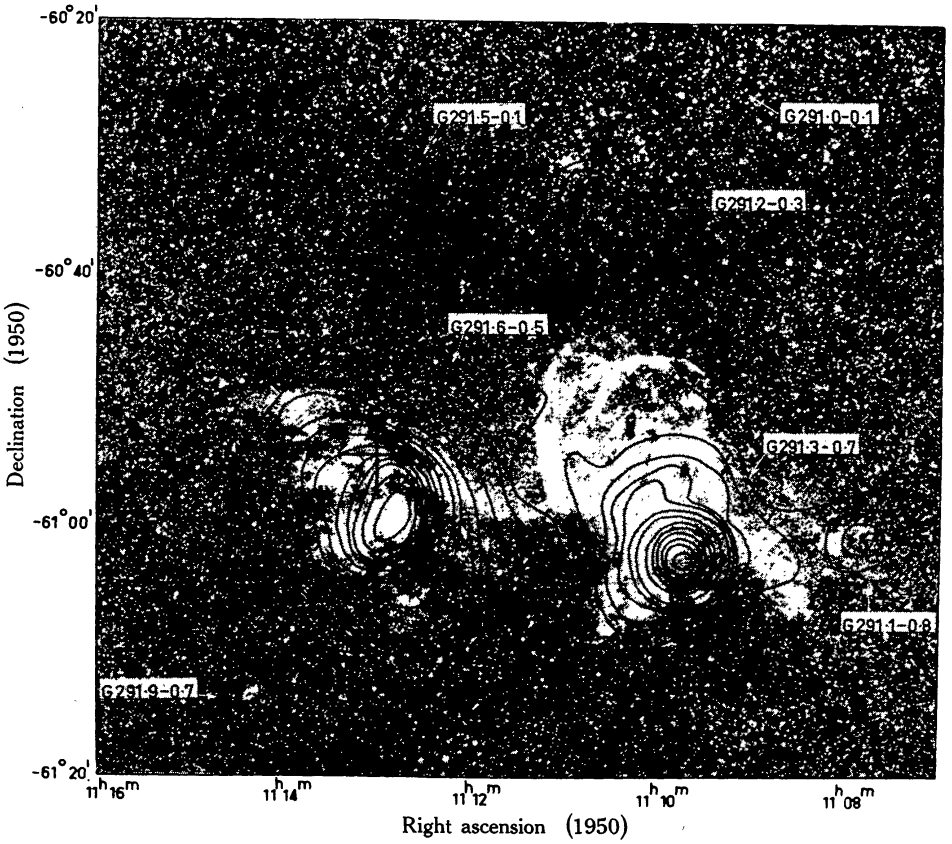

Fig. 4(*i*).—RCW 57. 5000 MHz contours are shown superimposed on an Hα photograph taken by G. Lyngå with the 20/26 in. Uppsala Schmidt telescope at Mount Stromlo Observatory. The OH emission source associated with G291.6−0.5 is indicated by a cross (Manchester, Robinson, and Goss 1970).

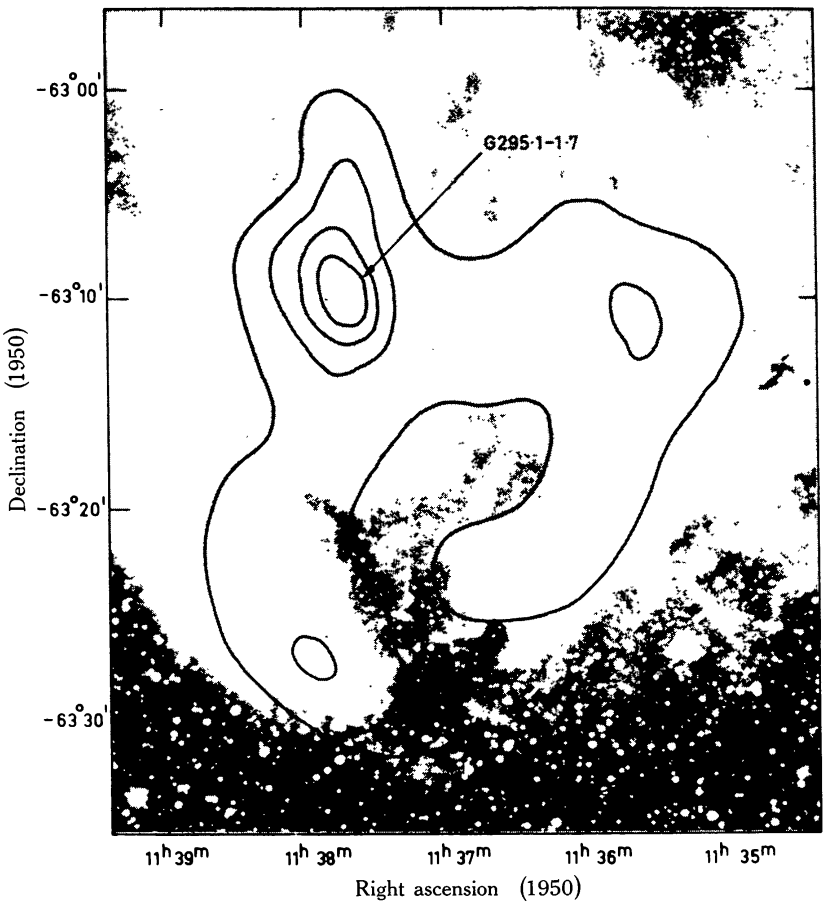

Fig. 4(*j*).–λ Cen Nebula. 408 MHz contours are shown superimposed on an Hα photograph taken by G. Lyngå with the 20/26 in. Uppsala Schmidt telescope at Mount Stromlo Observatory.

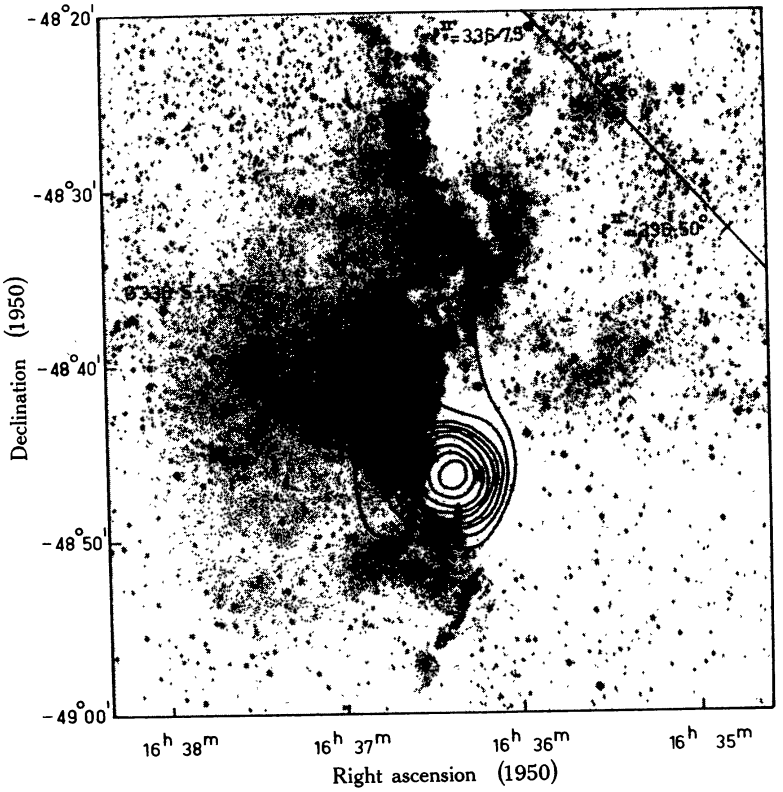

Fig. 4(*k*).–RCW 108. 5000 MHz contours are shown superimposed on a photograph taken from the Mathews extension of the Palomar Sky Survey.

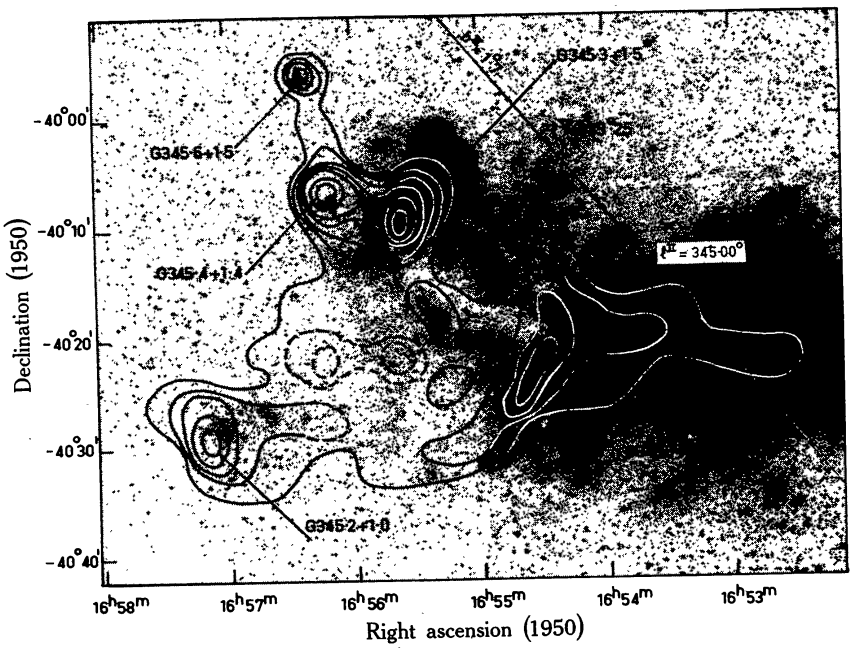

Fig. 4(*l*).–CTB 35. 408 MHz contours are shown superimposed on a photograph taken from the Whiteoak extension of the Palomar Sky Survey.

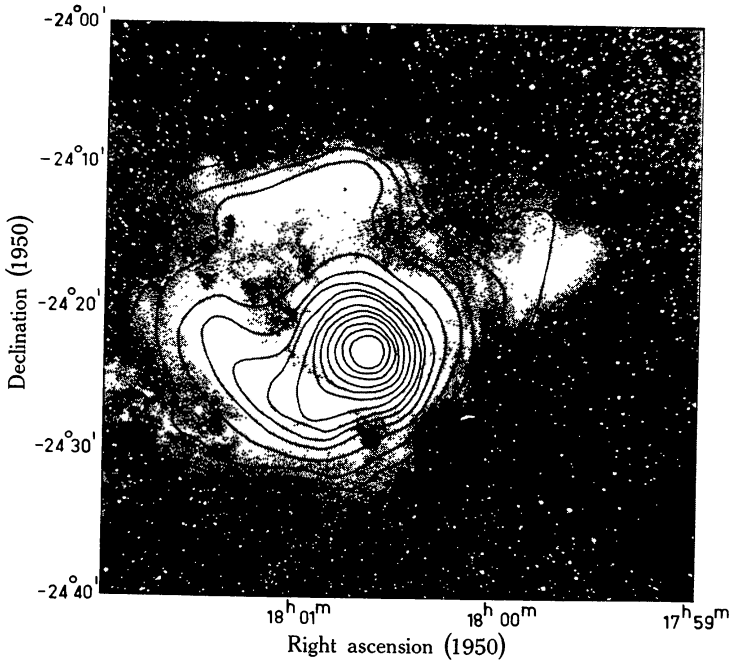

Fig. 4(*m*).—M8. 5000 MHz contours are shown superimposed on an Hα photograph taken by R. R. Shobbrook with the 74 in. reflector at Mount Stromlo Observatory, with the kind permission of Professor O. J. Eggen.

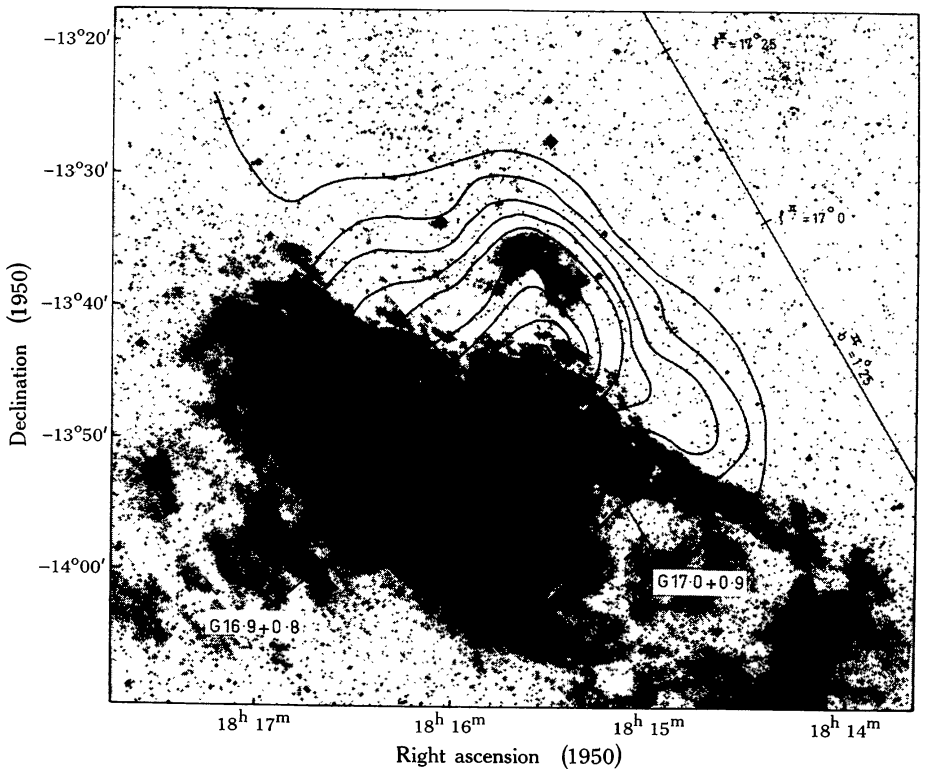

Fig. 4(*n*).—M16. 5000 MHz contours are shown superimposed on the red plate of the Palomar Sky Atlas.

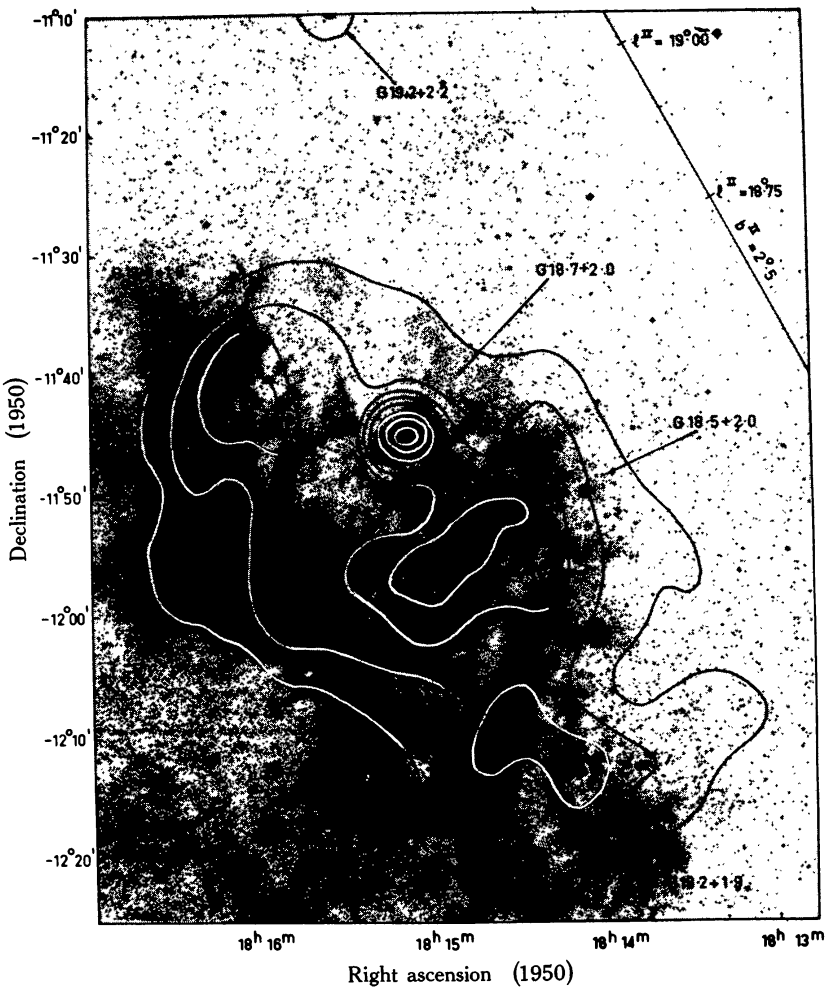

Fig. 4(*o*).–NGC 6604. 5000 MHz contours are shown superimposed on the red plate of the Palomar Sky Survey.

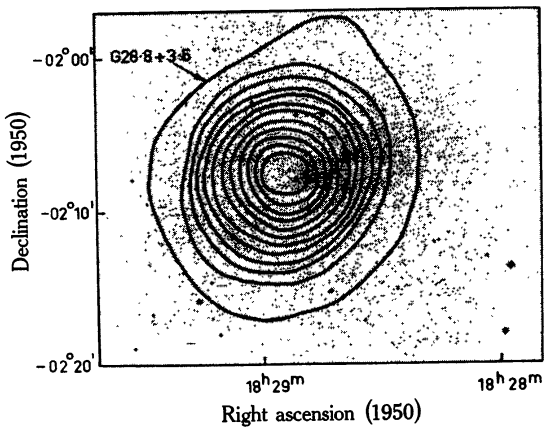

Fig. 4(*p*).–RCW 174. 5000 MHz contours are shown superimposed on the red plate of the Palomar Sky Survey.

About 40% of the thermal sources have been optically identified, and one-third of these identifications were made for the first time in the present study. Generally the strong thermal radio sources are associated with regions containing many bright-rim structures and sharp variations in opacity. The radio peaks are themselves often heavily obscured. Situations of this kind are exemplified by RCW 57 (Fig. 4(*i*)) and RCW 108 (Fig. 4(*k*)). The appearance of the nebula is sometimes determined by the actual distribution of the ionized gas, and sometimes by the foreground obscuring matter. By way of contrast, regions of extended low emission such as the Rosette Nebula in Figure 4(*a*) and the λ Cen Nebula in Figure 4(*j*) appear to contain very little obscuration at all. They were probably formed initially from clouds of rather low density (see Section IV). It is evident that, as the sensitivity and resolution of the radio observations are improved, more and more of the complexity apparent in the optical photographs can be seen.

There are very few cases in which optical emission has been observed from the direction of nonthermal galactic radio sources; only G320.4–1.4 (RCW 89), RCW 103, and W28 have been optically identified in the present study. Generally there are only a few filaments to be seen and these often form arcs about the radio shell.

IV. THERMAL SOURCES

(*a*) *Electron Temperatures*

If a thermal source is opaque and well-resolved at any frequency, its brightness temperature at that frequency is equal to the electron temperature. High resolution observations at low frequency therefore enable an estimate of the electron temperature to be made which is independent of theories for the relative populations of the excited levels of atoms and ions needed for methods using spectral lines. Shaver (1969*a*) has given a detailed description of the method used, and has applied it to 16 sources. Here we extend the method to a further 34 sources which were selected from Table 1 on the basis of their size (apparent source width greater than half the 408 MHz beamwidth) and opacity ($\tau_{408} \geqslant 1$).

The results for all 50 sources are summarized in Table 4. The baselevels for the 408 MHz contour maps in Part II are not at 0°K; since most of the 50 sources are at small distances, it is assumed here that these baselevels represent background emission only and not foreground emission. A small correction ($< 5\%$) then has to be applied in determining the electron temperature and these baselevels must be known. They were estimated from the 408 MHz galactic surveys of Large, Mathewson, and Haslam (1961) and Komesaroff (1966) and are listed in column 2 of Table 4. Columns 3 and 4 give the observed peak brightness temperature T_{1b} of the source averaged over the effective beam solid angle and the restored peak brightness temperature T_1' of the source (see Shaver (1969*a*) for a description of the restoration method); both have been corrected for the baselevel of the 408 MHz contour maps. In column 5 is listed the restored peak brightness temperatures T_2' at 5000 MHz assuming a Gaussian source and beam and multiplied by the ratio of optical depths at 408 and 5000 MHz. The derived values of the 408 MHz opacity τ_1 and the electron temperature T_{ec} are given in columns 6 and 7.

The computed electron temperatures are all considerably less than 10 000°K. If there is any unresolved fine structure at 408 MHz in the nebula, however, the temperatures will be underestimated (Le Marne and Shaver 1969; Shaver and Mills 1969), so they must all be regarded as lower limits. Uncertainties in the derived electron temperatures due to temperature calibration errors are only ~ 10% (standard error) for sources of high opacity, but for $\tau_1 \sim 1$ they can be as high as 25%. The lower limits listed for the components G287.4–0.6 and G287.6–0.6 suggest high electron temperatures, but the optical depths are too small here to permit any significant conclusions.

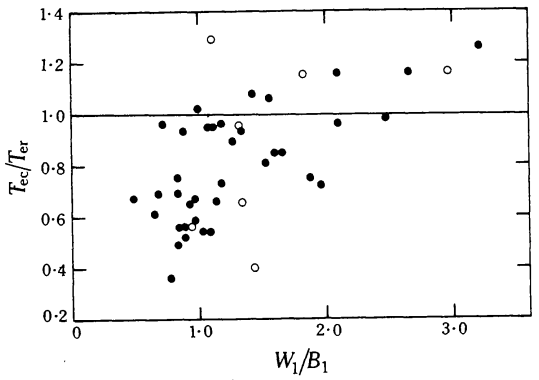

Fig. 5.–Dependence of the ratio T_{ec}/T_{er} on the degree of resolution of the source at 408 MHz. The open circles represent cases that are uncertain for reasons indicated in the footnotes to Table 4.

It is of interest to compare the electron temperatures determined above with those obtained from the H109α recombination line observations of Wilson *et al.* (1970) for the southern sources and Reifenstein *et al.* (1970) for the northern sources. The temperatures obtained using the H109α recombination lines are listed as T_{er} in column 8 of Table 4, and are compared with the present results in column 9. Figure 5 shows the ratio T_{ec}/T_{er} plotted against W_1/B_1, where

$$W_{1\alpha}^2 = M_{1\alpha}^2 - B_{1\alpha}^2 , \qquad W_{1\delta}^2 = M_{1\delta}^2 - B_{1\delta}^2 , \qquad (8, 9)$$

$$W_1 = (W_{1\alpha}\, W_{1\delta})^{1/2} , \qquad B_1 = (B_{1\alpha}\, B_{1\delta})^{1/2} . \qquad (10, 11)$$

Here, W is the corrected source width and the ratio W_1/B_1 is a measure of the degree of resolution of the source at 408 MHz.

Sources that are poorly resolved (small W_1/B_1) tend to have small values of T_{ec}/T_{er}. There are a variety of reasons for this, all based on resolution effects. The principal solution obtained in restoring the 408 MHz maps cannot distinguish features less than 2′ arc in extent; therefore small sources will not be fully restored. If such a source is optically thick, the inadequacy of the resolution process completely explains the low value of T_{ec}. For small sources that are not very opaque, it can be shown that the correction for finite opacity is also underestimated as a result of the inadequacy of the resolution at 408 MHz. Furthermore, some of these sources appear small only because they are at great distances; it is shown below that such distant sources are often composed of several unresolved components. Therefore the values of T_{ec} for distant sources, as well as for sources with small opacities, will be further underestimated because of the existence of unresolved fine structure.

1970AuJPA..14..133S

TABLE 4

Electron Temperatures

(1) G Number	(2) Base-Level of 408 MHz Map (^oK)	(3) Observed 408 MHz Peak Brightness Temp. T_{1b} (^oK)	(4) Restored 408 MHz Peak Brightness Temp. T_1' (^oK)	(5) Restored Value of T_2 T_2' (^oK)	(6) 408 MHz Optical Depth τ_1	(7) Continuum Estimate of Electron Temp. T_{ec} (^oK)	(8) H109α Line Estimate of Electron Temp. T_{er} (^oK)	(9) $\frac{T_{ec}}{T_{er}}$
206.5-16.4	0	3900	6380	18600	2.7	6850	7700	0.89
208.9-19.3	0	1610	3510	7150	1.6	4400	6366	0.69
209.0-19.4	0	6800	8550	92000	10.8	8550	7348	1.16
265.1+1.5	30	2930	5900	11300	1.5	7600	7468	1.02
268.0-1.1*	50	5150	7500	160000	21.3	7500	7939	0.95
282.0-1.2	60	3010	6300	17300	2.5	6850	7330	0.93
284.3-0.3	70	5470	6850	16200	2.1	7750	6690	1.16
285.3-0.0*	70	2250	4500	12200	2.4	4950	8893	0.56
287.4-0.6*	70	5420	7000	10000	≤ 1.2	≥ 8600	7407	≥ 1.16
287.6-0.6*	70	4770	6600	9100	≤ 1.2	≥ 8100	6469	≥ 1.25
291.3-0.7	70	3270	7300	178000	24.4	7300	7591	0.96
291.6-0.5	70	4770	6400	18600	2.7	6800	6929	0.98
298.2-0.3	70	2120	3950	20600	5.3	4000	8108	0.49
298.9-0.4	70	2570	4300	8100	1.5	5600	5962	0.94
305.2+0.0	90	1590	2800	5350	1.5	3700	5141	0.72
305.4+0.2*	90	2260	3300	13600	4.1	3350	5181	0.65
316.8-0.1	140	2540	4250	23700	5.6	4300	5878	0.73
320.2+0.8	140	1590	2900	10400	3.5	3000	8311	0.36
326.6+0.6	240	2240	4050	8900	1.9	4800	6370	0.75
327.3-0.6	240	2020	3400	98000	28.8	3400	6048	0.56
328.3+0.4	300	1280	2400	5600	2.2	2700	4854	0.56
330.9-0.4	350	1450	2400	7900	3.7	2450	4693	0.52

1970AuJPA..14..133S

331.5-0.1	350	2950	4800	16000	3.4	5000	5234	0.96
332.2-0.4	350	1750	3600	25000	7.6	3600	5392	0.67
333.0-0.4	350	2400	3150	6000	1.2	4000	3705	1.08
333.1-0.4	350	2400	3400	7500	1.9	4000	4730	0.85
333.3-0.4	350	1850	3300	28600	9.5	3300	5024	0.66
333.6-0.2	350	3250	6700	153000	23.8	6700	7097	0.95
337.1-0.2	350	2050	3400	20800	6.1	3400	5049	0.67
337.9-0.5	350	1850	3700	23500	6.4	3700	5384	0.69
345.2+1.0	250	1500	2900	12300	4.5	2900	4791	0.61
345.4+1.4	250	2050	3400	18000	5.6	3400	4538	0.75
348.7-1.0	350	3050	4900	25000	5.4	4950	5243	0.95
351.1+0.7	0	1740	2090	3100	1.0	3200	-	-
351.2+0.7	0	2330	3300	5350	1.7	4600	-	-
351.2+0.5	0	1480	1940	3300	1.3	2600	-	-
351.4+0.7*	0	3600	5000	8150	1.3	7000	6030	1.16
353.1+0.7	0	3440	4750	9750	1.7	5800	6019	0.96
353.2+0.9	0	4100	6830	26500	4.0	6900	6501	1.06
6.0-1.2	250	2950	4600	8350	1.4	6100	7200	0.85
10.2-0.3*	250	3550	6050	29300	5.0	6100	4707	1.29
10.3-0.2	250	2150	4200	12000	2.7	4500	7000	0.65
15.0-0.7	0	6400	7850	48600	6.3	7850	6228	1.26
15.1-0.7	0	7200	8400	-	-	8400	-	-
25.4-0.2	120	1820	3600	6700	1.5	4850	9000	0.54
29.9-0.0*	120	1420	2200	4450	1.7	2700	6900	0.40
30.8-0.0*	120	3420	5900	14300	2.3	6500	5640	1.15
43.2-0.0	0	2240	4350	22000	5.1	4400	7435	0.59
49.4-0.3	0	1900	3400	8300	2.2	3800	7035	0.54
49.5-0.4	0	2680	4650	32000	7.0	4650	5750	0.81

* See further notes for these sources on following page.

1970AuJPA..14..133S

*Notes to Table 4:

G268.0–1.1. The restoration procedure used on the 408 MHz map yielded two separate peaks, separated by 1′.5 arc; since the principal solution cannot in this case distinguish features separated by less than 2′ arc, at least one of these peaks must be spurious. One peak was located very close to the original maximum in the unrestored contour map, but the other was near the sharp edge to the north-east; as any slight error in the contours near this edge could result in a very large over-restoration, it is likely that this second peak is not real. As a check, another contour map made from a different set of observations of G268.0–1.1 was restored and this time only one broad peak was obtained, located near the maximum in the unrestored contour map. This result was used in Table 4. It seems that the difference was due to small errors in drawing the contour map and measuring it in preparation for restoration.

G285.3–0.0. Some structure $< 2'$ in extent was produced in the restored contour map, and the computed electron temperature may not be accurate (see notes on G268.0–1.1).

G287.4–0.6, G287.6–0.6. The lower limits on T_{ec} for these two sources were computed with the estimated errors in calibration of the observations taken into account. They are suggestive, but in view of the low optical depths they cannot be taken too seriously. There is no evidence of any nonthermal emission in the area.

G305.4+0.2. Some structure $< 2'$ in extent was produced in the restored contour map, and the computed electron temperature may not be accurate (see notes on G268.0–1.1).

G351.4+0.7. The 15.4 GHz observations of Schraml and Mezger (1969) indicate that this source is very poorly resolved at 5000 MHz. The value of T_2' is therefore too low, and T_{ec} too high. Rough calculations indicate that it may be $> 10\%$ too high.

G10.2–0.3. This is the only source in Table 4 for which the values of T_{er} obtained from the northern (Reifenstein *et al.* 1970) and southern (Wilson *et al.* 1970) H109α line surveys differ by $> 20\%$. If the northern value is used, we obtain $T_{ec}/T_{er} = 1.03$.

G29.9–0.0. Some structure $< 2'$ in extent was produced in the restored contour map, and the computed electron temperature may not be accurate (see notes on G268.0–1.1).

G30.8–0.0. The half-power width of this source measured at 15.4 GHz (Schraml and Mezger 1969) is about half the value obtained at 5000 MHz. This discrepancy is due to the poorer resolving power at 5000 MHz and the peculiar shape of the source. Evidently T_2' in Table 4 has been underestimated, and T_{ec} is too high by about 10%.

At high W_1/B_1 the situation is different and, if spatially small-scale temperature fluctuations are not severe, T_{ec} should be a good estimate of the electron temperature on the near side of the nebula averaged over the beam solid angle and weighted by the square of the electron density. In particular, T_{ec}/T_{er} should be close to unity if there are no large temperature gradients in the nebula. From Figure 5 we infer that in general $T_{ec}/T_{er} \approx 1$; it may be that this ratio is slightly greater than unity for large values of W_1/B_1. Most of these well-resolved sources have large optical depths at 408 MHz; for each of them T_{ec} refers to a region on the near side of the nebula, and the mean distance from the centre of the nebula depends on the density distribution and total optical depth along the line of sight. Since T_{er} is an average temperature over the whole nebula, the existence of a positive temperature gradient in the nebula could explain any excess in the ratio T_{ec}/T_{er}.

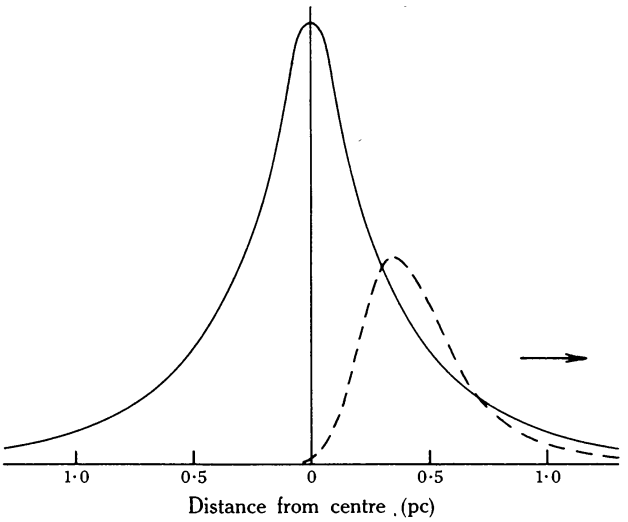

Fig. 6.—Relative electron density distribution in the Orion Nebula from Menon's (1961) model (solid curve), and the integrand in equation (12) (dashed curve). The arrow points towards the observer.

As an illustration of the weighting effects that occur we consider Menon's (1961) model of the Orion Nebula. This model is based on a constant electron temperature, and the relative electron density distribution is shown in Figure 6 as a solid curve. The 408 MHz brightness temperature is given by

$$T_b = T_e \int_0^\tau \exp(-t)\, dt \,, \qquad (12)$$

where t is the optical depth ($t \propto \int N_e^2\, dl$) measured from the near side of the nebula to the element under consideration and τ is the total optical depth through the nebula. Also shown in Figure 6 (dashed curve) is the integrand of equation (12) for Menon's model. The observed brightness temperature is then an average of the electron temperature (appropriately weighted) on the near side of the nebula; the centroid of the integrand is located at a distance of 0.45 pc from the centre. Thus the observed brightness temperature refers primarily to conditions near $r = 0.5$ pc.

The above considerations may explain the possible excess in T_{ec}/T_{er} for the well-resolved sources if the temperature gradient proposed by Mezger and Ellis (1968) for the Orion Nebula is a general phenomenon. From observations of the H109α line they found a high-temperature ring (up to 8500°K) concentric with the nebula and

TABLE 5

Properties of HII Regions

(1)	(2)	(3)	(4)	(5)	(6)	(7)	(8)	(9)	(10)	(11)	(12)	(13)	(14)	(15)
	Width at (MHz)		Emiss.	Electron	Near		Electron		Excit.	Far		Electron		Excit.
G	408	5000	Measure	Temp.	Dist.	Diam.	Density	Mass	Param.	Dist.	Diam.	Density	Mass	Param.
Number	W_1	W_2	EM	T_e	D_n	$2R$	N_e	M	U	D_f	$2R$	N_e	M	U
	(min of arc)		(pc cm^{-6})	(^{o}K)	(kpc)	(pc)	(cm^{-3})	(M_o)	(pc cm^{-2})	(kpc)	(pc)	(cm^{-3})	(M_o)	(pc cm^{-2})
206.3 -2.0	55.0	-	8.6E 3	-	1.4	33.0	18	7.7E 3	113.5	-	-	-	-	-
206.5-16.4	3.8	2.8	7.9E 5	7700	0.6	0.7	1052	4.5E 0	36.9	-	-	-	-	-
208.5-19.2	-	3.3	7.3E 3	-	0.5	0.7	102	4.2E-1	7.7	-	-	-	-	-
208.9-19.3	2.0	2.5	2.8E 5	6366	0.5	0.5	713	1.3E 0	21.6	-	-	-	-	-
209.0-19.4	6.2	3.2	3.8E 6	7348	0.5	0.7	2339	9.0E 0	60.6	-	-	-	-	-
265.1 +1.5	2.7	2.4	4.5E 5	7468	1.0	1.0	655	8.8E 0	39.3	-	-	-	-	-
267.8 -0.9	7.1	7.8	4.4E 4	5974	1.0	3.3	115	5.1E 1	39.4	-	-	-	-	-
268.0 -1.1	3.7	1.7	6.5E 6	7939	1.0	0.7	2971	1.4E 1	76.5	-	-	-	-	-
268.1 -1.0	5.5	5.3	6.8E 4	-	1.0	2.3	173	2.4E 1	35.2	-	-	-	-	-
282.0 -1.2	2.5	2.0	7.0E 5	7330	7.0	6.1	339	9.0E 2	147.5	-	-	-	-	-
283.1 -1.0	3.6	3.1	3.2E 4	-	-	-	-	-	-	-	-	-	-	-
283.3 -0.6	7.0	8.8	1.1E 4	-	-	-	-	-	-	-	-	-	-	-
283.3 -1.0	5.5	4.5	2.4E 4	-	-	-	-	-	-	-	-	-	-	-
283.5 -1.0	4.8	4.7	2.9E 4	-	3.8	7.6	62	3.3E 2	59.8	-	-	-	-	-
284.0 -1.0	4.6	7.6	1.5E 4	4077	5.0	16.4	30	1.6E 3	78.9	-	-	-	-	-
284.3 -0.3	7.6	5.5	6.4E 5	6690	5.0	11.7	235	4.4E 3	222.2	-	-	-	-	-
284.6 -0.2	6.2	6.3	2.1E 4	-	-	-	-	-	-	-	-	-	-	-
284.6 -0.5	5.1	5.2	1.3E 4	-	-	-	-	-	-	-	-	-	-	-
285.3 -0.0	2.7	1.9	5.3E 5	8893	5.3	4.3	349	3.4E 2	107.7	-	-	-	-	-
287.4 -0.6	7.0	6.7	3.0E 5	7407	2.7	7.8	196	1.1E 3	130.6	-	-	-	-	-
287.6 -0.6	6.8	6.0	2.9E 5	6469	2.7	6.9	205	8.1E 2	120.3	-	-	-	-	-
287.8 -0.8	8.3	-	4.0E 4	6847	2.7	9.6	76	8.0E 2	86.3	-	-	-	-	-
287.9 -1.0	5.2	-	7.7E 4	4500	2.7	6.0	97	2.5E 2	63.2	-	-	-	-	-
288.0 -0.8	5.8	-	3.6E 4	8140	2.7	6.7	98	3.5E 2	71.0	-	-	-	-	-
289.1 -0.4	3.2	3.3	9.7E 4	13340	8.5	12.0	90	1.8E 3	120.3	-	-	-	-	-

289.8 -1.2	7.4	6.9	4.2E 4	9090	8.8	26.1	40	8.4E 3	152.6	-	-	-	-	-
289.9 -0.8	2.1	1.6	1.1E 5	-	-	-	-	-	-	-	-	-	-	-
290.6 -1.2	3.4	-	1.4E 4	-	-	-	-	-	-	-	-	-	-	-
291.1 -0.8	2.3	3.4	3.1E 4	-	-	-	-	-	-	-	-	-	-	-
291.2 -0.3	5.0	5.3	1.7E 4	-	-	-	-	-	-	-	-	-	-	-
291.3 -0.7	2.1	1.1	8.3E 6	7591	3.6	1.8	2182	1.4E 2	147.3	-	-	-	-	-
291.5 -0.1	6.4	5.0	2.1E 4	-	-	-	-	-	-	-	-	-	-	-
291.6 -0.5	7.2	5.0	7.5E 5	6929	8.4	17.9	205	1.4E 4	311.2	-	-	-	-	-
291.9 -0.7	1.6	1.4	1.7E 5	6947	2.3	1.4	352	1.1E 1	33.9	6.2	3.7	214	1.3E 2	65.7
295.0 -1.8	20.0	20.0	1.0E 4	-	2.2	18.8	23	1.9E 3	77.1	-	-	-	-	-
295.1 -1.7	3.9	6.4	1.5E 4	3785	2.2	6.1	49	1.3E 2	40.6	-	-	-	-	-
295.2 -0.6	3.5	4.6	5.2E 4	7141	12.5	24.4	46	8.0E 3	157.3	-	-	-	-	-
298.2 -0.8	-	1.0	2.9E 5	-	-	-	-	-	-	-	-	-	-	-
298.2 -0.3	2.4	2.0	8.5E 5	8108	11.8	10.2	289	3.7E 3	223.2	-	-	-	-	-
298.9 -0.4	3.9	3.3	3.1E 5	5962	11.5	16.3	137	7.1E 3	217.0	-	-	-	-	-
301.0 +1.2	1.5	1.0	2.9E 5	6074	5.2	2.2	363	4.8E 1	56.6	-	-	-	-	-
301.1 +1.0	0.8	0.8	6.6E 5	9090	5.2	1.8	608	4.1E 1	64.2	-	-	-	-	-
305.1 +0.1	5.7	5.4	4.8E 4	5170	3.3	7.6	80	4.2E 2	70.4	8.2	18.9	50	4.0E 3	129.1
305.2 +0.0	5.7	3.8	1.9E 5	5141	3.5	5.7	182	4.0E 2	91.8	8.0	13.1	121	3.2E 3	159.3
305.2 +0.2	5.5	5.8	1.6E 5	5724	3.4	8.4	137	9.7E 2	111.9	8.1	20.1	89	8.5E 3	199.6
305.3 +0.1	2.6	2.9	1.1E 5	-	-	-	-	-	-	-	-	-	-	-
305.4 +0.2	3.9	2.8	5.0E 5	5181	3.4	4.0	353	2.8E 2	101.0	8.2	9.8	227	2.5E 3	181.6
305.5 +0.4	1.6	1.5	1.4E 5	-	-	-	-	-	-	-	-	-	-	-
305.6 +0.0	5.0	4.8	7.3E 4	4605	4.2	8.7	91	7.1E 2	88.1	7.4	15.3	69	2.9E 3	128.5
308.6 +0.6	4.1	4.7	5.0E 4	10075	4.6	9.3	73	7.0E 2	81.4	7.9	16.0	56	2.7E 3	116.7
311.1 -0.3	5.1	7.1	1.3E 4	-	-	-	-	-	-	-	-	-	-	-
311.3 +0.1	4.0	6.2	9.6E 3	-	-	-	-	-	-	-	-	-	-	-
311.5 +0.4	3.6	3.7	3.6E 4	5118	6.6	10.5	59	8.0E 2	79.2	-	-	-	-	-
311.5 -0.5	4.0	4.1	2.2E 4	-	-	-	-	-	-	-	-	-	-	-
311.6 +0.3	0.2	0.2	6.0E 6	3292	6.6	0.6	3247	7.0E 0	61.9	-	-	-	-	-
311.9 +0.1	2.8	2.4	1.2E 5	4613	3.4	3.5	181	9.4E 1	56.4	9.9	10.2	106	1.4E 3	115.0
311.9 +0.2	3.4	3.3	6.7E 4	4279	3.6	5.1	116	1.8E 2	59.9	9.8	13.7	70	2.2E 3	116.8
314.2 +0.3	2.6	3.5	2.5E 4	-	-	-	-	-	-	-	-	-	-	-
314.2 +0.4	2.3	2.8	5.5E 4	3012	3.8	4.5	110	1.2E 2	52.4	10.2	12.2	67	1.5E 3	101.1
316.4 -0.4	3.5	-	2.5E 4	-	-	-	-	-	-	-	-	-	-	-

1970AuJPA..14..133S

(1)	(2)	(3)	(4)	(5)	(6)	(7)	(8)	(9)	(10)	(11)	(12)	(13)	(14)	(15)
	Width at (MHz)		Emiss.	Electron	Near		Electron		Excit.	Far		Electron		Excit.
G	408	5000	Measure	Temp.	Dist.	Diam.	Density	Mass	Param.	Dist.	Diam.	Density	Mass	Param.
Number	W_1	W_2	EM	T_e	D_n	$2R$	N_e	M	U	D_f	$2R$	N_e	M	U
	(min of arc)		(pc cm^{-6})	(^{o}K)	(kpc)	(pc)	(cm^{-3})	($M_\odot$)	(pc cm^{-2})	(kpc)	(pc)	(cm^{-3})	($M_\odot$)	(pc cm^{-2})
316.8 -0.1	3.4	1.8	9.0E 5	5878	2.5	1.9	682	5.9E 1	75.0	12.1	9.4	310	3.0E 3	214.6
317.0 +0.3	7.5	7.1	2.7E 4	4139	3.3	10.0	52	6.2E 2	69.5	11.3	34.3	28	1.3E 4	158.0
317.3 +0.2	6.7	7.3	1.0E 4	2704	3.3	10.4	31	4.1E 2	51.4	11.4	35.8	17	9.2E 3	117.5
319.2 -0.4	5.6	4.9	4.3E 4	11058	1.6	3.3	114	5.1E 1	39.3	13.6	28.5	39	1.1E 4	163.6
319.4 -0.0	4.0	3.4	7.7E 4	7416	1.0	1.5	230	8.6E 0	27.5	14.3	21.0	61	6.7E 3	162.2
320.1 -0.5	2.8	4.0	1.5E 4	-	-	-	-	-	-	-	-	-	-	-
320.2 +0.8	2.2	1.4	4.5E 5	8311	2.5	1.5	548	2.2E 1	50.1	-	-	-	-	-
320.3 -0.3	3.0	2.9	1.0E 5	8420	5.0	6.2	128	3.5E 2	78.2	10.3	12.7	89	2.2E 3	126.6
320.3 -0.2	2.3	1.5	2.5E 5	5160	0.5	0.3	866	3.6E-1	14.9	14.9	9.8	159	1.8E 3	143.1
320.4 +0.2	2.8	3.1	2.3E 4	-	-	-	-	-	-	-	-	-	-	-
321.0 -0.5	2.9	2.7	1.0E 5	4895	4.4	5.2	139	2.3E 2	69.4	-	-	-	-	-
321.1 -0.5	4.2	4.0	4.7E 4	4396	3.9	6.6	84	2.9E 2	63.5	-	-	-	-	-
322.2 +0.6	1.0	1.0	1.2E 6	5384	3.6	1.5	865	3.8E 1	69.9	-	-	-	-	-
324.2 +0.2	4.0	-	2.8E 4	-	-	-	-	-	-	-	-	-	-	-
324.2 +0.1	0.4	0.4	1.9E 6	4260	6.9	1.2	1264	2.5E 1	69.1	9.3	1.6	1089	5.2E 1	84.3
326.3 +0.8	20.0	20.0	1.0E 4	-	2.7	23.1	21	3.1E 3	88.4	-	-	-	-	-
326.4 +0.9	0.9	0.9	9.6E 5	7076	2.7	1.0	963	1.3E 1	50.7	13.9	5.4	424	7.7E 2	151.2
326.6 +0.6	5.3	3.3	3.4E 5	6370	3.1	4.4	279	2.8E 2	93.9	-	-	-	-	-
327.2 -0.6	12.0	12.0	2.5E 4	-	3.5	18.0	37	2.6E 3	100.0	-	-	-	-	-
327.3 -0.6	2.4	1.0	4.4E 6	6048	3.5	1.5	1713	6.8E 1	107.2	-	-	-	-	-
327.6 -0.4	4.1	3.9	3.2E 4	3302	4.8	8.1	63	3.9E 2	63.9	12.1	20.3	40	4.0E 3	118.3
327.8 -0.4	1.5	2.4	8.3E 4	-	-	-	-	-	-	-	-	-	-	-
327.8 +0.1	5.4	5.8	1.2E 4	-	-	-	-	-	-	-	-	-	-	-
328.0 -0.1	2.1	2.0	1.1E 5	5922	3.2	2.8	199	5.0E 1	47.3	13.8	12.0	96	1.9E 3	125.2
328.1 +0.1	1.3	1.6	3.7E 4	-	-	-	-	-	-	-	-	-	-	-
328.3 +0.4	2.5	2.2	1.9E 5	4854	7.6	7.3	163	7.5E 2	108.7	9.5	9.1	146	1.3E 3	126.2
330.7 -0.4	1.8	2.3	5.3E 4	-	-	-	-	-	-	-	-	-	-	-
330.9 -0.4	2.5	1.8	2.8E 5	4693	4.1	3.1	299	1.1E 2	70.4	13.4	10.3	166	2.1E 3	155.0
331.0 -0.2	4.3	4.7	3.2E 4	3222	6.5	13.1	50	1.3E 3	88.3	11.0	22.1	38	4.9E 3	125.4
331.1 -0.5	1.8	1.4	1.6E 5	4501	4.9	2.9	234	6.8E 1	55.2	12.6	7.5	146	7.2E 2	103.6

331.3 -0.2	1.4	1.4	2.1E 5	5621	6.1	3.7	242	1.4E 2	71.0	11.4	6.8	177	6.7E 2	107.8
331.3 -0.3	3.2	2.4	1.1E 5	3414	4.7	4.9	153	2.1E 2	69.9	12.8	13.3	93	2.6E 3	136.4
331.4 +0.5	3.1	5.0	1.3E 4	-	-	-	-	-	-	-	-	-	-	-
331.4 -0.0	3.1	2.5	1.0E 5	5366	5.8	6.3	127	3.8E 2	79.6	11.8	12.8	89	2.2E 3	127.8
331.5 -0.1	3.3	2.3	5.7E 5	5234	6.5	6.5	297	9.5E 2	143.9	11.1	11.0	227	3.6E 3	205.6
332.2 -0.4	1.2	1.2	8.9E 5	5392	4.1	2.1	644	7.5E 1	79.7	13.6	7.1	353	1.5E 3	177.3
332.5 -0.1	2.2	1.4	8.7E 4	2156	4.2	2.5	187	3.4E 1	40.7	13.6	8.1	104	6.5E 2	89.2
332.7 -0.6	3.5	3.7	1.3E 5	4072	3.5	5.6	153	3.2E 2	80.2	-	-	-	-	-
332.8 -0.8	2.8	2.8	1.9E 4	-	-	-	-	-	-	-	-	-	-	-
332.8 -0.6	5.5	4.6	8.4E 4	4925	4.3	8.6	99	7.4E 2	91.7	-	-	-	-	-
332.8 -0.3	1.7	2.0	1.3E 4	-	-	-	-	-	-	-	-	-	-	-
333.0 -0.6	4.2	4.8	2.7E 4	-	-	-	-	-	-	-	-	-	-	-
333.0 -0.4	4.0	4.3	1.9E 5	3705	4.1	7.6	158	8.2E 2	110.8	13.7	25.3	86	1.7E 4	247.7
333.1 -0.4	4.6	4.0	2.6E 5	4730	4.2	7.1	190	8.2E 2	117.7	13.6	23.1	105	1.5E 4	257.6
333.1 +0.0	4.2	4.3	2.0E 4	-	-	-	-	-	-	-	-	-	-	-
333.2 -0.1	3.9	5.3	4.2E 4	4838	6.6	15.1	53	2.1E 3	105.9	11.2	25.6	40	8.0E 3	150.6
333.3 +0.1	1.1	2.9	3.5E 4	-	-	-	-	-	-	-	-	-	-	-
333.3 -0.4	3.2	1.8	1.0E 6	5024	3.8	2.9	598	1.8E 2	103.4	14.1	10.8	310	4.7E 3	247.8
333.6 -0.1	4.4	4.5	6.7E 4	4193	4.1	8.0	92	5.5E 2	81.2	13.8	26.8	50	1.1E 4	182.3
333.6 -0.2	3.1	1.1	7.1E 6	7097	3.7	1.8	1982	1.4E 2	142.0	14.2	6.9	1011	4.0E 3	348.1
333.7 -0.5	4.4	4.2	1.5E 4	2444	3.8	6.8	46	1.7E 2	43.6	14.1	25.1	24	4.5E 3	104.6
335.7 -0.2	5.1	4.1	4.3E 4	4457	4.1	7.1	78	3.4E 2	65.1	14.0	24.4	42	7.3E 3	147.7
336.0 +0.1	3.6	3.2	2.9E 4	-	-	-	-	-	-	-	-	-	-	-
336.4 -0.2	5.6	4.8	2.6E 4	2164	5.3	10.8	49	7.3E 2	72.0	13.0	26.5	31	6.9E 3	131.0
336.4 -0.3	4.4	4.8	3.8E 4	3620	6.4	13.2	54	1.5E 3	94.1	11.9	24.5	39	6.9E 3	142.2
336.5 +0.0	3.8	4.0	1.7E 4	2862	5.4	9.3	43	4.0E 2	56.7	13.0	22.3	28	3.6E 3	101.9
336.5 -1.5	1.5	0.7	2.1E 6	9669	2.1	0.6	1852	5.4E 0	47.1	-	-	-	-	-
336.5 -0.2	4.7	6.9	2.6E 4	3200	6.6	19.5	37	3.2E 3	107.4	11.7	34.5	27	1.3E 4	157.3
336.8 +0.0	7.2	8.1	9.1E 4	5999	6.0	20.8	66	7.1E 3	169.9	12.4	43.0	46	4.3E 4	275.7
337.1 -0.2	2.7	1.4	7.3E 5	5049	5.6	3.4	461	2.2E 2	102.1	12.8	7.8	305	1.7E 3	177.1
337.3 -0.1	6.0	4.0	4.1E 4	3900	4.4	7.6	73	3.8E 2	66.6	14.1	24.4	41	7.0E 3	144.8
337.5 -0.3	-	6.6	1.3E 4	-	-	-	-	-	-	-	-	-	-	-
337.6 -0.0	5.2	4.7	2.7E 4	4725	4.5	9.0	54	4.7E 2	64.8	14.0	28.1	31	8.1E 3	138.0
337.7 -0.3	2.4	3.3	1.5E 4	-	-	-	-	-	-	-	-	-	-	-
337.9 -0.5	2.3	1.4	8.8E 5	5384	3.4	2.0	658	6.6E 1	77.0	15.1	9.0	312	2.7E 3	208.0

1970AuJPA..14..133S

(1)	(2)	(3)	(4)	(5)	(6)	(7)	(8)	(9)	(10)	(11)	(12)	(13)	(14)	(15)
	Width at (MHz)		Emiss.	Electron	Near		Electron		Excit.	Far		Electron		Excit.
G	408	5000	Measure	Temp.	Dist.	Diam.	Density	Mass	Param.	Dist.	Diam.	Density	Mass	Param.
Number	W_1	W_2	EM	T_e	D_n	$2R$	N_e	M	U	D_f	$2R$	N_e	M	U
	(min of arc)		(pc cm^{-6})	(^{o}K)	(kpc)	(pc)	(cm^{-3})	(M_o)	(pc cm^{-2})	(kpc)	(pc)	(cm^{-3})	(M_o)	(pc cm^{-2})
338.0 -0.1	8.2	5.9	2.8E 4	3527	4.4	11.1	50	8.2E 2	75.6	14.2	35.8	28	1.5E 4	165.1
338.1 +0.0	5.2	3.1	6.7E 4	3537	3.6	4.8	119	1.5E 2	57.6	15.0	19.9	58	5.4E 3	149.1
338.1 -0.2	6.6	4.4	2.8E 4	3227	4.3	8.0	59	3.6E 2	61.0	14.3	26.7	32	7.3E 3	135.8
338.4 +0.2	5.2	5.0	1.1E 5	-	-	-	-	-	-	-	-	-	-	-
338.4 -0.2	2.3	1.7	1.4E 5	4789	0.4	0.3	687	1.9E-1	11.2	18.2	13.0	102	2.7E 3	142.3
338.4 +0.0	6.4	6.7	1.0E 5	4909	3.2	9.1	105	9.5E 2	102.0	15.4	44.0	48	4.9E 4	290.6
338.5 -0.3	1.3	1.3	7.7E 4	-	-	-	-	-	-	-	-	-	-	-
338.7 +0.6	2.2	2.3	4.4E 4	-	-	-	-	-	-	-	-	-	-	-
338.9 +0.6	3.8	3.4	8.6E 4	4984	5.4	7.8	105	5.9E 2	86.5	13.3	19.1	67	5.6E 3	157.8
338.9 -0.1	2.8	1.9	9.5E 4	5707	3.5	2.9	181	5.1E 1	46.0	15.1	12.4	87	2.0E 3	122.0
338.9 +0.4	3.3	2.5	3.0E 4	-	-	-	-	-	-	-	-	-	-	-
340.2 -0.2	20.0	20.0	6.5E 3	-	3.9	33.4	14	6.1E 3	96.5	14.9	127.6	7	1.8E 5	235.9
340.3 -0.2	2.7	2.1	1.1E 5	5387	3.9	3.5	176	9.2E 1	55.5	14.9	13.5	90	2.6E 3	135.6
340.8 -1.0	0.8	0.8	1.4E 6	4970	2.5	0.9	1281	9.7E 0	50.7	-	-	-	-	-
340.9 -1.0	3.1	-	6.4E 4	-	2.5	3.4	146	6.5E 1	46.5	-	-	-	-	-
343.5 -0.0	3.1	3.6	1.1E 5	7800	3.2	4.9	149	2.1E 2	69.4	16.0	24.6	67	1.2E 4	202.8
345.0 +1.5	6.4	8.9	1.9E 4	5666	2.1	8.0	49	2.9E 2	53.4	-	-	-	-	-
345.2 +1.0	1.8	1.5	4.3E 5	4791	1.1	0.7	768	3.4E 0	30.2	-	-	-	-	-
345.3 +1.5	3.3	3.6	1.0E 5	5770	1.9	2.9	185	5.5E 1	47.4	-	-	-	-	-
345.4 +1.4	2.3	1.4	6.3E 5	4538	1.8	1.1	767	1.1E 1	45.2	-	-	-	-	-
345.6 +1.5	1.3	1.2	1.2E 5	-	-	-	-	-	-	-	-	-	-	-
348.7 -1.0	3.0	1.9	9.3E 5	5243	2.0	1.6	756	3.8E 1	67.2	-	-	-	-	-
351.1 +0.7	8.1	6.6	1.1E 5	-	1.0	2.8	199	5.3E 1	48.1	-	-	-	-	-
351.2 +0.7	3.4	3.4	2.0E 5	-	1.0	1.4	374	1.3E 1	37.4	-	-	-	-	-
351.2 +0.5	4.8	4.2	1.2E 5	-	1.0	1.8	263	1.8E 1	36.5	-	-	-	-	-
351.4 +0.7	8.2	7.3	3.1E 5	6030	1.0	3.1	312	1.1E 2	72.1	-	-	-	-	-
351.6 +0.5	-	1.7	6.1E 4	-	-	-	-	-	-	-	-	-	-	-
353.1 +0.4	-	7.9	6.6E 4	7600	1.0	3.4	140	6.5E 1	45.7	-	-	-	-	-
353.1 +0.7	5.8	5.6	3.6E 5	6019	1.0	2.4	387	6.5E 1	64.1	-	-	-	-	-
353.2 +0.7	20.0	20.0	5.7E 4	-	1.0	8.6	81	6.1E 2	80.4	-	-	-	-	-

353.2	+0.9	4.3	3.0	1.0E 6	6501	1.0	1.3	900	2.2E 1	59.6	-	-	-	-	-
5.9	-0.4	2.5	5.9	1.2E 5	6400	3.0	7.6	125	6.4E 2	94.7	16.9	42.6	53	4.9E 4	299.9
6.0	-1.2	4.5	4.2	3.4E 5	7200	1.4	2.5	370	6.8E 1	64.3	-	-	-	-	-
6.1	-0.1	7.5	-	6.3E 4	2014	-	-	-	-	-	-	-	-	-	-
6.6	-0.1	3.7	-	3.8E 4	3707	-	-	-	-	-	-	-	-	-	-
7.0	-0.3	5.7	5.6	7.7E 4	7300	1.5	3.6	145	8.2E 1	50.1	-	-	-	-	-
9.9	-0.7	4.8	4.1	2.2E 4	-	-	-	-	-	-	-	-	-	-	-
10.2	-0.3	3.1	2.1	1.0E 6	4704	9.0	8.2	356	2.3E 3	204.8	-	-	-	-	-
10.3	-0.2	2.6	1.7	4.9E 5	7000	1.8	1.3	619	1.6E 1	46.9	17.8	12.8	197	4.9E 3	215.9
10.5	+0.0	-	1.3	1.0E 5	-	-	-	-	-	-	-	-	-	-	-
10.6	-0.4	3.3	2.0	1.9E 5	5400	0.1	0.1	1508	1.1E-2	5.6	19.6	16.6	108	5.9E 3	188.0
12.7	-0.2	5.3	4.1	7.4E 4	-	-	-	-	-	-	-	-	-	-	-
12.8	-0.2	0.8	0.8	4.8E 6	7800	4.4	1.5	1774	7.3E 1	110.9	-	-	-	-	-
15.0	-0.7	9.1	5.2	1.8E 6	6228	2.4	5.4	581	1.1E 3	187.6	-	-	-	-	-
16.9	+0.7	8.1	8.1	6.9E 4	6100	2.2	7.6	96	5.0E 2	79.3	-	-	-	-	-
17.0	+0.9	11.1	11.3	5.3E 4	-	2.2	10.6	70	1.0E 3	90.9	-	-	-	-	-
18.5	+1.9	40.0	40.0	1.4E 4	-	3.2	54.8	16	3.1E 4	173.7	-	-	-	-	-
18.7	+2.0	2.7	2.7	1.3E 5	-	3.2	3.7	190	1.1E 2	60.5	-	-	-	-	-
19.2	+2.2	-	1.9	3.8E 4	-	-	-	-	-	-	-	-	-	-	-
22.8	-0.5	2.8	1.6	1.1E 5	-	-	-	-	-	-	-	-	-	-	-
22.8	-0.2	3.9	3.5	1.7E 4	6400	6.2	9.3	43	4.2E 2	57.4	12.2	18.4	31	2.3E 3	90.1
23.1	+0.6	3.8	-	2.0E 4	-	-	-	-	-	-	-	-	-	-	-
23.4	-0.2	2.9	2.2	1.7E 5	6300	7.5	7.2	154	6.8E 2	103.1	10.9	10.4	128	1.7E 3	132.3
23.6	-0.0	6.3	5.8	2.3E 4	-	-	-	-	-	-	-	-	-	-	-
23.7	+0.2	0.6	0.6	6.0E 5	-	-	-	-	-	-	-	-	-	-	-
23.9	-0.1	3.5	2.1	2.7E 4	-	-	-	-	-	-	-	-	-	-	-
24.0	+0.2	1.1	0.5	1.0E 6	-	-	-	-	-	-	-	-	-	-	-
24.4	+0.1	3.4	-	2.4E 4	-	-	-	-	-	-	-	-	-	-	-
24.5	+0.5	1.1	-	2.2E 6	-	-	-	-	-	-	-	-	-	-	-
24.5	-0.2	3.0	-	6.9E 4	4500	8.3	10.8	69	1.0E 3	91.0	9.9	12.9	63	1.6E 3	102.3
24.7	-0.2	3.1	-	4.2E 4	-	-	-	-	-	-	-	-	-	-	-
24.8	+0.1	5.0	-	2.8E 4	8000	9.0	19.1	51	4.2E 3	131.7	-	-	-	-	-
25.3	+0.3	5.7	5.1	8.5E 3	-	-	-	-	-	-	-	-	-	-	-
25.4	-0.2	3.2	2.9	2.9E 5	9000	4.7	5.8	224	5.2E 2	107.0	13.4	16.5	133	7.1E 3	215.1
25.4	+0.0	2.8	3.4	1.8E 4	-	-	-	-	-	-	-	-	-	-	-

(1)	(2)	(3)	(4)	(5)	(6)	(7)	(8)	(9)	(10)	(11)	(12)	(13)	(14)	(15)
	Width at (MHz)		Emiss.	Electron	Near		Electron		Excit.	Far		Electron		Excit.
G	408	5000	Measure	Temp.	Dist.	Diam.	Density	Mass	Param.	Dist.	Diam.	Density	Mass	Param.
Number	W_1	W_2	EM	T_e	D_n	$2R$	N_e	M	U	D_f	$2R$	N_e	M	U
	(min of arc)		(pc cm^{-6})	(^{o}K)	(kpc)	(pc)	(cm^{-3})	(M_o)	(pc cm^{-2})	(kpc)	(pc)	(cm^{-3})	(M_o)	(pc cm^{-2})
28.8 +3.5	5.8	5.4	1.2E 5	8500	0.7	1.6	273	1.4E 1	34.1	-	-	-	-	-
29.9 -0.0	4.3	3.2	1.7E 5	6900	7.3	10.0	130	1.6E 3	128.9	10.0	13.8	111	3.4E 3	159.0
30.2 -0.1	3.2	1.8	6.4E 4	3800	8.1	6.3	101	3.0E 2	68.0	9.1	7.0	95	4.0E 2	73.5
30.4 -0.2	4.3	4.4	2.5E 4	-	-	-	-	-	-	-	-	-	-	-
30.5 -0.3	6.5	6.4	1.6E 4	-	-	-	-	-	-	-	-	-	-	-
30.6 +0.0	3.3	1.6	7.2E 4	-	14.0	9.5	87	9.0E 2	93.6	-	-	-	-	-
30.7 -0.3	3.7	2.9	4.7E 4	-	-	-	-	-	-	-	-	-	-	-
30.8 -0.0	5.5	4.1	5.2E 5	5640	7.1	12.4	205	4.7E 3	216.3	-	-	-	-	-
31.1 +0.1	-	4.1	2.7E 4	6700	8.1	14.4	43	1.5E 3	88.5	9.0	16.0	41	2.0E 3	95.0
31.1 +0.5	-	1.5	5.8E 4	-	-	-	-	-	-	-	-	-	-	-
35.1 -1.5	5.3	5.4	1.5E 4	-	-	-	-	-	-	-	-	-	-	-
35.2 -1.8	1.5	1.4	8.7E 5	6500	3.4	2.0	652	6.5E 1	76.6	13.0	7.8	334	1.9E 3	187.2
35.4 -1.8	5.3	3.9	2.1E 4	-	-	-	-	-	-	-	-	-	-	-
37.5 -0.1	5.2	4.8	2.2E 4	5600	4.0	8.2	52	3.4E 2	57.0	11.9	24.3	30	5.1E 3	117.9
37.7 +0.1	5.5	5.0	1.6E 4	-	-	-	-	-	-	-	-	-	-	-
37.8 -0.2	2.9	3.1	5.8E 4	-	-	-	-	-	-	-	-	-	-	-
37.9 -0.4	5.3	2.6	1.1E 5	6500	4.2	4.7	150	1.8E 2	66.0	11.5	12.8	91	2.3E 3	129.1
39.3 -0.0	3.5	-	2.0E 4	-	-	-	-	-	-	-	-	-	-	-
43.2 -0.0	3.2	2.6	9.2E 5	7435	13.9	15.5	244	1.1E 4	301.5	-	-	-	-	-
45.1 +0.1	1.9	-	8.2E 4	-	-	-	-	-	-	-	-	-	-	-
45.5 +0.1	1.9	1.7	3.3E 5	-	-	-	-	-	-	-	-	-	-	-
48.6 +0.0	2.8	3.8	7.7E 4	8254	1.5	2.4	178	3.0E 1	38.3	11.7	18.9	64	5.1E 3	150.8
48.6 +0.2	-	3.7	1.6E 4	-	-	-	-	-	-	-	-	-	-	-
49.0 -0.3	7.0	5.6	1.2E 5	6454	6.6	15.7	87	4.0E 3	153.5	-	-	-	-	-
49.1 -0.4	5.2	4.8	6.0E 4	4259	6.5	13.4	67	1.9E 3	110.6	-	-	-	-	-
49.2 -0.3	1.4	1.5	6.1E 5	5266	6.5	4.1	385	3.2E 2	109.5	-	-	-	-	-
49.4 -0.3	3.6	3.5	3.3E 5	7035	4.5	6.8	219	8.1E 2	123.4	8.5	12.8	160	4.0E 3	188.5
49.5 -0.4	5.3	3.1	1.3E 6	5750	5.8	7.6	408	2.1E 3	208.3	7.2	9.4	366	3.6E 3	240.5

having a radius of 0.9 pc. In view of the asymmetries known to exist in the density distribution of the nebula it is reasonable to suggest that there is a high-temperature zone surrounding the nebula which is causing both the ring observed by Mezger and Ellis, and also the high value of T_{ec} (8550°K). If this is the case, the T_{ec} and T_{er} values are consistent. The existence of such a high-temperature zone in the outer parts of an HII region has long been anticipated theoretically; it is due to the hardening of the stellar u.v. radiation as the opacity in the Lyman limit increases. Rubin (1969) has summarized evidence that electron temperatures increase to the outside in nebulae.

Little can be said about the other well-resolved HII regions. If they all have positive temperature gradients a correlation should exist between T_{ec}/T_{er} and optical depth. Such a correlation has been found but it is very weak; the number of well-resolved HII regions is too small. The apparent correlation suggested in Shaver (1969*a*) has not been confirmed.

We conclude that the electron temperatures determined from the H109α line work can be reconciled with those obtained from the continuum observations. Departures from local thermodynamic equilibrium of the relative populations of the atomic energy levels do not seem to be significant for the nebulae studied here. In the work that follows the values of electron temperature obtained from the H109α line observations are assumed to be the true electron temperatures weighted by the square of the electron density throughout the nebula.

(*b*) *General Properties*

All of the HII regions observed are listed in Table 5. It is difficult to decide exactly what features on the contour maps are single HII regions. In most cases the individual thermal sources in Table 1 were taken to be single HII regions. However, there were some cases, such as the Rosette Nebula, in which it seemed clear that the source was more complex. In seven such cases a source was fabricated out of a number of components, and given an "equivalent Gaussian representation" (equivalent in the sense that the total flux and angular size were consistent with the actual source). The details for individual cases are noted in the Appendix.

The galactic source numbers in column 1 of Table 5 refer to the centroids of the HII regions, and the entries in columns 2 and 3 are respectively the 408 and 5000 MHz corrected geometric mean half-power source widths W_1 and W_2 defined above by equation (10). The emission measure *EM* in column 4 refers to a line of sight through the centre of the HII region. It was computed from equation (7) of Schraml and Mezger (1969) whenever values of W_2 were available; otherwise it was calculated from the observed 408 MHz parameters allowing for finite optical depth. In all of these calculations the electron temperature T_e in column 5, which was computed from equation (1) of Schraml and Mezger (1969) using the H109α line observations, was used whenever possible; otherwise a value of 6000°K was assumed.

In 13 cases listed in Table 6 the source did not substantially broaden the beam at either or both frequencies, and the half-power source widths could not be measured. However, in all but 1 of these cases the emission measure of the source was high enough to permit the turnover frequencies ν_t to be determined, and the half-power source widths W in Table 5 could be calculated using the method of Mezger, Schraml, and Terzian (1967). For the single remaining case a half-power source width of 1′ arc was assumed.

Before the linear dimensions and density of an HII region can be determined, its distance must be known and a model must be assumed for the distribution of matter within the HII region. Kinematic distances from the H109α line observations have generally been used. In many cases there are two possible distances for a given HII region and both the near (D_n) and far (D_f) distances have to be determined. When there is no such ambiguity the distance has been listed in column 6 of Table 5 under D_n. For some HII regions there are other sources of information regarding the distance, such as OH and HI line absorption data and optical work; unambiguous distances that have been obtained by these methods are listed under D_n and the references used for them are given in Table 7. Altogether there are 75 sources in Table 5 with unambiguous distances.

TABLE 6

Unresolved HII Regions

G Number	Turnover Frequency ν_t (MHz)	Computed Widths W (min arc)	G Number	Turnover Frequency ν_t (MHz)	Computed Widths W (min arc)
301.0+1.2	–	1.0*	340.8–1.0	800	0.8
301.1+1.0	500	0.8	12.8–0.2	1350	0.8
311.6+0.3	1350	0.2	23.7+0.2	500	0.6
322.2+0.6	750	1.0	24.0+0.2	700	0.5†
324.2+0.1	900	0.4	35.2–1.8	600	1.4†
326.4+0.9	600	0.9	49.2–0.3	500	1.4
336.5–1.5	850	0.7†			

* A value of $W_2 = 1'.0$ was assumed for this source.

† Sources were resolved at 408 MHz and only W_2 values were determined from ν_t.

A homogeneous sphere has been adopted as the model for these HII regions. This crude approximation is adequate for the purposes of the present work, although its consequences should be kept in mind. The actual geometry of an HII region depends on its stage of evolution, but for many of the strong HII regions the brightness temperature distribution due to a homogeneous spherical nebula is too broad (Menon 1961) and the computed turnover in the radio spectrum is too sharp as compared with observations of optically thick nebulae. However, more important consequences stem from the assumption of homogeneity alone. Suppose the nebula is actually composed of a number of blobs of uniform density distributed in an otherwise empty volume. If the ratio of the total volume of all the blobs together to that of the nebula is α, the density determined from these radio observations, assuming homogeneity, is less than that in the blobs by a factor $\alpha^{-1/2}$ and the computed mass is greater than the true mass by the same factor. Typically $\alpha \sim 1/25$ (Osterbrock and Flather 1959; Meaburn 1969) so that the effect is substantial. However, the excitation parameter is not affected (Rubin 1967). For an ionization-bounded HII region the excitation parameter is a measure of the Lyman continuum flux from the exciting star(s) and should be approximately constant throughout most of the lifetime of the nebula (Hjellming 1968). For a density-bounded HII region the value of the excitation parameter calculated here will underestimate the power of the exciting star(s).

TABLE 7

References for Distances of HII Regions

G Number	Distance* (kpc)	References†	G Number	Distance* (kpc)	References†
206.3−2.0	1.4	1	336.5−1.5	2.1	D_n
206.5−16.4	0.6	2	340.8−1.0	2.5	D_n
208.5−19.2	0.5	3	340.9−1.0		
208.9−19.3			345.0+1.5	2.1	D_n
209.0−19.4			345.2+1.0	1.1	D_n
265.1+1.5	1.0	4	345.3+1.5	1.9	D_n
267.8−0.9	1.0	4	345.4+1.4	1.8	D_n
268.0−1.1			348.7−1.0	2.0	D_n
268.1−1.0			351.1+0.7	1.0	10, 11, D_n
282.0−1.2	7.0	5	351.2+0.7		
283.5−1.0	3.8	6	351.2+0.5		
284.3−0.3	5.0	4, 5, 7	351.4+0.7		
287.4−0.6	2.7	8	353.1+0.4	1.0	12, D_n
287.6−0.6			353.1+0.7		
287.8−0.8			353.2+0.7		
287.9−1.0			353.2+0.9		
288.0−0.8			6.0−1.2	1.4	3, 12, D_n
291.3−0.7	3.6	9	7.0−0.3	1.5	13, 14
291.6−0.5	8.4	9	10.2−0.3	9.0	5
295.0−1.8	2.2	8	12.8−0.2	4.4	5
295.1−1.7			15.0−0.7	2.4	D_n
320.2+0.8	2.5	D_n	16.9+0.7	2.2	3, 13, D_n
321.0−0.5	4.4	D_n	17.0+0.9		
321.1−0.5	3.9	D_n	18.5+1.9	3.2	13, D_n
322.2+0.6	3.6	D_n	18.7+2.0		
326.6+0.6	3.1	D_n	28.8+3.5	0.7	5
327.2−0.6	3.5	D_n	30.6+0.0	14.0	15
327.3−0.6			30.8−0.0	7.1	16
332.7−0.6	3.5	D_n	43.2−0.0	13.9	17
332.8−0.6	4.3	D_n			

* The distances listed here are usually consistent with the H109α line radial velocities; exceptions are noted in the Appendix.

† References are: 1, Allen (1963); 2, Courtès (1960); 3, Becker and Fenkart (1963); 4, Manchester, Robinson, and Goss (1970); 5, Radhakrishnan (personal communication); 6, Gum (1955); 7, Westerlund (1960); 8, Sher (1965*a*); 9, Goss and Radhakrishnan (1969); 10, Roslund (1966); 11, Clark, Radhakrishnan, and Wilson (1962); 12, Cederblad (1946); 13, Miller (1968); 14, Pottasch (1965); 15, Robinson, Goss, and Manchester (1970); 16, Mezger and Höglund (1967); 17, Sato, Akabane, and Kerr (1967). D_n indicates that the near kinematic distance has been adopted if the source has been observed optically, and if the far kinematic distance from the H109α line work is greater than 10 kpc and also greater than twice the near distance.

The values of linear diameter $2R$, electron density N_e, mass M, and excitation parameter U in columns 12–15 of Table 5 have been computed for the spherical model from equations (3), (5), (6), and (8) respectively in Schraml and Mezger (1969). The data in Table 5 can now be used to study the physical and astronomical properties of HII regions.

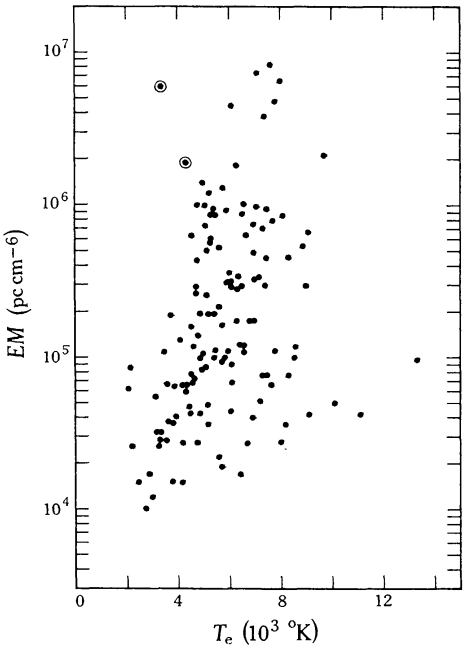

Fig. 7.—Correlation between emission measure EM and electron temperature T_e as determined from the H109α lines.

(*c*) *Collisional De-excitation*

In high density HII regions it is expected that the effectiveness of cooling agents such as oxygen and neon ions will be diminished due to collisional de-excitation (Osterbrock 1965) and that the electron temperature will be higher in these regions. Because of selection effects described below, the electron densities for the HII regions in Table 5 are strongly correlated with the emission measures. It is therefore expected that high emission measure sources will have electron temperatures greater than a certain value and that this limit will decrease with decreasing emission measure. Such a situation appears to be present in Figure 7, although the statistics are weak.

The fact that an inverse correlation between electron temperature and emission measure is not seen in Figure 7 may be considered to be further evidence against line enhancement for the hydrogen α recombination lines (Dyson 1969). Since for the HII regions studied here the emission measure is approximately proportional to the density, we can use the theoretical curves of Hjellming, Andrews, and Sejnowski (1969) to predict a relation between electron temperature and emission measure; for the H109α line and for $T_e \sim 7500°$K, we expect $T_e \propto EM^{0.2}$ approximately. No such correlation can be seen in Figure 7. In fact if line enhancement is at all important, the evidence presented in Figure 7 underestimates the effects of collisional de-excitation. It should be noted that the two unresolved sources with the highest overall turnover frequencies of all unconfused sources, G311.6+0.3 and G324.2+0.1 (circled points in Fig. 7), have unusually low values of T_{er}; it may be that maser effects are becoming important at the corresponding "true" emission measures ($\sim 10^8$ pc cm^{-6}).

(*d*) *Clustering of HII Regions*

If there are systematic errors in the 75 unambiguous distances, then the linear sizes computed for the sources would be correlated with their distances. That a correlation does exist can readily be seen from Figure 8, where the more distant HII

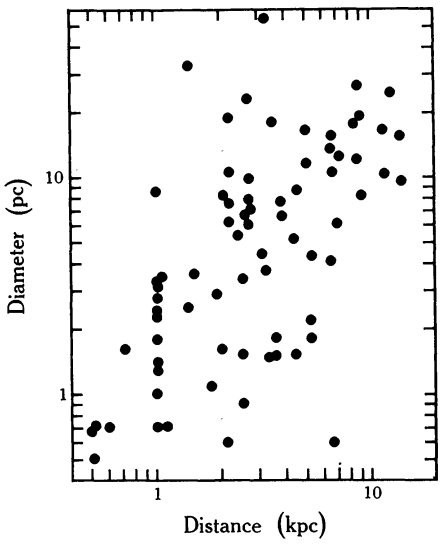

Fig. 8.—Dependence of the apparent diameters of HII regions on their distances.

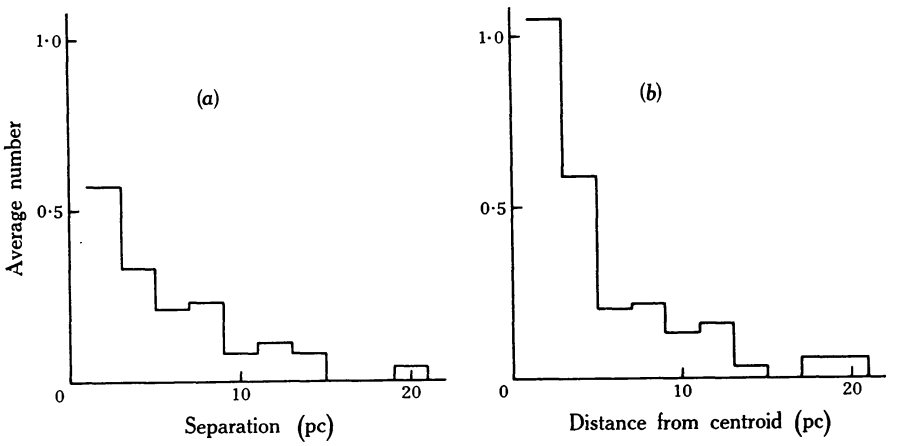

Fig. 9.—Frequency distributions of (*a*) nearest-neighbour distances for HII regions, and (*b*) distances of HII regions from the cluster centroids.

regions appear to be the bigger ones. However, there is a possibility that this correlation is caused by resolution effects. This possibility was investigated by measuring the linear separation of each HII region from its nearest neighbour. This could only be done for sources with known distances and in each case the area had to be free of contamination from sources with unknown distances; lower limits on the separation that could be measured were set by the finite resolution of the observations and upper limits by the extent of the uncontaminated area. These limits were different for different contour maps, and when the results were averaged for each separation range a fairly reliable mean distribution of nearest-neighbour distances was obtained from 1–20 pc, as shown in Figure 9(*a*). It is obvious that HII regions tend to cluster together. Figure 9(*b*) was made in a similar way and shows a histogram for the distances of sources from the cluster centroid. The determination of the centroid in each case is necessarily subjective, but the "mean cluster profile" in Figure 9(*b*) is certainly qualitatively correct. Its size is comparable to the mean diameter of ~ 5–6 pc for the more concentrated parts of open star clusters (Hogg 1959).

NGC 6334 and 6357 are good examples of this clustering property of HII regions; if they were at a distance of > 7 kpc, each would appear as a single source in a $4'$ arc beam. The distant "giant" HII regions are therefore likely to be unresolved clusters of individual sources. Recently Wynn-Williams (1969) has resolved W49A (G43.2–0.0) into two components, and indicates that one of these has a complex structure and may be a composite of three smaller sources.

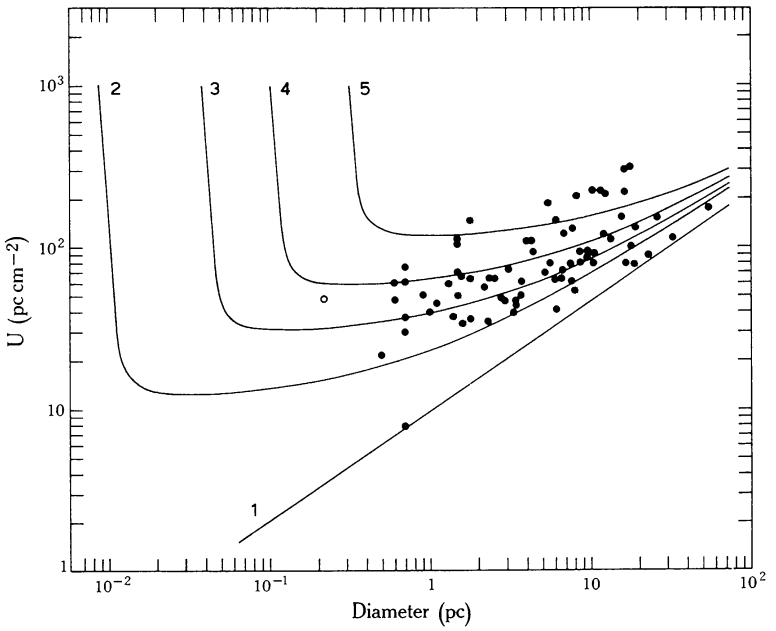

Fig. 10.–Relation between excitation parameter U and diameter for HII regions. The open circle represents the northern source DR 21. Curves 1–5 are sensitivity limits, explained in the text.

(*e*) *Excitation Parameters*

The densities, masses, and excitation parameters listed in Table 5 are all strongly correlated with the source diameters. However, these different correlations are equivalent to each other, and it suffices to discuss just one of them. In Figure 10 the excitation parameter U is plotted against diameter. From the foregoing discussion about the clustering of HII regions it is evident that the excitation parameters shown here will often be greater than expected for single HII regions, especially when the diameter is large. Part of the correlation in Figure 10 is certainly due to this effect, and it is likely that for "individual HII regions" the excitation parameter is rarely greater than $\sim$ 100–150 pc cm^{-2}.

Sensitivity limits also play a large role in causing this apparent correlation. Curve 1 in Figure 10 defines a sensitivity limit of 1°K (T_b) at 5000 MHz for well-resolved sources; few sources in this work have peak temperatures less than this value. Most of the sources observed are those in the southern H109α line survey for which a peak temperature of $T_b \geqslant 2$°K was required. Curves 2–5 in Figure 10 are 2°K (T_b) sensitivity limits for sources at distances of 0.5, 2, 5, and 15 kpc respectively and for a half-power beamwidth of $4'$ arc. In all of these cases, sources strong

enough to be observed are represented by points lying above the relevant sensitivity limits. Curves 2–5 are flatter than curve 1 at low diameters because they take into account the finite resolution of the observations. The steep portions on the left side of the graph show the sensitivity limits when the source is optically thick at 5000 MHz; if the upper observing frequency had been higher than 5000 MHz these limits would have been even further to the left.

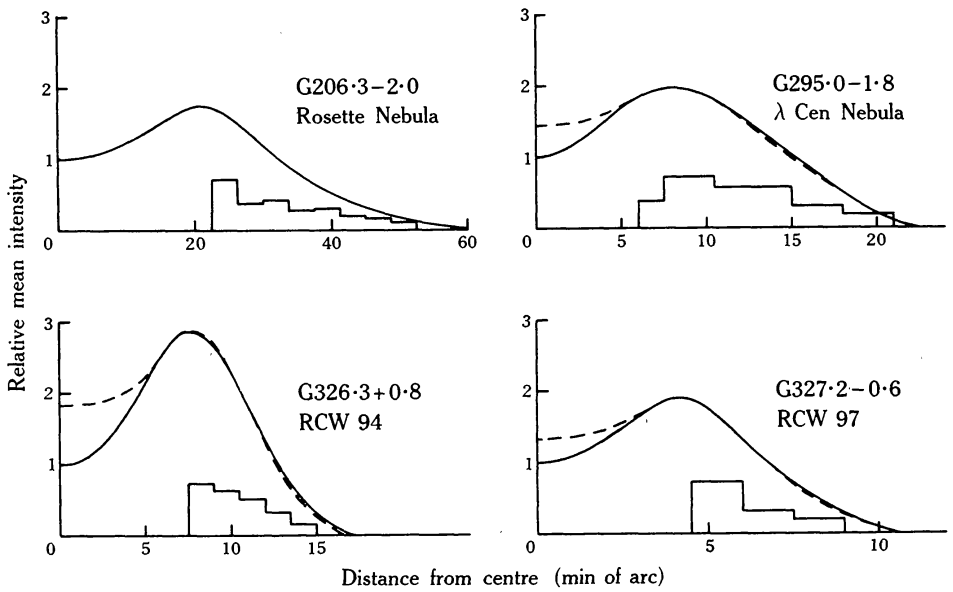

Fig. 11.—Mean profiles of shell-type HII regions. The histograms represent relative model shell emissivities; the solid and dashed curves are observed and computed mean profiles respectively.

Evidently the sensitivity restrictions set by the observations impose upper limits on the diameters of observable sources, and lower limits on the excitation parameters. However, there appears to be a low-diameter limit also ($\sim$ 0.5 pc) and this is certainly not caused by the restrictions imposed by sensitivity. This limit is related to the fact that not one out of the 218 HII regions in Table 5 has a turnover frequency above 1400 MHz. Generally speaking, no sources were found with electron densities $> 5 \times 10^3$ cm^{-3} averaged over regions > 0.1 pc in extent.

Small-diameter sources are expected to evolve very quickly and not many are likely to be found. However, it may be that 0.5 pc is the smallest diameter of the initial Stromgren sphere for the HII regions observed here ($U \sim 50$ pc cm^{-2}). Then such HII regions at an earlier stage of evolution would be very weak radio sources and fall below the (horizontal) sensitivity limits in Figure 10. A corollary of this hypothesis would be that if the largest O stars are initially surrounded by "cocoons" of very high density ($\geqslant 10^4$ cm^{-3}), these cocoons must be density-bounded. In any case it seems that a search for young HII regions requires very high sensitivity above all; the observing frequency need not be much higher than 5000 MHz. Northern observers have found a few radio sources suspected of being extremely dense HII regions, and the most reliable case (DR 21) is shown in Figure 10 as an open circle.

(*f*) *Shell Structure*

Among the largest and least dense HII regions observed in this study are four sources showing pronounced shell structure. They are G206.3–2.0 (Rosette Nebula), G295.0–1.8 (λ Cen Nebula), G326.3+0.8 (RCW 94), and G327.2–0.6 (RCW 97). They have all been analysed using the method of Hill (1967) and the results are illustrated in Figure 11. The solid curves are the mean observed profiles, and the histograms represent the relative emissivities of the derived composite shells. In the case of the Rosette Nebula the shell emissivities are those deduced by Hill (1967). For the other three sources the dashed line is the average profile computed from the shell emissivities shown. The observed and computed profiles agree closely except near the centre of the shell, where the computed profile is always too large. Hill's results for the Rosette Nebula show the same features. The discrepancy at the shell centre could be explained if the four HII regions are actually rings of emission which all happen to be facing us. An alternative explanation seems more likely. In Hill's method the thickness of individual shells is always half of the half-power beamwidth; if thinner shells were used with spacings in between, far lower central intensities could be obtained. Such thin shells may correspond to filaments known to exist from optical observations. In general the overall shell thickness is about one-quarter of the diameter.

It can be seen from Figure 11 that the emissivity (or electron density) is always greatest on the inside of the shell. This type of structure is in excellent agreement with the calculations of Mathews (1967) on the effects of radiation pressure on dust in HII regions. It seems likely that such shell-type structures are common in HII regions, especially those with low density for which the dust grains have the greatest chance of survival (Mathews 1969).

V. NONTHERMAL SOURCES

(*a*) *Extragalactic Sources*

In sorting out galactic and extragalactic sources located in the galactic plane, it can be assumed as a first-order approximation that all "point" sources are extragalactic and all extended sources are galactic. This is based on information gained from high latitude surveys and the properties of known galactic sources (in particular, surface brightness). However, some extragalactic sources are extended and some galactic sources have small angular diameters, and for these cases additional information is required.

Kesteven (1968*a*) has discussed the assumption that small-diameter extragalactic sources located in the galactic plane can usually be distinguished on the basis of their angular sizes alone. He demonstrated that sources with flux densities > 4 f.u. and angular sizes $< 1'$ arc are distributed fairly isotropically in b^{II}, and that the areal density of such sources near the galactic plane is similar to that at high latitudes. However, these conclusions are biased by confusion effects in the galactic plane. Sources of small angular size tend to be merged with other larger sources in the $1'.5 \times 4°.2$ arc fan beam used by Kesteven, and the number of small-diameter sources in the galactic plane is underestimated.

While this criterion appears reliable for Kesteven's work, it is inadequate here and additional criteria are necessary in distinguishing extragalactic from galactic sources.

The extragalactic sources have nonthermal spectra and sometimes rather large net polarization. Sources located in the galactic plane that are optically identified with nebulosities are almost certain to be galactic. HI line absorption measurements can provide lower limits for the distances of sources and extended galactic nonthermal sources can usually be identified on the basis of their arc-like radio contours.

In cases where no other information is available, unresolved nonthermal sources listed in Table 1 have been taken to be extragalactic. Two sources which are extended (G309.6+1.7 and G309.8+1.8) were assumed to be components of a single extragalactic source, for reasons given in the Appendix. All of these sources are listed in Table 8, along with their spectral indices and 408 MHz flux densities.

TABLE 8

Extragalactic Sources

G Number	Spectral Index α	408 MHz Flux Density S_{408} (f.u.)	G Number	Spectral Index α	408 MHz Flux Density S_{408} (f.u.)
207.1−1.3	$\leqslant -1.05$	3.5	336.5+0.1	−0.35	1.2
283.2−1.1	$\leqslant -0.80$	1.8	337.2+0.1	−0.27	1.4
287.7−1.3	$\leqslant -0.60$	3.0	22.9−0.1	$\leqslant -0.58$	2.0
290.4−0.9	$\leqslant -0.19$	1.7	24.2+0.6	$\leqslant -0.56$	1.7
307.1+1.2	−0.80	28.4	25.3−0.1	$\leqslant -0.91$	4.8
309.6+1.7	−0.67	45.8	37.4−0.2	$\leqslant -0.20$	1.3
309.8+1.8	−0.75	136.5	39.4−0.6	$\leqslant -0.74$	1.6
319.9+0.8	−0.15	1.6	49.2−1.0	$\leqslant -1.05$	3.8

Except for G307.1+1.2, G309.6+1.7, and G309.8+1.8, all of these sources were found by chance in the observations. High latitude surveys (e.g. Pooley and Ryle 1968) have shown that 14 extragalactic sources with $S_{408} > 1$ f.u. should be found by chance in the area covered (55 sq deg). The actual number found (13) agrees well with this estimate. However, this agreement must be to some extent fortuitous because of the small size of the sample. The spectral indices of the 13 sources seem to be divided into two groups (see Fig. 3(*c*)). One of them is centred at $\alpha \sim -0.8$ in good agreement with the results of Fanti *et al.* (1969) on a homogenous sample of 4C radio sources. The other is centred at $\alpha \sim -0.2$ and many of these sources may not be extragalactic. It is interesting to note that not one unresolved nonthermal source has been found in the region within 20° of the galactic centre, while about five were expected.

(*b*) *Supernova Remnants*

The other nonthermal components in Table 1 are thought to comprise supernova remnants. Table 9 lists the observed and computed properties of these supernova remnants. There are 34 of them, and about half have not been previously recognized as such. In cases where a supernova remnant has been made up from two or more components from Table 1 the galactic source number in column 1 refers to the centroid of the supernova remnant, and the spectral index in column 2 is the average for all of the components. Individual cases are described in more detail in the Appendix. The

1970AuJPA..14..133S

TABLE 9

Properties of Supernova Remnants

(1) G Number	(2) Spectral Index α	(3) Angular Diameter θ (min arc)	(4) Flux Density at 1000 MHz S_{1000} (f.u.)	(5) Distance D (kpc)	(6) Displ. from Galactic Plane Z (pc)	(7) Diameter $2R$ (pc)	(8) Power Output at 1000 MHz P_{1000} (W Hz^{-1})	(9) Total Power $\int P_\nu d\nu$ (erg sec^{-1})
290.1-0.8	-0.58	12.0	41.6	3.9	-52	14	7.7 E 16	4.5 E 33
291.0-0.1	-0.18	10.0	20.4	5.1	-7	15	6.3 E 16	5.1 E 33
292.0+1.8	-0.20	4.8	17.6	7.9	+242	11	1.3 E 17	1.0 E 34
298.5-0.3	-0.36	5.3	5.4	9.7	-59	15	6.1 E 16	4.1 E 33
298.6-0.0	-0.30	7.1	4.3	8.7	-3	18	3.9 E 16	2.8 E 33
304.6+0.1	-0.54	8.4	13.6	6.1	+13	15	6.1 E 16	3.7 E 33
311.5-0.3	-0.49	3.9	3.7	12.5	-74	14	6.9 E 16	4.3 E 33
316.3-0.0	-0.47	13.0	24.3	4.2	-1	16	5.2 E 16	3.2 E 33
320.4-1.2	-0.53	26.0	58.4	2.4	-51	18	3.9 E 16	2.4 E 33
328.0+0.3	-0.55	5.9	2.4	10.9	+54	19	3.5 E 16	2.1 E 33
328.4+0.2	-0.15	4.2	17.5	8.5	+33	10	1.5 E 17	1.3 E 34
332.0+0.2	-0.48	12.0	9.1	5.5	+16	19	3.3 E 16	2.0 E 33
332.4-0.4	-0.52	9.0	27.6	5.0	-33	13	8.4 E 16	5.1 E 33
332.4+0.1	-0.47	15.0	26.2	3.8	+8	17	4.6 E 16	2.9 E 33
333.0+0.8	-0.17	2.6	8.3	13.1	+176	10	1.7 E 17	1.4 E 34
336.7+0.5	-0.49	11.0	6.3	6.3	+56	20	2.9 E 16	1.8 E 33
337.0-0.1	-0.47	14.0	17.1	4.4	-6	18	3.9 E 16	2.5 E 33
337.8-0.1	-0.51	6.5	17.7	6.7	-10	13	9.4 E 16	5.7 E 33

338.1+0.4	-0.42	12.0	4.5	6.4	+49	22	2.2 E 16	1.4 E 33
338.3-0.0	-0.65	8.9	15.1	5.8	-4	15	6.1 E 16	3.5 E 33
338.5+0.1	-0.30	8.2	28.3	5.3	+9	13	9.4 E 16	6.7 E 33
6.4-0.1	-0.44	42.0	310.1	1.3	-3	15	5.8 E 16	3.7 E 33
10.0-0.3	-0.83	7.8	2.9	9.0	-39	20	2.8 E 16	1.7 E 33
11.2-0.3	-0.52	4.6	22.6	7.6	-46	10	1.6 E 17	9.6 E 33
21.8-0.5	-0.52	20.0	69.0	2.6	-23	15	5.8 E 16	3.5 E 33
22.7-0.2	-0.57	26.0	33.0	2.7	-9	20	2.9 E 16	1.7 E 33
23.3-0.3	-0.50	27.0	70.3	2.2	-12	17	4.2 E 16	2.6 E 33
23.6+0.3	-0.34	9.8	7.6	6.4	+34	18	3.7 E 16	2.6 E 33
24.5+0.2	-0.22	7.2	10.0	7.1	+30	15	6.1 E 16	4.7 E 33
24.7+0.6	-0.38	14.0	13.4	4.6	+47	19	3.4 E 16	2.3 E 33
29.7-0.2	-0.60	2.1	11.4	13.8	-60	8	2.6 E 17	1.5 E 34
39.2-0.3	-0.44	6.7	20.9	6.3	-34	12	1.0 E 17	6.3 E 33
43.3-0.2	-0.47	4.8	38.7	6.6	-22	9	2.0 E 17	1.3 E 34
49.2-0.5	-0.25	26.0	159.8	1.9	-17	14	6.9 E 16	5.1 E 33

high resolution observations used here clearly show that the spectral index does not vary significantly from one part of a supernova remnant to another. Column 3 gives the angular diameter θ of the source. In cases where the shell structure is not resolved this is the apparent diameter for a spherical model; in general it refers to the outer edge of the shell. The interpolated 1000 MHz flux density is listed in column 4.

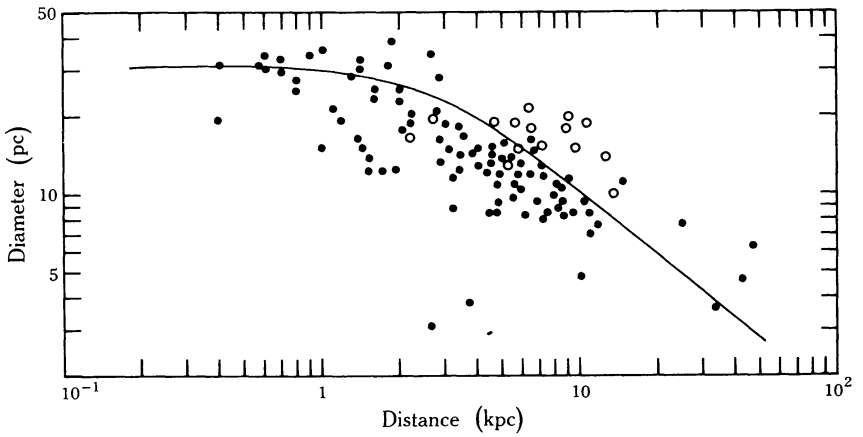

Fig. 12.—Relation between the diameters and distances of supernova remnants. The filled circles represent sources listed in Milne's (1970) catalogue. The open circles represent newly identified supernova remnants from the present work. The curve is a sensitivity limit, explained in the text.

A relation found by Kesteven (1968*b*) to hold between the total power output and the diameter of a supernova remnant enables the distance to be calculated from the observed flux density and the angular diameter. For a mean value of the spectral index $\alpha = -0.5$, we can write

$$P_{1000} = k_1 R^{-2.5} \tag{13}$$

and

$$D^{4.5} = k_2 S_{1000}^{-1} \theta^{-2.5} , \tag{14}$$

where P_{1000} is the power output in watts per hertz at 1000 MHz, R and D are the radius and distance of the supernova remnant in parsecs respectively, S_{1000} is the flux density in W m^{-2} Hz^{-1} at 1000 MHz, and θ is the angular diameter in minutes of arc. The constants k_1 and k_2 are related by $k_2 = 32.5\ k_1$. Using Milne's (1970) tabulation of supernova remnants with known distances, we obtain values for k_2 of 0.5×10^{20}, 7×10^{20}, and 3×10^{20} for type I and type II supernova remnants and for the average of all supernova remnants respectively. Distances computed from equation (14) using the average value of k_2 are accurate to within 40% (standard error); type I supernova remnants are placed ~ 50% too far, and type II about 25% too close. If it is known that a supernova remnant is either type I or type II, its distance can be estimated more precisely. This is not generally known for the supernova remnants studied here and the overall average relation has to be used. Columns 5–9 of Table 9

list respectively the computed distance D of the supernova remnants, the displacement Z above or below the galactic plane, the linear diameter $2R$, the power output P_{1000} at 1000 MHz, and the total power output for the supernova remnant obtained by assuming a constant spectral index and cutoff frequencies of 10 and 10^4 MHz.

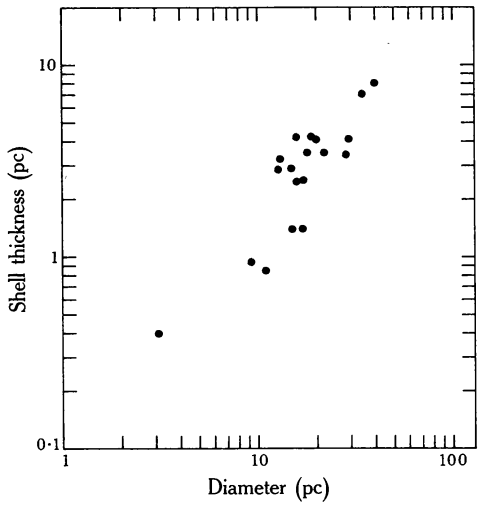

Fig. 13.–Correlation between shell thickness and diameter of well-resolved supernova remnants.

Observational selection effects in the detection of supernova remnants can readily be seen in Figure 12, which shows diameter versus distance for the 98 supernova remnants listed by Milne (1970) (filled circles) and the 15 new supernova remnants presented in this paper (open circles). Most of the supernova remnants in Milne's catalogues were found in early galactic surveys made with rather large beams. In order to roughly define the observational selection effects for these sources a sensitivity limit is shown in Figure 12 derived from equation (13) for a minimum detectable brightness temperature of 5°K at 1000 MHz and a half-power beamwidth of 30′ arc. Sources strong enough to be observed (and to enable the determination of their spectral indices) are represented by points lying below this sensitivity limit. Although the selection criterion differs from one supernova remnant to another in Milne's catalogue, this sensitivity limit defines the distribution of filled circles quite well. The new supernova remnants (open circles) are generally larger and more distant than the others. It is interesting to note that there is a scarcity of close small-diameter supernova remnants. A likely explanation is that observations with poor sensitivity of a source with a bright feature and an extended low-emission region will detect the bright feature and miss the rest; the estimated flux density and angular size of the supernova remnant will be too small, and the computed distance much too big (though the linear diameter is not much affected).

The high resolution of the present observations enables an estimate to be made of the shell thicknesses for a number of supernova remnants. This is plotted against the linear diameter in Figure 13. Similar measurements have been made for some supernova remnants not observed in the present work such as Cas A, and these are also shown in Figure 13. In estimating the shell thickness, corrections were made for finite resolution but the values obtained are still rather uncertain. Nevertheless the strong correlation shown in the graph is undoubtedly real, and it appears that the shell thickness remains a constant fraction (~ 15%) of the diameter as the supernova remnant evolves. Such

a situation is described by Shklovsky's original model of a supernova remnant, but Kesteven (1968*b*) has shown that the empirical relation between power output and diameter (equation (13)) is much more closely described by a variant of Shklovsky's model in which the shell thickness remains constant during the evolution of the supernova remnant. The situation is further complicated by the fact that there is some observational evidence supporting Van der Laan's (1962) model (Whiteoak and Gardner 1968; Shaver 1969*b*) which predicts yet another relation between the power output and the diameter of a supernova remnant. More high resolution observations and polarization work should help to clarify the issue. At the same time detailed theoretical calculations are needed which take into account the effects of filaments and other inhomogeneities in the expanding shell.

(*c*) *Association of Thermal and Nonthermal Galactic Radio Sources*

Stars are expected to form in groups rather than singly – about 15% of all stars are formed in open clusters and the rest in associations (Von Hoerner 1968). The life span of massive OB stars is short ($\sim 10^7$ years) compared with the dynamical lifetime of open star clusters ($\sim 10^9$ years), but smaller stars survive for much longer and are much more likely to be dispersed from the cluster because of their low mass. Therefore it is expected that OB stars will be found almost exclusively in clusters and associations, whereas smaller stars will be widely spread. This explains why HII regions (excited by O and B stars) are often found to cluster together. Shklovsky (1960) made the suggestion that type II supernova remnants result from explosions of O and B stars; since observable supernova remnants have ages less than ~ 50 000 years they too will be found still within the original associations, and often close to HII regions. On the other hand, it is believed that older less massive stars give rise to type I supernova remnants and therefore that these remnants will be more generally dispersed throughout the Galaxy.

Observational evidence concerning these ideas is rather meagre. The few known type I supernova remnants are all farther away from the galactic plane than the average $|Z|$ distance for the supernova remnants in Milne's (1970) catalogue; this is to be expected if most of the nonthermal galactic radio sources are supernova remnants of type II. The half-widths of the Z distributions for supernova remnants and HII regions are both ~ 100 pc (Murdin and Sharpless 1968; Milne 1970), the same as for O–B5 stars (Blaauw 1965). Furthermore the distribution in galactic longitude of supernova remnants is just as strongly dominated by spiral arm tangential directions as is the distribution of HII regions (Kesteven 1968*b*). So far the observations are consistent with expectations: type I supernova remnants are generally located in the disk of the Galaxy, and type II supernova remnants (which comprise most of the nonthermal galactic radio sources) are extreme population I spiral arm features as are HII regions and OB stars. However, it is difficult to go beyond this point and show conclusively that supernova remnants (of type II) are always found in OB associations and clusters. The distances of the remnants are generally not well enough known.

Nevertheless the existence of such a close association between type II supernova remnants and regions of early-type stars and ionized gas has been demonstrated for some individual cases. Westerlund (1969*a*, 1969*b*) gives several examples of known supernova remnants located in OB associations. The present observations have shown a few more such cases. The three supernova remnants in Norma, G332.0+0.2, G332.4–0.4, and G332.4+0.1 are all at a distance of ~ 4.5 kpc and separated from each other by

~ 40 pc (projected distance). The HII region G332.7–0.6 (RCW 106) is at about the same distance (3.5 kpc) and its projected separation from the supernova remnants is also ~ 40 pc. These sources could easily all be part of a single association (typical diameter ~ 100 pc). Similarly, G6.4–0.1 (W28) has a distance of ~ 1.3 kpc, in very close agreement with the distances of the HII regions G6.0–1.2 (M8) and G7.0–0.3 (M20), namely 1.4 and 1.5 kpc respectively. The projected separations in this case are all less than 30 pc. However, it should be noted that there are cases, such as G49.2–0.5 (W51) (see Appendix), in which thermal and nonthermal sources appear to be very close together along the line of sight and yet are actually well separated from each other.

The fact that there are three supernova remnants all probably in the same association in Norma indicates that supernova remnants can cluster together as HII regions do. However, the clustering is not as severe in this case; with an observable lifetime of ~ 50 000 years and a frequency of occurrence of ~ 100 year^{-1} for the whole Galaxy, the average number of observable supernova remnants per association is ~ 1–2 and, per open star cluster, $\ll 1$. It is therefore not surprising that no resolution problems have been encountered in detecting individual supernova remnants.

VI. CONCLUSIONS

By combining high resolution observations at 408 and 5000 MHz we have obtained spectral information for over 250 galactic radio sources. Thermal sources form 86% of this sample. The line to continuum temperature ratio for hydrogen α recombination lines is closely related to spectral index.

Electron temperatures have been determined for 50 sources which are optically thick at 408 MHz. These temperatures are considerably less than 10^4 °K. In most cases the electron temperatures T_{ec} determined from continuum brightness temperature measurements are consistent with those from hydrogen α recombination line observations (T_{er}). Hence the values of T_{er} are not seriously affected by departures from local thermodynamic equilibrium. For some cases it may be that T_{ec}/T_{er} increases slightly for well-resolved sources with large emission measures. This effect could be due to positive temperature gradients in the nebulae.

VII. ACKNOWLEDGMENTS

The authors are indebted to Professor B. Y. Mills and Dr. B. J. Robinson for their assistance in arranging this work and also to Dr. G. Lyngå for generously providing his Uppsala Schmidt Hα photographs. One of us (P.A.S.) gratefully acknowledges the support of a Sydney University Post-graduate Research Studentship, while W.M.G. acknowledges the support of a NATO Postdoctoral Fellowship in the initial stages of this investigation.

VIII. REFERENCES

Allen, C. W. (1963).–"Astrophysical Quantities." (Univ. London Press.)

Altenhoff, W. (1968).–*In* "Interstellar Ionized Hydrogen". (Ed. Y. Terzian.) p. 519. (W. A. Benjamin: New York.)

Beard, M. (1966).–*Aust. J. Phys.* **19**, 141.

Beard, M., and Kerr, F. J. (1966).–*Aust. J. Phys.* **19**, 875.

Beard, M., and Kerr, F. J. (1969).–*Aust. J. Phys.* **22**, 121.

Beard, M., Thomas, B. M., and Day, G. A. (1969).–*Aust. J. Phys. astrophys. Suppl.* No. 11, 27.
Becker, W., and Fenkart, R. (1963).–*Z. Astrophys.* **56**, 257.
Blaauw, A. (1965).–*In* "Stars and Stellar Systems". (Eds A. Blaauw and M. Schmidt.) Vol. 5, p. 435. (Univ. Chicago Press.)
Bottinelli, L., and Gouguenheim, L. (1964).–*Annls Astrophys.* **27**, 685.
Cederblad, S. (1946).–*Meddn Lunds astr. Obs.* (2d ser.) No. 119.
Clark, B. G., Radhakrishnan, V., and Wilson, R. W. (1962).–*Astrophys. J.* **135**, 151.
Courtes, G. (1960).–*Annls Astrophys.* **23**, 115.
Day, G. A., Thomas, B. M., and Goss, W. M. (1969).–*Aust. J. Phys. astrophys. Suppl.* No. 11, 11.
Day, G. A., Warne, W. G., and Cooke, D. J. (1970).–*Aust. J. Phys. astrophys. Suppl.* No. 13, 11.
Dyson, J. E. (1969).–*Astrophys. Space Sci.* **4**, 401.
Fanti, C., Fanti, R., Londrillo, P., and Padrielli, L. (1969).–*Astr. Astrophys.* **2**, 477.
Gardner, F. F., and Morimoto, M. (1968).–*Aust. J. Phys.* **21**, 881.
Gardner, F. F., Morris, D., and Whiteoak, J. B. (1969).–*Aust. J. Phys.* **22**, 79.
Goss, W. M., and Day, G. A. (1970).–*Aust. J. Phys. astrophys. Suppl.* No. 13, 3.
Goss, W. M., and Radhakrishnan, V. (1969).–*Astrophys. Lett.* **4**, 199.
Gum, C. S. (1955).–*Mem. R. astr. Soc.* **67**, 155.
Hill, E. R. (1967).–*Aust. J. Phys.* **20**, 297.
Hjellming, R. M. (1968).–*In* "Interstellar Ionized Hydrogen". (Ed. Y. Terzian.) p. 171. (W. A. Benjamin: New York.)
Hjellming, R. M., Andrews, M. H., and Sejnowski, T. J. (1969).–*Astrophys. Lett.* **3**, 111.
Hogg, H. S. (1959).–*In* "Handbuch der Physik". (Ed. S. Flügge.) Vol. 53, p. 129. (Springer-Verlag: Berlin.)
Hughes, V. A., and Butler, R. (1969).–*Astrophys. J.* **155**, 1061.
Hughes, V. A., and Routledge, D. (1969).–*Astr. J.* **74**, 604.
Kerr, F. J., and Westerhout, G. (1965).–*In* "Stars and Stellar Systems". (Eds A. Blaauw and M. Schmidt.) Vol. 5, p. 167. (Univ. Chicago Press.)
Kesteven, M. J. L. (1968*a*).–*Aust. J. Phys.* **21**, 369.
Kesteven, M. J. L. (1968*b*).–*Aust. J. Phys.* **21**, 739.
Komesaroff, M. M. (1966).–*Aust. J. Phys.* **19**, 15.
Large, M. I., Mathewson, D. S., and Haslam, C. G. T. (1961).–*Mon. Not. R. astr. Soc.* **123**, 112.
Le Marne, A. E., and Shaver, P. A. (1969).–*Proc. astr. Soc. Aust.* **1**, 216.
Manchester, R. N., Robinson, B. J., and Goss, W. M. (1970).–18 cm observations of galactic OH, longitudes 128° to 300°. *Aust. J. Phys.* (in press).
Mathews, W. G. (1967).–*Astrophys. J.* **147**, 965.
Mathews, W. G. (1969).–*Astrophys. J.* **157**, 583.
Meaburn, J. (1969).–*Astrophys. Space Sci.* **3**, 600.
Menon, T. K. (1961).–*Publ. natn Radio Astr. Obs.* **1**, 1.
Mezger, P. G., and Ellis, S. A. (1968).–*Astrophys. Lett.* **1**, 159.
Mezger, P. G., and Höglund, B. (1967).–*Astrophys. J.* **147**, 490.
Mezger, P. G., Schraml, J., and Terzian, Y. (1967).–*Astrophys. J.* **150**, 807.
Milne, D. K. (1969).–*Aust. J. Phys.* **22**, 613.
Milne, D. K. (1970).–*Aust. J. Phys.* **23**, 425.
Milne, D. K., and Hill, E. R. (1969).–*Aust. J. Phys.* **22**, 211.
Milne, D. K., Wilson, T. L., Gardner, F. F., and Mezger, P. G. (1969).–*Astrophys. Lett.* **4**, 121.
Miller, J. S. (1968).–*Astrophys. J.* **151**, 473.
Mills, B. Y., and Shaver, P. A. (1968).–*Aust. J. Phys.* **21**, 95.
Murdin, P., and Sharpless, S. (1968).–*In* "Interstellar Ionized Hydrogen". (Ed. Y. Terzian.) p. 249. (W. A. Benjamin: New York.)
Oster, L. (1961).–*Rev. mod. Phys.* **33**, 525.
Osterbrock, D. E. (1965).–*Astrophys. J.* **142**, 1423.
Osterbrock, D. E., and Flather, E. (1959).–*Astrophys. J.* **129**, 26.
Pooley, G. G., and Ryle, M. (1968).–*Mon. Not. R. astr. Soc.* **139**, 515.

Pottasch, S. R. (1965).–*In* "Vistas in Astronomy". (Ed. A. Beer.) Vol. 6, p. 149. (Pergamon Press: London.)
Reifenstein, E. C., Wilson, T. L., Burke, B. F., Mezger, P. G., and Altenhoff, W. (1970).–*Astr. Astrophys.* **4**, 357.
Robinson, B. J., Goss, W. M., and Manchester, R. N. (1970).–*Aust. J. Phys.* **23**, 363.
Roslund, C. (1966).–*Ark. Astr.* **4**, 101.
Rubin, R. H. (1967).–Stromgren radii as a function of spectral type. NRAO Internal Rep., December 1967.
Rubin, R. H. (1969).–*Astrophys. J.* **157**, 1461.
Sato, F., Akabane, K., and Kerr, F. J. (1967).–*Aust. J. Phys.* **20**, 197.
Schraml, J., and Mezger, P. G. (1969).–*Astrophys. J.* **156**, 269.
Shaver, P. A. (1969*a*).–*Mon. Not. R. astr. Soc.* **142**, 273.
Shaver, P. A. (1969*b*).–*Observatory* **89**, 227.
Shaver, P. A., and Goss, W. M. (1969).–*Proc. astr. Soc. Aust.* **1**, 280.
Shaver, P. A., and Mills, B. Y. (1969).–*Proc. astr. Soc. Aust.* **1**, 217.
Sher, D. (1965*a*).–*Q. Jl R. astr. Soc.* 6, 299.
Sher, D. (1965*b*).–*Mon. Not. R. astr. Soc.* **129**, 237.
Shklovsky, I. S. (1960).–*Soviet Astr. AJ* **4**, 355.
Smith, Lindsey F., and Batchelor, R. A. (1970).–*Aust. J. Phys.* **23**, 203.
Terzian, Y., and Balick, B. (1969).–*Astr. J.* **74**, 76.
Thomas, B. M., and Day, G. A. (1969*a*).–*Aust. J. Phys. astrophys. Suppl.* No. 11, 3.
Thomas, B. M., and Day, G. A. (1969*b*).–*Aust. J. Phys. astrophys. Suppl.* No. 11, 19.
Van der Laan, H. (1962).–*Mon. Not. R. astr. Soc.* **124**, 179.
Von Hoerner, S. (1968).–*In* "Interstellar Ionized Hydrogen". (Ed. Y. Terzian.) p. 101. (W. A. Benjamin: New York.)
Westerlund, B. E. (1960).–*Ark. astr.* **2**, 419.
Westerlund, B. E. (1969*a*).–*Astr. J.* **74**, 879.
Westerlund, B. E. (1969*b*).–*Astr. J.* **74**, 882.
Whiteoak, J. B., and Gardner, F. F. (1968).–*Astrophys. J.* **154**, 807.
Wilson, T. L., Mezger, P. G., Gardner, F. F., and Milne, D. K. (1970).–A survey of H109α recombination line emission in galactic HII regions of the southern sky. *Astr. Astrophys.* (in press).
Wynn-Williams, C. G. (1969).–*Mon. Not. R. astr. Soc.* **142**, 453.
Zisk, S. H. (1966).–*Science, N.Y.* **153**, 1107.

APPENDIX

Notes on Individual Sources

G206.0–1.7 to G206.6–1.7. The 408 MHz flux density of 320 f.u. (Part II) for the Rosette Nebula is consistent with the thermal spectrum shown by Bottinelli and Gouguenheim (1964), indicating that the nebula is optically thin at 408 MHz. In Section IV the four components have been combined into one source representative of the Rosette Nebula, G206.3–2.0.

G283.3–1.0. The spectrum for this source is flat, suggesting that the source is thermal. No H109α line was found, but for such a weak source an upper limit of 2.5% is not very significant (see notes on G284.6–0.2).

G283.5–1.0. This HII region is excited by the Wolf–Rayet star HD 89358 (Smith and Batchelor 1970).

G284.6–0.2. The optical identification of this source and its proximity to RCW 49 suggest that it is thermal. However, no H109α line was found in the source; the upper limit of $T_L/T_C < 2.3\%$ gives a line width > 700 kHz for $T_e < 10\,000°K$. It is likely that G284.6–0.2 is part of an expanding shell of compressed matter, in which large turbulent motions can be expected. The large line width coupled with the weakness of the source could then explain the negative line results.

G287.4–0.6 and G287.6–0.6. The 5000 MHz data of Gardner and Morimoto (1968) were used in Tables 4 and 5.

G287.7–0.8, G287.9–1.0, and G288.0–0.8. From a comparison of the 408 MHz contour map (Part II) with the 2650 MHz map of Beard and Kerr (1966) it appears that these three sources have flat spectra.

G291.0–0.1. The 85 MHz position of MSH 11–62 is midway between this source and the two strong HII regions G291.3–0.7 and G291.6–0.5, supporting the conclusion that G291.0–0.1 is nonthermal.

G291.3–0.7. The 408 MHz position of this source is ~ 1′ east of the 5000 MHz position, indicating that there must be at least two components in this source with very different emission measures.

G291.6–0.5. If this source is at the indicated distance of 8.4 kpc (Goss and Radhakrishnan 1969), the excitation parameter corresponding to its total integrated flux density is ~ 350 pc cm^{-2}, making it by far the most powerful galactic HII region yet observed. The largest single component in W49A (G43.2–0.0) has an excitation parameter of only ~ 265 pc cm^{-2}, and even this may be overestimated. Only the 30 Doradus Nebula in the Large Magellanic Cloud is more powerful, with an excitation parameter of ~ 600 pc cm^{-2}. Each of these big HII regions must be excited by a large number of O stars; in the case of G291.6–0.5, excitation is provided by the compact cluster NGC 3603 (Sher 1965*b*).

G292.0+1.8. HI absorption measurements (Radhakrishnan, personal communication) provide weak evidence that this source is at a distance ⩽ 4 kpc. The estimate of 7.9 kpc in Table 9 will be too large if the low-emission wings have been underestimated and the diameter and flux density of the source are too small. Alternatively if G292.0 +1.8 is a type I supernova remnant the estimated distance is decreased to about 5 kpc (see Section V).

G295.1–1.7. In Section IV this source is treated as a separate HII region, and the rest of the λ Cen Nebula is called G295.0–1.8.

G298.5–0.3 and G298.6–0.0. The 85 MHz position of MSH 12–61 is close to G298.6–0.0, supporting the conclusion that these sources are nonthermal. The entire ring showing up, especially on the 408 MHz contour map (Part II), may be a supernova remnant, but its spectrum is rather flat.

G307.1+1.2. On the basis of its small angular size and steep nonthermal spectrum, this source appears to be extragalactic. Further evidence supports this conclusion: HI absorption measurements (Radhakrishnan, personal communication) set a lower limit of 6 kpc for the distance; the source is highly polarized at centimetre wavelengths and has a very high rotation measure (Gardner, Morris, and Whiteoak 1969).

G309.6+1.7 and G309.8+1.8. The appearance of the radio contours (Parts I and II) is suggestive of an external galaxy. HI line absorption measurements (Radhakrishnan, personal communication) indicate that the source is more distant than 6.5 kpc, and

support the assumption that it is extragalactic. If it is a supernova remnant at a distance > 6.5 kpc, it is unusually powerful even for a type II supernova remnant.

G316.2+0.0 and G316.3−0.0. These sources are assumed to be components of a single supernova remnant, G316.3−0.0.

G320.2−1.4 to G320.5−1.0. All five of these sources appear to be components of a single supernova remnant, G320.4−1.2. A matted nebulosity (RCW 89), about 6′ in diameter, is located at the position of G320.4−1.0.

G324.2+0.2. At 2650 MHz this source is partly confused with G324.2+0.1 (Day, Thomas, and Goss 1969); the total flux density for both sources is ~ 8 f.u., and this is consistent with a flat spectrum for G324.2+0.2.

G326.2+0.7. The complete thermal ring is included in Section IV as a single source, and is called G326.3+0.8.

G327.3−0.6. The main ring of emission is listed as G327.2−0.6 in Table 5 and G327.3−0.6 is taken to be a separate source.

G328.0+0.3 and G328.4+0.2. The 85 MHz position of MSH 15−57 is midway between these two nonthermal sources, and the 85 MHz flux density is far greater than they can account for alone. It may be that G328.0+0.3 is part of a much larger nonthermal ring that extends to the south and east.

G332.0+0.2 and G332.0+0.1. These sources are regarded as components of a single supernova remnant, G332.0+0.2.

G332.4+0.2 and G332.5+0.0. These two nonthermal sources are assumed to be components of a single supernova remnant, G332.4+0.1.

G333.0−0.4 and G333.1−0.4. These two thermal sources listed in Tables 1 and 5 are clearly shown on the 5000 MHz map (Part I) but at 408 MHz they appear to be merged into one source (G333.1−0.5). These sources and G333.3−0.4 form a very thin crescent of emission which is very opaque at 408 MHz. It appears that some expansion process has caused a great compression of matter into a thin shell.

G336.7+0.5 and G336.8+0.6. These sources are assumed to be components of a single supernova remnant, G336.7+0.5.

G337.0−0.1. This source clearly has a nonthermal spectrum, and yet it also has a strong H109α line. The 408 MHz position is 2′.5 north of the 5000 MHz position, suggesting that the source is made up of a nonthermal component located just north of a thermal component. A model was constructed which adequately fits the data; in it the thermal source is optically thin at 408 MHz and the nonthermal source is 3′ to the north and has a spectral index of −0.47. The nonthermal source is assumed to be part of a supernova remnant which has a diameter of 14′ and is centred about 6′ north-east of the 408 MHz peak in G337.0−0.1.

G338.2+0.4. This nonthermal source is part of the supernova remnant G338.1+0.4.

G338.3−0.1. This source and the small source ~ 6′ west of it both seem to be nonthermal, and are assumed to be components of a single supernova remnant, G338.3−0.1.

G340.3−0.2. The ring associated with this source was taken to be a separate HII region in Section IV, G340.2−0.2.

G340.9−1.0. This source appears to have a flat spectrum down to 408 MHz.

G353.1+0.4 to G353.2+0.9. The basic ring of emission in NGC 6357 was taken to be a separate HII region in Section IV, G353.2+0.7.

G5.9–0.4. This source appears to be very small at 408 MHz and yet it is quite extended at 5000 MHz; this suggests that it is made up of several components, some of which have very high turnover frequencies and contribute little to the 408 MHz flux density. The 5000 MHz continuum measurements of Reifenstein *et al.* (1970) have been used in Table 5.

G6.0+0.0 to G6.7–0.3. This is the supernova remnant W28 (G6.4–0.1). The integrated flux density of W28 at 408 MHz is 460 f.u. and at 2650 MHz, 200 f.u. (Goss and Day 1970); the spectral index is –0.44. It is likely that most of the individual sources in the region of W28 are nonthermal; many of them are crescent-shaped as expected for a supernova remnant. However, some of them (G6.1–0.1, G6.5+0.1, G6.6–0.1, and G6.7–0.3) exhibit H109α recombination lines. Using the 5000 MHz continuum data of Wilson *et al.* (1970) we obtain $T_2/T_1 \sim 1.27$ and 2.70 for G6.1–0.1 and G6.6–0.1 respectively, showing that both of these sources are thermal. However, for G6.5+0.1 and G6.7–0.3, $T_2/T_1 \sim 0.63$ and 0.78, and they are certainly nonthermal, but may be confused by some weak thermal emission.

G7.0–0.3. The continuum parameters given by Reifenstein *et al.* (1970) were used in Table 5.

G10.2–0.3. HI absorption measurements (Radhakrishnan, personal communication) give a definite lower limit of 8 kpc. Combined with the H109α velocity this implies a distance of 17.2 kpc. However, there is weak HI evidence that suggests that the source is not beyond the galactic centre. A distance of 9 kpc has been assumed here. It differs from the H109α line distance, but the latter may not be reliable in this case because the assumption of circular motion is not valid near the galactic centre.

G10.6–0.4. This source appears to be composed of a central peak of small angular size and very high density and an extended halo of low emission.

G15.0–0.7. There are two components in this source that are not resolved by the present observations (Zisk 1966; Schraml and Mezger 1969); the emission measure and density given in Table 5 are therefore underestimated.

G18.2+1.9 to G18.9+1.8. In Section IV, G18.7+2.0 was regarded as a separate source, but the others were taken to be components of a single HII region, G18.5+1.9.

G21.8–0.6 and G21.9–0.4. Both sources are assumed to be components of a supernova remnant, G21.8–0.5

G22.7–0.1 and G22.8–0.2. This whole region appears to be nonthermal, except for the small thermal source G22.8–0.2, and is assumed to be a supernova remnant (G22.7–0.2).

G23.1–0.2, G23.3–0.3, and G23.4–0.2. The central peak in G23.4–0.2 is a thermal source, but the more extended part of G23.4–0.2 is nonthermal and together with G23.1–0.2 and G23.3–0.3 comprises the supernova remnant G23.3–0.3.

G39.2–0.3. With a spectral index of –0.44 this source (NRAO 593) is clearly nonthermal. Hughes and Butler (1969) recently studied the source in some detail, and they concluded that it has a thermal spectrum; however, they had difficulties with resolution effects at the lower frequencies, which the present observations have overcome.

G39.3–0.0. Hughes and Butler (1969) concluded that this source (NRAO 591) contains a small component with a very high turnover frequency. However, the 408 MHz flux density (3.0 f.u.) is consistent with a single source having a flat spectrum between 408 MHz and 10.5 GHz.

G43.2–0.0. The radio spectrum for this source is shown in Figure 14. All the flux density measurements quoted by Mezger, Schraml, and Terzian (1967) and Milne and Hill (1969) are shown here, as well as the 408 and 5000 MHz values from Table 1 and an estimate of the 2650 MHz flux density (62 f.u. ±10%) made from the map of Day, Warne, and Cooke (1970). A single smooth curve adequately fits all the points, and the turnover frequency is ~ 1000 MHz. There is no evidence for the high density component W49 A2 postulated by Mezger, Schraml, and Terzian (1967); Mathews (1969) has recently shown that the excitation requirements of this hypothetical component are in conflict with the properties of even the most massive stars. However, the gentle turnover of the spectrum suggests that a few components with different emission measures may be present, and high resolution observations (Wynn-Williams 1969) have shown that this is so.

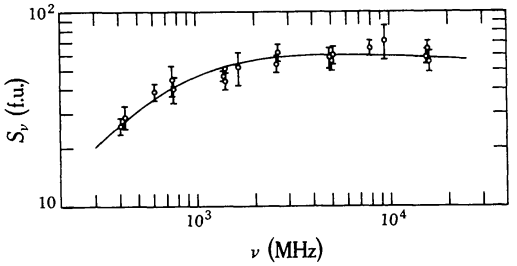

Fig. 14.–Radio continuum spectrum of G43.2–0.0 (W49A). References for the flux densities are given in the text.

G43.3–0.2. The value of T_L/T_C for this source is from the H109α line observations reported by Mezger and Höglund (1967).

G45.5+0.1. The value of T_2/T_1 = 2.04 for this source strongly suggests that the source is thermal. However, this conclusion is difficult to reconcile with the negative H109α line result ($T_L/T_C < 1.1\%$).

The radio continuum spectrum of G45.5+0.1 has been studied in some detail. Peak brightness temperatures at 2650 MHz (Day, Warne, and Cooke 1970), 3240 MHz (Hughes and Routledge 1969), and 15375 MHz (Schraml and Mezger 1969) are all consistent with the 5000 MHz value when the different beamwidths are taken into account, and the spectrum is evidently flat over this range. Flux density measurements give the same result although these are highly uncertain due to the very extended low-brightness component of this source (for example, the 15.4 GHz observations are not sensitive enough even to detect the north-west ridge showing up on the 408 and 5000 MHz maps, and the 15.4 GHz flux density quoted by Schraml and Mezger (1969) is likely to be far too small). The spectrum appears to turn over at ~ 1000 MHz. Obviously this conclusion depends entirely on the 408 MHz observations. Therefore the source has been observed several times at 408 MHz and the calibration checked in several ways; the same result has always been obtained. The source is resolved in the present observations, and is therefore unlikely to be an extragalactic source (Kesteven 1968*a*). On the basis of its spectrum then, G45.5+0.1 appears to be a thermal source.

The H109α line observations set a lower limit on T_e of 14 000°K for a line width of 1000 kHz, which are rather large values even for planetary nebulae; however, such high temperatures are possible if collisional excitation is important. Another curious feature of this source is the arc extending to the north-west. It may be related to a large crescent-shaped radio source about 30′ to the east (Hughes and Routledge 1969) which was observed at 408 MHz, and together these features may comprise a

shell with G45.5+0.1 located on the edge. The arc-like component of G45.5+0.1 appears to have a flat spectrum down to 408 MHz, and the source 30′ to the east may be non-thermal ($\alpha \sim -0.3$) but both of these results are highly uncertain. It is interesting to speculate that G45.5+0.1 is a cloud of gas which has been collisionally excited by an energetic expanding shell of some sort. More continuum and line observations of this source would be of great interest.

G49.0–0.6 and G49.2–0.7. These sources are assumed to be components of a supernova remnant, G49.2–0.5. If this supernova remnant is actually at the distance of the thermal sources G49.0–0.3, G49.1–0.4, and G49.2–0.3 (i.e. 6.5 kpc) then it is quite unusually powerful, even for a type II supernova remnant. Since these sources lie in a direction tangential to a spiral arm (Kerr and Westerhout 1965) where both thermal and nonthermal sources are common, it is likely that the positional coincidence is due to a chance superposition of the sources in the line of sight.